

ALMA MATER STUDIORUM · UNIVERSITÀ DI BOLOGNA

Scuola di Scienze
Dipartimento di Fisica e Astronomia
Corso di Laurea Magistrale in Fisica

Quantum Information Protocols in Complex Entangled Networks

Supervisor:

Prof. Cristian Degli Esposti
Boschi

Presented by:

Francesca Sansavini

Co-supervisor:

Prof. Valentina Parigi

Academic Year 2018/2019

A mio padre Antonio
A mio nonno Aride

Acknowledgements

This is the end of an incredibly long journey.

Thanks to Valentina, who gave me the opportunity to work on this subject at the LKB with the Quantum Optics group, who helped me producing my first results, who introduced me to research. I'm glad I had the chance to work with her and I'm glad I will continue to do so for my PhD. A big thanks also to professor Degli Esposti Boschi, who took the responsibility to follow this project from Bologna. Thanks to the Quantum Optics group, for sharing a wonderful *ambiance*, knowledge, lunches and funny stories, thank you guys because it's a pleasure to work with you.

Grazie mamma, per avermi lasciato intraprendere questo percorso e per il tuo supporto incondizionato, per avermi resa ciò che sono, per essere la mia migliore amica. Grazie babbo, per avermi insegnato ad arrivare dove volevo, ad essere forte e determinata, per le notti trascorse sul terrazzo del mare a guardare le stelle. Grazie Simo, per le ore passate su Spyro con me, per aver giocato alla Luna Nera con la luce spenta prima di addormentarsi, per far parte delle fondamenta della mia vita. Grazie ai nonni, per l'infanzia meravigliosa, per avermi fatto costruire castelli con sedie e tavoli e mangiare cappelletti al ragù e Gibi-Gibi. Grazie Daniele tutte quelle volte in cui abbiamo volato sugli aeroplani alla segavecchia. Grazie a tutta la mia famiglia, agli zii, ai cugini, grazie a Romeo.

Grazie Terry. Per esserci in ogni istante e in ogni momento, per avermi accompagnato nelle mie cadute e aver detto sempre la cosa giusta per farmi rialzare, per essere irriverente e controcorrente, per le Goccioline e i cookies, le birre alla Collina, le pizze e i crescioni divisi a metà.

Grazie Linda. Per essere un'ancora e una certezza, per gli attacchi di nervi condivisi davanti alle macchinette del caffè, perché con te mi sento sempre a casa, per le ore passate ad ascoltare musica improbabile.

Grazie Dia. Per il tuo ottimismo e il tuo farti in quattro per un'amica, per la tua voglia di viaggiare, per i messaggi vocali di trenta minuti.

Grazie Ale. Per Rue de l'Abreuvoir, per aver condiviso con me i miei crampi notturni, per la tua carbonara. Il mio primo anno a Parigi non sarebbe stato lo stesso senza di te: l'hai reso molto più speciale.

Grazie Lucia per tutti i pomeriggi passati alla Esse, grazie Ciap per aver condiviso con me gli *angoli* più belli della mia vita, Mef per tua voglia di vivere e per avermi fatto alzare tutte quelle mattine per fare colazione, Marica per esserci dall'anno zero, Martino per il tuo umorismo insopportabile, Brice per gli sticker con i cactus e i caffè da Descartes,

Lillo per il tuo metro e novanta di buonumore, Pier per aver cucinato tutte quelle cose buone per me, Luciana, Klaudio e Vins perché vivere con voi è stato meraviglioso anche se nessuno comprava le lampadine. Grazie Mariella per il gioco dell'oca e i giardini pubblici, grazie Maurizio, Maria Assunta e Maura per avermi incoraggiata a leggere, scoprire, imparare.

Thanks Emma for every *remblai* night and for sharing *bonbons* with me, thanks Lalou for your Rocky Horror soul, thanks Onir for your sarcasm, thanks Lucìa for your strength and your light, thanks Paul, for tolerating me all these hours, for sharing with me chocolate bars and for sitting on the grass sometimes even if you hate it, thanks Alex, for that wonderful playlist and for teaching me how to properly clean teacups, thanks *the kids* for all the nights, the laughters and the catfights, thanks Jeff, from the University of Nothing in Taos, New Mexico.

Thank you Gabriel. For being always there for me, for standing me when I vent and I shout and I hurt your ears, for that first *balade souterraine*.

Thank you Nicolas. For making room for me into your life, your house and your balcony with my pink flowerpot and my sunflower. For keeping me awake at night searching for mosquitoes and turning on that stupid fan. Thank you for everything that makes you you, even *le coulommiers*, the pshit and CSGO. Except for your food taste, the pizza of Casa Mario was disgusting and I think it will take you two or three months to make up for it.

Abstract

Quantum entangled networks represent essential tools for Quantum Communication, i.e. the exchange of Quantum Information between parties. This work consists in the theoretical study of continuous variables (CV) entangled networks - which can be deterministically generated via multimode squeezed light - with complex topology. In particular we investigate CV complex quantum networks properties for quantum communication protocols. We focused on the role played by the topology in the implementation and the optimization of given characteristics of our entangled resource that are useful for a specific quantum communication task, i.e. the creation of an entanglement link between two arbitrary nodes of the resource we are provided with. We implemented an analytical procedure for the generation of entangled complex networks, their optimization and their manipulation via global linear optics operations. We also developed a numerical procedure, based on an evolutionary algorithm, for manipulating entanglement connections via local linear optics operations. Finally, we analyzed the re-shaping of our entangled resource via homodyne measurements.

Contents

Introduction	1
1 Quantum Light	3
1.1 From classical to quantum light	3
1.2 Common states in quantum optics	5
1.2.1 Fock states	5
1.2.2 Coherent states	6
1.2.3 Squeezed states	8
1.2.4 Multimode Generalization	9
1.2.5 Pure states and mixed states	11
1.3 Wigner functions	12
1.3.1 Basic properties	12
1.3.2 Examples of Wigner functions	14
1.4 Gaussian states and Gaussian unitaries	16
1.4.1 Gaussian states	16
1.4.2 Gaussian Unitaries	17
1.4.3 The real symplectic group in quantum optics	18
1.4.4 Homodyne detection	20
2 CV quantum information	23
2.1 From DV quantum Information to CV quantum information	23
2.2 Entanglement and the EPR state	25
2.2.1 The EPR paradox	25
2.2.2 Bipartite entanglement	26
2.2.3 Bipartite entanglement: the two-mode squeezed vacuum	27
2.3 Quantum teleportation	30
2.3.1 Quantum teleportation in the Heisenberg representation	30
2.3.2 Quantum teleportation in the Wigner representation	31
2.3.3 Fidelity	33
2.3.4 The Q-function	34
2.4 One Way Quantum Computation	35
2.4.1 Quantum Gates and Universality	36
2.4.2 Teleportation gate	37
2.4.3 Universal Quantum Computation	38

3	Cluster states	41
3.1	Continuous variable cluster states via C_Z gate	42
3.1.1	Definition	42
3.1.2	Stabilizers and Nullifiers	42
3.1.3	Wigner representation of Cluster States	44
3.1.4	The effect of finite squeezing	44
3.2	Implementation via multimode squeezing and linear optics	46
3.3	Building cluster states	48
3.3.1	Shot noise	48
3.3.2	Optimization protocol	49
3.3.3	Implementation of regular clusters	49
3.3.4	Implementation of complex clusters	54
3.3.5	Comparison of complex graphs	61
4	Transformations on Cluster States	63
4.1	Global transformations for entanglement percolation	63
4.1.1	Global transformation from cluster to cluster	63
4.1.2	EPR vs two-mode cluster state with equal squeezing	65
4.1.3	Is the 3-modes cluster an EPR channel?	65
4.1.4	Global linear optics transformations on Quantum Network to get an EPR state	67
4.2	Local linear optics transformations for entanglement percolation	68
4.2.1	Local transformations for two parties	69
4.2.2	Derandomized Evolution Strategy (DES)	69
4.2.3	Fitness function for the creation of an EPR channel via local transformations	73
4.2.4	Creation of an EPR channel via local transformations on given graphs	74
4.3	Measurement of nodes in cluster states	78
4.3.1	Measurements in the characteristic function formalism	78
4.3.2	Homodyne detection for node removal or wire-shortening	80
	Conclusions	87
	Appendices	89
	Bibliography	97

Introduction

At the beginning of the 20th century the discovery of the wave-particle duality of weak light fields and microscopic particles, such as electrons, laid the foundation for what has been called the *first quantum revolution*. During this period we were merely observers: nature taught us about quantization, superposition, uncertainty and other remarkable peculiarities of the quantum world, such as *entanglement*. This latter quantum feature has been at the core of the debate on the completeness of quantum mechanics with the EPR paper [1] and of its non-locality with Bell's article [2]. Nowadays it is also at the heart of a *second quantum revolution*, that enabled us to switch our role in the quantum world: from spectators we became actors. The second revolution promises the development of *quantum technology*, i.e. the engineering of tools and devices with better performances than classical ones. With the aim of reaching these goals, recent years have seen the parallel development of various fields concerning the quantum world. We will concentrate on *Quantum Information theory*, which explores the ways we can exploit quantum properties to process and transmit information [3, 4].

Nowadays, we follow mostly two different approaches for the encoding of quantum information: one exploits discrete variables (DV), mainly belonging to a two dimensional space (qubits), while the other is a continuous variables (CV) approach that employs variables with a continuous spectrum of values (qumodes). The two approaches have been used in quantum cryptography and quantum computing with different realizations and experimental techniques, with the aim of reaching intrinsically secure protocols in quantum cryptography and computationally efficient protocols in quantum computing [5, 6].

Here we focus on the implementation of CV entanglement networks, based on a photonic setup, which can be exploited both as a resource for measurement based (“one way”) quantum computing and for multiparty quantum communication protocols. CV entanglement networks have the advantage that, differently from the DV counterpart, they can be deterministically generated via multimode squeezed light [7, 8]. One-way quantum computing is implemented by the means of a series of measurements and feed-forward operations done at the price of destroying the entanglement of the resource, a particular type of entanglement networks named *cluster states*. It is important to mention, however, that in CV such a resource is always imperfect, as opposed to a DV resource, due to the impossibility of reaching an infinite amount of squeezing to create our CV resource out of squeezed modes of light [9, 10].

Quantum communication concerns the exchange of quantum information by employ-

ing both a quantum channel (i.e. entanglement) and a classical channel. Quantum networks are essential tools for allowing long-distance quantum communication between parties and for implementing multiparty delegated quantum computing or a quantum internet [11, 12]. It is known that classical world-wide communication networks have complex topology (neither regular nor simply random). Thus, if we wish to implement quantum communication networks, it is important to investigate the role played by the topology for various quantum communication tasks, in order to search for the existence of resilient structures, as in the classical domain [13].

Classically, complex networks are used to describe a huge variety of situations that we may find in science, arts, social sciences or, in general, in everyday life. Some of the most intuitive examples are the World Wide Web, a social network made of people who know each other, a biological neural network. Various models of complex networks have been proposed with different network topology in order to better describe their statistical properties [14]. It is natural to ask ourselves what happens when we cross the border between the classical world and the quantum world. In other words: what happens when our classical complex network becomes a quantum complex network? Does the topology play any role in quantum communication tasks? Which topologies are the most resilient to error and failure? Which topologies are the best for entanglement percolation, the ability to establish entanglement between two particular nodes?

Here we consider the implementation of quantum networks via parametric processes, which generate multimode squeezed resources, and the equivalent of linear optical manipulations, which can be experimentally implemented via mode-dependent measurements, as done at the Laboratoire Kastler Brossel [15]. The main advantage of this implementation is that we can easily build the networks and reconfigure their shape, according to the task we want to perform. During this dissertation, we focused on the role played by the topology in the implementation and the optimization of given characteristic of our resource for a specific quantum communication task, i.e. the creation of an entanglement link between two given nodes of the graph we are provided with. At first, we will study the implementation of entanglement networks with complex shapes in a realistic scenario: we will see how we can generate them with a finite amount of squeezing, how we can optimize them and what are their peculiar features. In addition, we will investigate network manipulation: we will allow global linear optical operations to be performed after the generation of the resource, via an analytic procedure, and local linear optical operations to be performed after its distribution to two parties, using a numerical procedure based on an evolutionary algorithm for experimental quantum control [16]. In this work, the evolutionary algorithm was adapted accordingly to search, over a continuous landscape, optimized parameters for the construction of suitable unitaries subjected to certain constraints, with the aim of creating an entanglement link between the two parties. Finally, the re-shaping of cluster states via homodyne measurements will be studied and analyzed in our framework for a paradigmatic case.

The results of this work reveal general theoretical features of quantum complex networks and, at the same time, they involve protocols which are close to the possible experimental realisations.

Chapter 1

Quantum Light

The study of light began more than 2500 years ago in ancient Greece, in strict connection with the study of visual perception. From that moment on many philosophers and scientists have tried to unravel the mysteries of its properties, through many theories and experiments of optics, and after centuries of brilliant intuitions and missteps, with the publication of Maxwell's paper *Electricity and Magnetism*, the classical electromagnetic theory is finally fully described: classical light is an electromagnetic radiation obeying Maxwell equations.

1.1 From classical to quantum light

Maxwell equations are thus the starting point for the quantization of the electromagnetic field [17, 18]. We consider an electromagnetic field in a region of space with volume V , expanding it over its *modes*, i.e. normalized solutions of the Maxwell equations. We may for example assume the plane wave ansatz and impose periodic boundary condition to obtain the expansion

$$\begin{aligned}\mathbf{E}(\mathbf{r}, t) &= \sum_{\mathbf{k}} \sqrt{\frac{\hbar\omega_{\mathbf{k}}}{2\varepsilon_0 V}} \boldsymbol{\epsilon}_{\mathbf{k}} [a_{\mathbf{k}} e^{i(\mathbf{k}\cdot\mathbf{r}-\omega_{\mathbf{k}}t)} + c.c.] \\ \mathbf{B}(\mathbf{r}, t) &= \sum_{\mathbf{k}} \sqrt{\frac{\hbar\omega_{\mathbf{k}}}{2\varepsilon_0 V}} \frac{\mathbf{k} \times \boldsymbol{\epsilon}_{\mathbf{k}}}{\omega_{\mathbf{k}}} [a_{\mathbf{k}} e^{i(\mathbf{k}\cdot\mathbf{r}-\omega_{\mathbf{k}}t)} + c.c.]\end{aligned}\tag{1.1}$$

where $\boldsymbol{\epsilon}_{\mathbf{k}}$ is the unit polarization vector, ε_0 is the vacuum permittivity, $\omega_{\mathbf{k}} = c|\mathbf{k}|$ and the summation is over the discrete values of $\mathbf{k} = (k_x, k_y, k_z)$ satisfying $k_i = 2\pi n_i/L$, with $n_i \in \mathbb{N}$, as imposed by the boundary conditions. The classical Hamiltonian for a free field in a region of space V is¹

$$\mathcal{H} = \frac{1}{2} \int_V dV (\varepsilon_0 \mathbf{E}^2 + \mu_0^{-1} \mathbf{B}^2) = \hbar \sum_{\mathbf{k}} \omega_{\mathbf{k}} |a_{\mathbf{k}} e^{-i\omega_{\mathbf{k}}t}|^2\tag{1.2}$$

¹To carry out the second equality we must note that $a_{\mathbf{k}} = a_{-\mathbf{k}}^*$ is a necessary condition for the fields to be real and that $\int d^3\mathbf{r} e^{i\mathbf{k}\cdot\mathbf{r}} e^{-i\mathbf{k}'\cdot\mathbf{r}} = V\delta_{\mathbf{k}',\mathbf{k}}$

and by defining

$$\begin{aligned} q_{\mathbf{k}} &= 4\text{Re} [a_{\mathbf{k}}e^{-i\omega_{\mathbf{k}}t}] \\ p_{\mathbf{k}} &= 4\text{Im} [a_{\mathbf{k}}e^{-i\omega_{\mathbf{k}}t}] \end{aligned}$$

or, equivalently,

$$Q_{\mathbf{k}} = \sqrt{\frac{\hbar}{m\omega_{\mathbf{k}}}} q_{\mathbf{k}} \quad (1.3)$$

$$P_{\mathbf{k}} = \sqrt{m\hbar\omega_{\mathbf{k}}} p_{\mathbf{k}} \quad (1.4)$$

and substituting them in the Hamiltonian (1.2) we can re-express the Hamiltonian of the free field as

$$\mathcal{H} = \frac{1}{4} \sum_{\mathbf{k}} \hbar\omega_{\mathbf{k}}(p_{\mathbf{k}}^2 + q_{\mathbf{k}}^2) = \sum_{\mathbf{k}} \frac{P_{\mathbf{k}}^2}{2m} + \frac{m\omega^2}{2} Q_{\mathbf{k}}^2 \quad (1.5)$$

This Hamiltonian enlightens the fact that the electromagnetic field can be regarded as a collection of quantum harmonic oscillators, corresponding to the different modes of the field, which are independent of one another. This allows us to quantize each mode separately, promoting the position and momentum coordinates to operators obeying the well-known commutation relations $[\hat{Q}_{\mathbf{k}}, \hat{P}_{\mathbf{k}'}] = i\hbar\delta_{\mathbf{k},\mathbf{k}'}$. The position and momentum operator $\hat{Q}_{\mathbf{k}}$ and $\hat{P}_{\mathbf{k}}$ can be expressed in terms of the creation and annihilation operators as

$$\hat{Q}_{\mathbf{k}} = \sqrt{\frac{\hbar}{2m\omega_{\mathbf{k}}}} (\hat{a}_{\mathbf{k}}^{\dagger} + \hat{a}_{\mathbf{k}}) \quad (1.6)$$

$$\hat{P}_{\mathbf{k}} = i\sqrt{\frac{\hbar m\omega_{\mathbf{k}}}{2}} (\hat{a}_{\mathbf{k}}^{\dagger} - \hat{a}_{\mathbf{k}}) \quad (1.7)$$

where the canonical commutation relation $[\hat{a}_{\mathbf{k}}, \hat{a}_{\mathbf{k}}^{\dagger}] = 1$ holds.

Given the relations (1.3), (1.4), (1.6) and (1.7), the *quadrature operators* $\hat{q}_{\mathbf{k}}$ and $\hat{p}_{\mathbf{k}}$ can be expressed as

$$\hat{q}_{\mathbf{k}} = \hat{a}_{\mathbf{k}}^{\dagger} + \hat{a}_{\mathbf{k}} \quad (1.8)$$

$$\hat{p}_{\mathbf{k}} = i(\hat{a}_{\mathbf{k}}^{\dagger} - \hat{a}_{\mathbf{k}}) \quad (1.9)$$

with the inverse relation

$$\hat{a}_{\mathbf{k}} = \frac{1}{2}(\hat{q}_{\mathbf{k}} + i\hat{p}_{\mathbf{k}})$$

$$\hat{a}_{\mathbf{k}}^{\dagger} = \frac{1}{2}(\hat{q}_{\mathbf{k}} - i\hat{p}_{\mathbf{k}})$$

The canonical commutation relations of the creation and annihilation operators lead to

$$[\hat{q}_{\mathbf{k}}, \hat{p}_{\mathbf{k}'}] = 2i\delta_{\mathbf{k},\mathbf{k}'} \quad (1.10)$$

$$[\hat{q}_{\mathbf{k}}, \hat{q}_{\mathbf{k}'}] = [\hat{p}_{\mathbf{k}}, \hat{p}_{\mathbf{k}'}] = 0 \quad (1.11)$$

This notation, which will be used throughout the whole dissertation, is not unique: many authors may adopt the convention with normalized commutation relations such that $[\hat{q}_{\mathbf{k}}, \hat{p}_{\mathbf{k}'}] = i\delta_{\mathbf{k}, \mathbf{k}'}$ and many others will prefer to have unity vacuum expectation values with the convention $[\hat{q}_{\mathbf{k}}, \hat{p}_{\mathbf{k}'}] = i/2\delta_{\mathbf{k}, \mathbf{k}'}$ [19].

From the generalization of Heisenberg uncertainty principle for two arbitrary observables [20, 21] we see that for the quadrature operators the relation

$$\Delta^2 q_i \Delta^2 p_i - \Delta^2 qp_i \geq 1 \quad (1.12)$$

where $\Delta^2 q_i$ and $\Delta^2 p_i$ denote respectively the variance² of the momentum quadrature and of the position quadrature of the mode labeled by i and $\Delta^2 qp_i$ denotes the covariance of the two, holds. States characterized by a vanishing covariance $\Delta^2 qp_i$ and that minimize the relation (1.12) are called *minimum uncertainty states* and we will analyze some of them, namely the *vacuum state*, *coherent states* and *squeezed states*, in the next section.

1.2 Common states in quantum optics

To get familiar with the most common states encountered in quantum optics, it is useful to confine for the moment the discussion to the single-mode field. An extensive dissertation of the subject can be found in most books of quantum optics, such as [17, 18, 22, 23].

1.2.1 Fock states

Using the relations (1.6) and (1.7), the Hamiltonian (1.5) may be rewritten, in the single-mode case, as

$$\hat{\mathcal{H}} = \hbar\omega \left(\hat{a}^\dagger \hat{a} + \frac{1}{2} \right)$$

and we define $\hat{n} = \hat{a}^\dagger \hat{a}$ as the *number operator*. As the Hamiltonian commutes with \hat{n} , there exists an orthonormal basis formed by common set of eigenstates of the two operators, namely the *Fock states* $\{|n\rangle\}_{n \in \mathbb{N}}$, that have thus a defined energy E_n and a defined number of photons n . The action of the creation and annihilation operators consists respectively in adding and removing a photon from the Fock state, resulting in the relations

$$\begin{aligned} \hat{a} |n\rangle &= \sqrt{n} |n-1\rangle \\ \hat{a}^\dagger |n\rangle &= \sqrt{n+1} |n+1\rangle \end{aligned}$$

If we identify as $|0\rangle$ the *vacuum state*, defined by $\hat{a}|0\rangle = 0$, we can express a Fock state as

$$|n\rangle = \frac{(\hat{a}^\dagger)^n}{\sqrt{n!}} |0\rangle \quad (1.13)$$

²Recall that the variance of an operator \hat{A} is defined as $\Delta^2 A = \langle A^2 \rangle - \langle A \rangle^2$

Considering the quadrature operators defined in (1.8) and (1.9) it is straightforward to obtain the variances

$$\Delta^2 q = \Delta^2 p = 2n + 1$$

from which we see that for $n = 0$, the vacuum state, the uncertainty relation is minimized.

It is interesting to evaluate the mean value and the variance of the electric field for a Fock state $|n\rangle$. Let's consider for simplicity the single-mode version of the electric field (1.1), promoted to an operator, propagating in the z direction

$$\hat{E}(z, t) = E_0 \hat{a} e^{i(kz - \omega t)} + c.c. \quad (1.14)$$

where $E_0 = \sqrt{\hbar\omega/2\varepsilon_0 V}$ is a constant³. We can calculate the mean field and the field variance, obtaining

$$\begin{aligned} \langle E \rangle &= 0 \\ \Delta^2 E &= E_0^2 (2n + 1) \end{aligned}$$

From these relations it is evident that Fock states exhibit properties that are far away from the classical regime. In fact we see that even for the vacuum state $|0\rangle$ the electric field undergoes zero-point oscillations. Moreover, regardless of the number of photons of the Fock state $|n\rangle$, the mean electric field vanishes and a measurement performed at any time t may lead to any outcome in the range determined by ΔE , which depends on n . This reflects the fact that a Fock state lacks any information about the phase of the electric field, which takes random values, leading to a behavior of the electric field that is different from the oscillating behavior we are familiar with.

1.2.2 Coherent states

To recover a classical oscillation behavior we may want to introduce *coherent states* or *Glauber states* [24], also considered the “most classical states of light”. Considering that the electric field is a linear combination of the creation and annihilation operators, if we want to keep the oscillating exponential of Eq. (1.14) from vanishing we need to search for eigenstates of \hat{a} or \hat{a}^\dagger . In particular, coherent states are defined as eigenstates of \hat{a} , such that

$$\hat{a} |\alpha\rangle = \alpha |\alpha\rangle \quad (1.15)$$

It is to keep in mind that since \hat{a} is not Hermitian its eigenvalues α are complex numbers and we can identify them by $\alpha = |\alpha| e^{i\theta}$. The expectation value for the single-mode electric field (1.1) propagating in the z direction gives

$$\langle \hat{E} \rangle = \langle \alpha | \hat{E} | \alpha \rangle = 2E_0 |\alpha| \cos(kz - \omega t + \theta)$$

³In terms of the quadrature operators the electric field operator reads $\hat{E}(z, t) = 2E_0(\hat{q} \cos \phi - \hat{p} \sin \phi)$ where $\phi = kz - \omega t$. From this expression it is evident that \hat{q} and \hat{p} are associated to observables of the electric field that oscillates out of phase by $\pi/2$, from which the name *quadratures*.

This expectation value reflects the sinusoidal behavior of the classical electric field, as we may see in Fig. 1.1 and for this reason the coherent states are the “most classical” states of light.

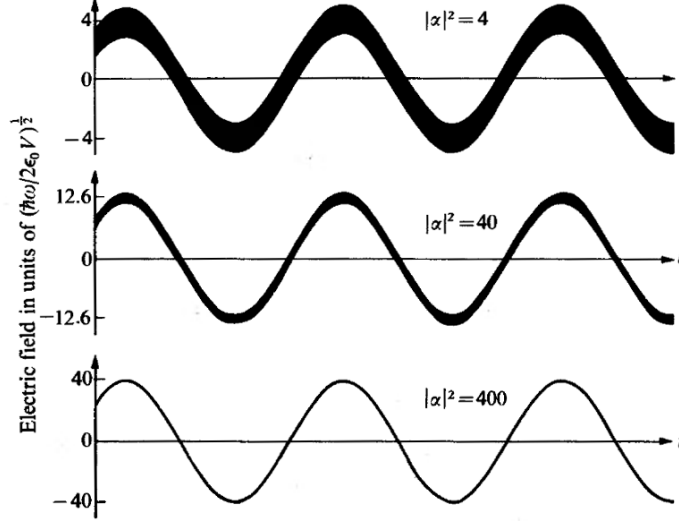


Figure 1.1: Electric field for a state $|\alpha\rangle$, where the vertical width of the sinusoidal wave represents the variance $\Delta E = E_0$ [22]. Note that the vertical scales are different for the three cases.

To construct coherent states we need to introduce the *Weyl displacement operator*

$$D(\alpha) = \exp(\alpha \hat{a}^\dagger - \alpha^* \hat{a}) \quad (1.16)$$

which is obviously unitary, since $D(\alpha)^\dagger = D(\alpha)^{-1}$. From the Baker-Campbell-Hausdorff formula and other properties of the exponentiation of operators⁴ [25] we may rewrite the expression (1.16) for $D(\alpha)$ as

$$D(\alpha) = e^{\alpha \hat{a}^\dagger} e^{-\alpha^* \hat{a}} e^{-|\alpha|^2/2} \quad (1.17)$$

which, subsequently, leads to

$$\begin{aligned} D(\alpha)^\dagger \hat{a} D(\alpha) &= \hat{a} + \alpha \\ D(\alpha)^\dagger \hat{a}^\dagger D(\alpha) &= \hat{a}^\dagger + \alpha^* \end{aligned}$$

that shows that the action of $D(\alpha)$ effectively displaces the creation and annihilation operators by a complex number, hence the name *displacement operator*. From the above properties we see that we can equivalently define a coherent state as

$$|\alpha\rangle \equiv D(\alpha) |0\rangle \quad (1.18)$$

⁴For operators \hat{A} and \hat{B} such that $[\hat{A}, [\hat{A}, \hat{B}]]$ and $[\hat{B}, [\hat{A}, \hat{B}]]$ are null reads $e^{\hat{A}+\hat{B}} = e^{\hat{A}} e^{\hat{B}} e^{-[\hat{A}, \hat{B}]/2}$. Moreover, for such operators the following identity holds: $e^{\hat{A}} \hat{B} e^{-\hat{A}} = \hat{B} + [\hat{A}, \hat{B}]$

This definition is equivalent to the one given in (1.15).

We can express a coherent state in a Fock state basis as $|\alpha\rangle = \sum_n |n\rangle \langle n|\alpha\rangle$, where the term $\langle n|\alpha\rangle$ can be calculated by means of the Equations (1.13), (1.15), (1.18) and (1.17) and we obtain

$$|\alpha\rangle = e^{-|\alpha|^2/2} \sum_n \frac{\alpha^n}{\sqrt{n!}} |n\rangle$$

from which it's evident that a coherent state doesn't have a well-defined number of photons. In fact, an explicit calculation of the photon number distribution leads us to the Poisson distribution, with expected value $\langle n\rangle = |\alpha|^2$.

It's worth to notice that for coherent states, independently from the complex number α , and thus from the mean number of photons, $\Delta^2 q = \Delta^2 p = 1$ and thus they satisfy the relation (1.12), which identifies them as minimum uncertainty states⁵. We can represent a coherent state in the optical phase space as it is shown in Fig. 1.2.

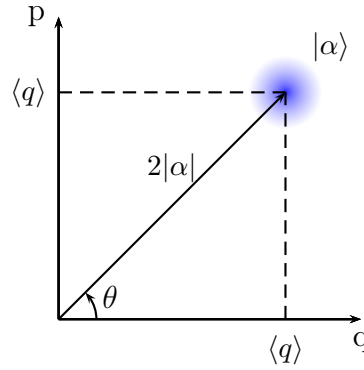


Figure 1.2: Representation of a coherent state in the optical phase space. $\langle q\rangle = \langle \alpha|\hat{q}|\alpha\rangle = 2|\alpha| \cos \theta$ and $\langle p\rangle = \langle \alpha|\hat{p}|\alpha\rangle = 2|\alpha| \sin \theta$ are the mean values of the position and the momentum respectively.

1.2.3 Squeezed states

Coherent states are minimum uncertainty states with the same noise, equal to vacuum noise, on both quadratures, but there exists minimum uncertainty states with less noise in one quadrature and more noise in the other one, such that they maintain the uncertainty relation (1.12): the *squeezed states*.

To obtain squeezed states we define the unitary squeezing operator

$$\hat{S}(\epsilon) = \exp[(\epsilon \hat{a}^2 - \epsilon^* \hat{a}^{\dagger 2})/2] \quad (1.19)$$

where ϵ is a complex number defined as $\epsilon = r e^{2i\theta}$. After some calculations⁶ we get to the

⁵This can be checked by explicitly evaluating the variance $\Delta^2 q = \langle \alpha|\hat{q}^2|\alpha\rangle - \langle \alpha|\hat{q}|\alpha\rangle^2$ using the relations (1.8) and (1.9) and by repeating the same steps for the momentum quadrature $\Delta^2 p$.

⁶We have to consider the expansion $e^{-\hat{A}\hat{B}e^{\hat{A}}} = \hat{B} + [\hat{B}, \hat{A}] + 1/2![[\hat{B}, \hat{A}], \hat{A}] + \dots$

following result:

$$\hat{S}(\epsilon)^\dagger \hat{a} \hat{S}(\epsilon) = \hat{a} \cosh r - e^{2i\theta} \hat{a}^\dagger \sinh r \quad (1.20)$$

$$\hat{S}(\epsilon)^\dagger \hat{a}^\dagger \hat{S}(\epsilon) = \hat{a}^\dagger \cosh r - e^{-2i\theta} \hat{a} \sinh r \quad (1.21)$$

Let's define phase-shifted quadrature operators as

$$\hat{q}^\theta + i\hat{p}^\theta = (\hat{q} + i\hat{p})e^{-i\theta} = 2\hat{a}e^{-i\theta} \quad (1.22)$$

$$\hat{q}^\theta - i\hat{p}^\theta = (\hat{q} - i\hat{p})e^{i\theta} = 2\hat{a}^\dagger e^{i\theta} \quad (1.23)$$

Using Eqs (1.20) and (1.21) we are able to see the action of the squeezing transformation on the two phase-shifted quadrature operators:

$$\hat{S}(\epsilon)^\dagger (\hat{q}^\theta + i\hat{p}^\theta) \hat{S}(\epsilon) = 2e^{-i\theta} (\hat{a} \cosh r - e^{2i\theta} \hat{a}^\dagger \sinh r) = \hat{q}^\theta e^r + i\hat{p}^\theta e^{-r}$$

that can be written more compactly as

$$\hat{S}(\epsilon)^\dagger \begin{pmatrix} \hat{q}^\theta \\ \hat{p}^\theta \end{pmatrix} \hat{S}(\epsilon) = \begin{pmatrix} e^r & 0 \\ 0 & e^{-r} \end{pmatrix} \begin{pmatrix} \hat{q}^\theta \\ \hat{p}^\theta \end{pmatrix} \quad (1.24)$$

It is evident that $\hat{S}(\epsilon)$ increases the variance of \hat{q}^θ (the *anti-squeezed* quadrature), which becomes $\Delta^2 q^\theta = e^{2r}$, and reduces the variance of \hat{p}^θ (the *squeezed* quadrature), which becomes $\Delta^2 p^\theta = e^{-2r}$. We define $s = e^{2r}$ as the *squeezing factor*. The value of these variances shows that we can identify squeezed states as minimum uncertainty states, as they satisfy Eq. (1.12). Moreover, the degree of squeezing depends on the *squeezing parameter* $|\epsilon| = r$ and it is often quantified in Decibels as

$$\text{degree of squeezing (dB)} = 10 \log_{10}(\Delta^2 \hat{\xi})$$

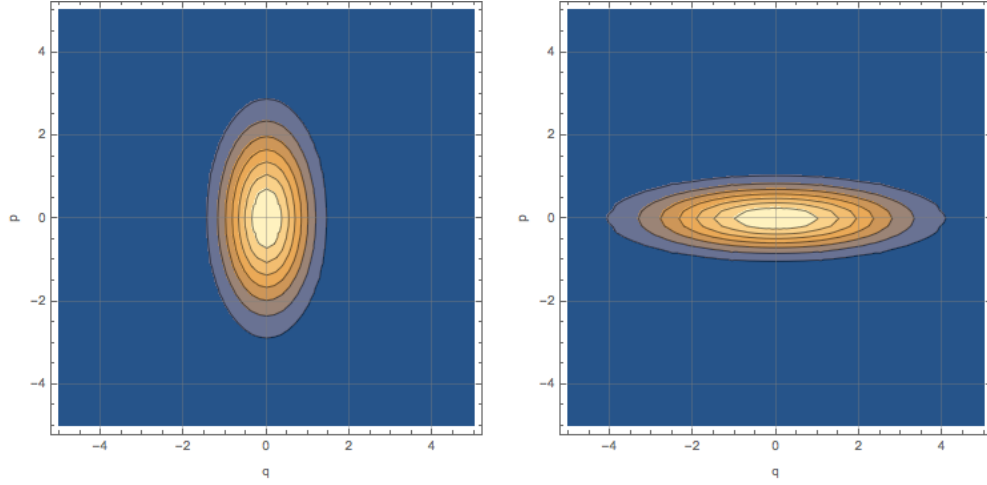
where $\hat{\xi} = \hat{q}, \hat{p}$ ⁷.

A *coherent squeezed state* is obtained by first squeezing the vacuum and then displacing it, while a *squeezed coherent state* is generated by acting on the vacuum inverting the order of the two operators. The order of these transformations is important, due to the fact that the squeezing operator and the displacement operator do not commute, so that in general $\hat{D}(\alpha)\hat{S}(\epsilon)|0\rangle \neq \hat{S}(\epsilon)\hat{D}(\alpha)|0\rangle$. In the present dissertation we will concentrate uniquely on squeezed vacuum states, depicted in Fig. 1.3 for $\theta = 0$. It is to note that squeezed vacuum states no longer represent a “true” vacuum state $|0\rangle$, void of photons, as their mean number of photons reads $\langle n \rangle = \sinh^2 r > 0$.

1.2.4 Multimode Generalization

All the single-mode states of light introduced in Section 1.2 can be easily generalized to the multi-mode case.

⁷We remark that the degree of squeezing is normalized with respect to the shot noise. In general it is equal to $10 \log_{10}(\Delta^2 \hat{\xi} / \Delta^2 \xi_0)$ where $\Delta^2 \xi_0$ is the variance of the vacuum



(a) -3 dB of squeezing in the q quadrature. (b) -6 dB of squeezing in the p quadrature

Figure 1.3: Contour plots of the Wigner function (see Section 1.3) of squeezed-vacuum states exhibiting different amounts of squeezing, respectively in the q quadrature and in the p quadrature

Having now multiple modes, Fock states can be generalized by adding a label to the number state, such that $|n_l\rangle$ state represents n photons in the single-particle mode labeled by l , whose creation and destruction operators are $\hat{a}_l, \hat{a}_l^\dagger$. A suitable basis state of the Fock space is

$$|\psi_{n_1, \dots, n_l, \dots}\rangle = |n_1, \dots, n_l, \dots\rangle = |n_1\rangle \otimes \dots \otimes |n_l\rangle \otimes \dots$$

so that a general state living in the Fock space can be represented in the Fock basis as

$$|\psi\rangle = \sum_{n_1, \dots} C_{n_1, \dots, n_l, \dots} |\psi_{n_1, \dots, n_l, \dots}\rangle$$

The multimode Fock state can be obtained from the multimode vacuum as

$$|n_1, \dots, n_l, \dots\rangle = \prod_l \frac{(\hat{a}_l^\dagger)^{n_l}}{\sqrt{n_l!}} |0\rangle^{\otimes N}$$

where $|0\rangle^{\otimes N}$ is the multimode vacuum for N modes.

We generalize the definition of coherent states in an arbitrary basis as a tensor product of single-mode coherent states

$$|\alpha\rangle = |\alpha_1\rangle \otimes \dots \otimes |\alpha_k\rangle \dots \quad (1.25)$$

where

$$\hat{a}_k |\alpha_k\rangle = \alpha_k |\alpha_k\rangle$$

The annihilation operator of such a state is $\hat{a} = \sum_k \alpha_k^* \hat{a}_k / \beta$, where $\beta = \sqrt{\sum_k |\alpha_k|^2}$ is a normalization factor, and its action on a multimode coherent state is

$$\hat{a} |\alpha\rangle = \sum_k \frac{\alpha_k^* \hat{a}_k}{\beta} |\alpha\rangle = \sum_k \frac{\alpha_k^* \alpha_k}{\beta} |\alpha\rangle = \beta |\alpha\rangle$$

It's thus demonstrated that $|\alpha\rangle$ is a coherent state as well, as it's the eigenstate of an annihilation operator. More precisely, we can identify its displacement operator with

$$D(\beta) = \exp(\beta \hat{a}^\dagger - \beta^* \hat{a})$$

and express the coherent state $|\alpha\rangle$ as the result of a displacement transformation acting on the multimode vacuum, namely

$$|\alpha\rangle = D(\beta) |0\rangle^{\otimes N}$$

It is to remark that by choosing the basis that corresponds to the operators \hat{a} and \hat{a}^\dagger the generalized coherent state we defined in Eq. (1.25) can be described by a single-mode field [26].

Lastly, even squeezed states can be generalized to the multimode case by applying a single-mode squeezing operator to each vacuum mode, as

$$|r_1, r_2, \dots\rangle = \otimes_j \hat{S}_j(r_j) |0\rangle^{\otimes N}$$

1.2.5 Pure states and mixed states

A *pure state* is a state that can be described by a vector $|\psi\rangle$ in the Hilbert space, such that its density matrix is of the form

$$\hat{\rho} = |\psi\rangle \langle\psi|$$

A *mixed state* is a statistical mixture, an *ensemble*, of pure states whose density matrix reads

$$\hat{\rho} = \sum_i p_i |\psi_i\rangle \langle\psi_i|$$

where p_i represents the probability for the state $|\psi_i\rangle$. Given the density matrix $\hat{\rho}$ of a state we can tell if it's pure or mixed by calculating $\text{Tr}\hat{\rho}^2$: we will obtain $\text{Tr}\hat{\rho}^2 = 1$ for pure states and $\text{Tr}\hat{\rho}^2 < 1$ for mixed states. To quantify the “degree of mixing” of a state we introduce the *Von Neumann entropy*, an extension of the Shannon entropy of classical information theory to the quantum case, defined as

$$S_{VN} = -\text{Tr}(\hat{\rho} \log \hat{\rho}) = \sum_i \lambda_i |i\rangle \langle i|$$

where in the second equality we expressed the density matrix according to its spectral decomposition. The Von Neumann entropy quantifies the quantum and classical information content of a state, but it is also useful to quantify the entanglement of a bipartite pure state.

When we have a coherent superposition of states the effect of *quantum interference* appears, since we have a well-defined relative phase between the states, whose information is contained in the off-diagonal terms of the density matrix. Mixed states can be regarded as *incoherent superposition* of states: here the word “incoherent” refers to the fact that we miss the information of the relative phase between the states that constitute the statistical mixture.

1.3 Wigner functions

From the deterministic point of view of classical mechanics, a state of a system of N particles is described by a point $P = \{q^i, p^i\}$ in a $6N$ dimensional phase space. Statistical mechanics and the *ensemble* theory shift to a probabilistic point of view, associating to a specific macrostate of the system a set of microstates (representative points) and identifying a probability density function $\rho(q^i, p^i)$, such that $\rho(q^i, p^i) \prod_i dq^i dp^i$ is the probability for the representative point to be in the infinitesimal volume $\prod_i dq^i dp^i$. In such a classical formalism the average expectation value of a function is

$$\langle f \rangle = \int \prod_i dq^i dp^i \rho(q^i, p^i, t) f(q^i, p^i, t) \quad (1.26)$$

Since there is no uncertainty principle in classical physics, it is possible to know a particle’s momentum and position at the same time to an arbitrary precision. But we cannot find such a probability distribution in quantum mechanics, because of the Heisenberg principle. We work indeed with $P(q) = |\psi(q)|^2$ and $P(p) = |\psi(p)|^2$.

The *Wigner function* [27] fulfills, in a way, this need for a probability density for both position and momentum in a *quantum phase space*. To be precise, the Wigner function is a *quasiprobability distribution*: it differs from classical probability distributions, presenting counterintuitive behaviors such as the presence of negative regions, but it permits the calculations of expectation values and it has other classical-like features.

The Wigner function for a N -mode quantum state described by the density matrix $\hat{\rho}$ can be defined as

$$W(\mathbf{q}, \mathbf{p}) = \left(\frac{1}{2\pi}\right)^N \int d^N \mathbf{y} e^{i\mathbf{p}\cdot\mathbf{y}} \langle \mathbf{q} - \mathbf{y} | \hat{\rho} | \mathbf{q} - \mathbf{y} \rangle \quad (1.27)$$

where the integration is over the whole space of the integration variable.

1.3.1 Basic properties

We will proceed to enunciate some of the basic properties of the Wigner distributions, emphasizing its classical-like features and also its differences with a classical probability distribution. For simplicity, to have a better understanding of the concept and a lighter notation, we will work on the single-mode case, but the generalization to the multi-mode case is straightforward. A detailed treatise on the Wigner function can be found in [28].

Firstly, from Eq. (1.27) is easy to demonstrate that the Wigner function is real, i.e. $W^*(q, p) = W(q, p)$ for hermitian operators $\hat{\rho}$ and that, as $\text{Tr}\hat{\rho} = 1$, it's normalized, i.e.

$$\iint W(q, p)dqdp = 1$$

Moreover, the marginal distributions give rise to the correct probabilities for position and momentum, namely

$$\int W(q, p)dq = \langle q|\hat{\rho}|q\rangle$$

$$\int W(q, p)dp = \langle p|\hat{\rho}|p\rangle$$

These marginal distributions play an important role in quantum state tomography for the reconstruction of a quantum state [28]. We note that the Wigner function in Eq. (1.27) involves the density operator $\hat{\rho}$, but we can generalize it for any operator \hat{O} , which is not even required to be Hermitian, to obtain a Wigner function $W_O(q, p)$. The *overlap formula*

$$\text{Tr}(\hat{A}\hat{B}) = 4\pi \iint W_A(q, p)W_B(q, p)dqdp$$

is an useful property⁸ that permits us to calculate the mean values of an observable when $\hat{A} = \hat{\rho}$, indeed

$$\langle \hat{B} \rangle = \text{Tr}(\hat{\rho}\hat{B}) = 4\pi \iint W(q, p)W_B(q, p)dqdp$$

which reflects the classical rule to calculate expectation values in statistical mechanics of Eq. (1.26): the Wigner function of the state corresponds to the classical probability density $\rho(q^i, p^i, t)$ while the Wigner function of the operator $W_B(q, p)$ plays the role of the function over the phase space $f(q^i, p^i, t)$ representing the physical quantity we're interested in.

Up to this moment the Wigner function seems to behave like a classical probability distribution. A sign of non-classical behavior emerges by noting that the Wigner function of a state can have negative regions, as it's the case for a Fock state with $n > 0$, clearly not present in a classical probability distribution, which is always positive. Another quantum feature is a constraint on the values that a realistic Wigner function may take, namely

$$|W(q, p)| \leq \frac{1}{2\pi},$$

a property that has no classical analogue.

Finally, it's useful to give an idea on how Wigner function change when the system is subjected to a measurement. Imagine a case in which we have a system with two modes

⁸We remark that in a multimode generalization we have to add a factor of 2π for each integrated mode

and we chose to measure one of them. For a positive-operator valued measure (POVM)⁹

$$p(m)\hat{\rho}_{2,|m\rangle} = \text{Tr}_1(\hat{\rho}_{1,2}|m\rangle\langle m| \otimes \mathbb{1}) \quad (1.28)$$

where $p(m)$ is the probability of obtaining the output m , $\hat{\rho}_{1,2}$ is the state of the whole system before the measurement, $\hat{\rho}_{2,|m\rangle}$ is the state after system 1 has been measured and Tr_1 denotes a partial trace over system 1 In [29]. In the Wigner formalism this can be translated as

$$p(m)W_{out}(q_2, p_2) = 4\pi \iint dq_1 dp_1 W_{1,2} W_{POVM} \quad (1.29)$$

where $W_{1,2}$ and W_{out} represent, respectively, the Wigner functions of the system before and after the measurement on the second mode and W_{POVM} is the Wigner function of the POVM operator¹⁰.

1.3.2 Examples of Wigner functions

It will be useful to show the plots of the Wigner function of the states we will encounter during this dissertation. The explicit calculation can be found in [28].

For a Fock state $|n\rangle$ with a given number of photons, the Wigner function reads

$$W_{|n\rangle} = \frac{(-1)^n}{2\pi} e^{-\frac{q^2}{2} - \frac{p^2}{2}} L_n(q^2 + p^2)$$

where $L_n(x)$ is the n-th Laguerre polynomial. The plots are shown in Fig 1.4 for some values of n and some of them clearly exhibit regions where the Wigner function takes negative values, behaving as a non-classical probability distribution. The Wigner function for the vacuum state $|0\rangle$ is a Gaussian function, as it can be seen from Fig. 1.4a.

We expect to obtain the Wigner function of a coherent state simply by displacing the Wigner function of the vacuum by the complex amplitude $2\alpha = (q_0 + ip_0)$ in the optical phase space. Indeed, displacing the vacuum state with the displacement operator defined in Eq. (1.16) results in the following expression for the Wigner function of a coherent state, depicted in Fig. 1.5:

$$W_{|\alpha\rangle} = \frac{1}{2\pi} e^{-\frac{(q-q_0)^2}{2} - \frac{(p-p_0)^2}{2}}$$

⁹A POVM is the complete set of operators $\{E_m\}_m$. The element E_m is defined as $E_m \equiv M_m^\dagger M_m$, where M_m is a measurement operator acting on a state $|\Psi\rangle$ such that the probability of outcome m is given by $p(m) = \langle\Psi|M_m^\dagger M_m|\Psi\rangle$

¹⁰For example, if we imagine to measure the momentum m of the first mode via a POVM $\Pi_m = |m\rangle\langle m|$, we get that $W_{POVM} \propto \delta(p_1 - m)$

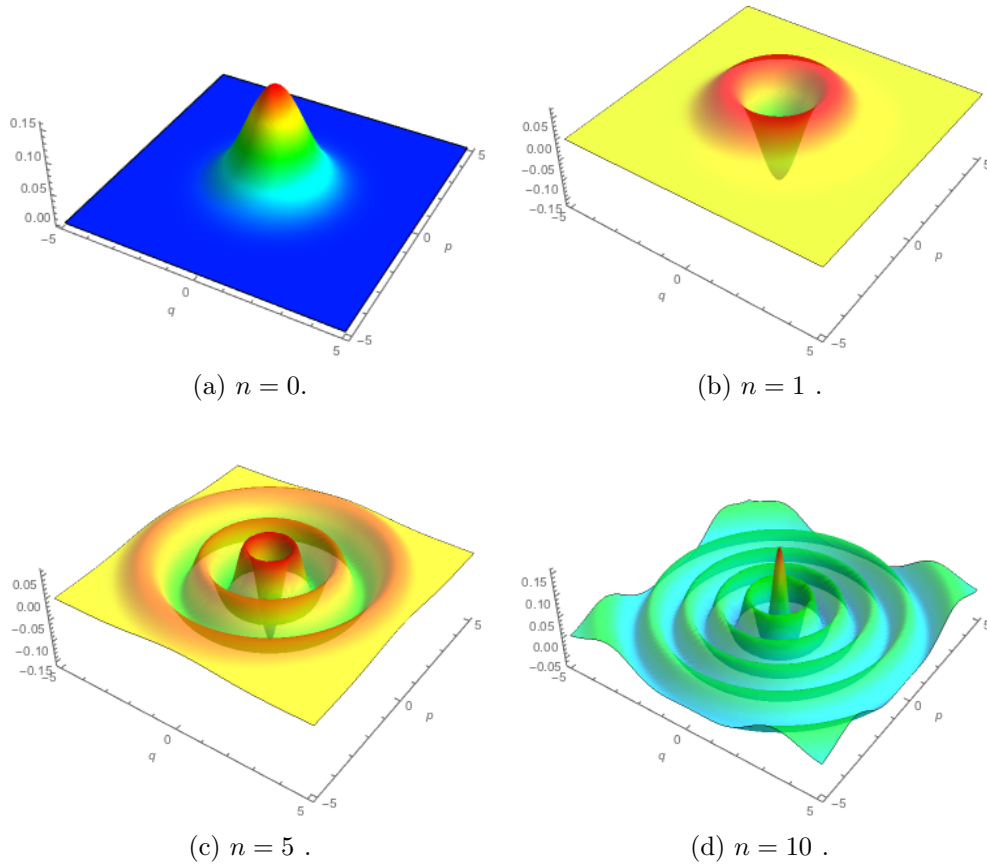


Figure 1.4: Wigner functions of Fock states states with different number of photons n . Note that (b), (c) and (d) exhibits negative regions.

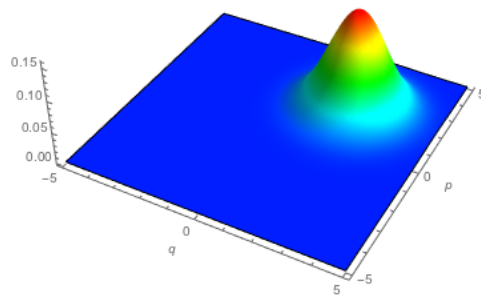


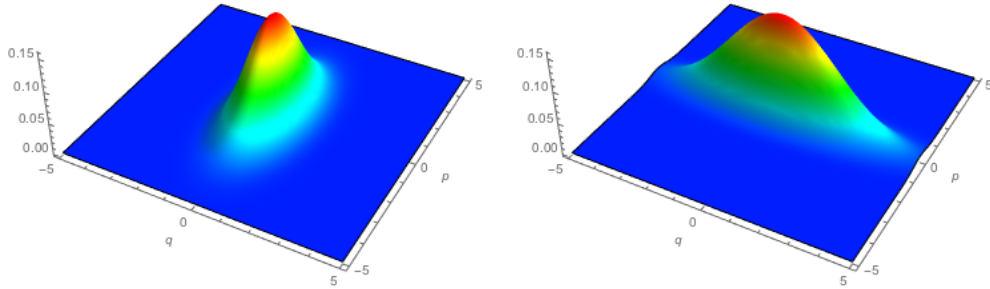
Figure 1.5: Wigner function of the coherent state $|\alpha\rangle$, with $q_0 = p_0 = 2$

Lastly, to obtain the Wigner function of a squeezed vacuum state we will act on the vacuum state with the squeezing operator defined in Eq. (1.19). The Wigner function

for the squeezed vacuum reads

$$W_{|r\rangle} = \frac{1}{2\pi} e^{-\frac{q^2}{2s} - \frac{sp^2}{2}} \quad (1.30)$$

where we recall that $s = e^{2r}$, and it is depicted in Fig 1.6.



(a) -3 dB of squeezing in the q quadrature. (b) -6 dB of squeezing in the p quadrature

Figure 1.6: Wigner functions of squeezed-vacuum states exhibiting different amounts of squeezing, respectively in the q quadrature and in the p quadrature. The corresponding contour plots are depicted in Fig 1.3

1.4 Gaussian states and Gaussian unitaries

There is a particular class of states that plays a central role in quantum optics, that includes some of the most common states described in Section 1.2, such as the vacuum state, coherent states and squeezed states: the class of *Gaussian states*. Even if they are subjected to many limitations, they are an essential resource for Quantum Information Processing in CV.

1.4.1 Gaussian states

A Gaussian state by definition is a state whose Wigner function is a normalized Gaussian distribution that can be written as

$$W(\boldsymbol{\xi}) = \frac{1}{(2\pi)^N \sqrt{\det \sigma}} \exp \left[-\frac{1}{2} (\boldsymbol{\xi} - \bar{\boldsymbol{\xi}})^T \sigma^{-1} (\boldsymbol{\xi} - \bar{\boldsymbol{\xi}}) \right] \quad (1.31)$$

where $\boldsymbol{\xi}^T = (q_1, \dots, q_N, p_1, \dots, p_N)$. With $\bar{\boldsymbol{\xi}}$ we denote the first statistical moment of the state, or mean value, which is defined as

$$\bar{\boldsymbol{\xi}} = \langle \hat{\boldsymbol{\xi}} \rangle = \text{Tr}(\hat{\boldsymbol{\xi}} \hat{\rho})$$

while σ is the second statistical moment, the covariance matrix, whose elements are defined as

$$\sigma_{ij} = \frac{1}{2} \langle \hat{\xi}_i \hat{\xi}_j + \hat{\xi}_j \hat{\xi}_i \rangle - \langle \hat{\xi}_i \rangle \langle \hat{\xi}_j \rangle \quad (1.32)$$

and characterize a matrix which is real, symmetric and positive definite. In the case of a Gaussian state the mean value and the covariance matrix are sufficient to completely describe the state.

1.4.2 Gaussian Unitaries

According to quantum mechanics, a closed quantum system dynamics is described by a unitary operator \hat{U} acting on a state. When we deal with an open system, i.e. a system which is coupled to an environment, we allow a more general class of transformations acting on it.

In the general case, a quantum operation is a completely positive linear map that acts on an input state $\hat{\rho}$

$$\mathcal{E}: \hat{\rho} \rightarrow \hat{\rho}'$$

In general, \mathcal{E} is a trace-decreasing map, i.e. $0 \leq \text{Tr}[\mathcal{E}(\hat{\rho})] \leq 1$. This includes also measurements, which are examples of non-trace-preserving maps. A trace preserving map is called a *quantum channel* and it is reversible if and only if it's unitary, so that

$$\hat{\rho} \rightarrow \hat{U} \hat{\rho} \hat{U}^\dagger$$

holds [29, 30]. A Gaussian unitary is defined as a Gaussian reversible quantum channel, that transforms Gaussian states into Gaussian states. We will restrict ourselves to these transformations, avoiding non-Gaussian operations.

Gaussian unitaries are operators of the form $\hat{U} = e^{-i\hat{H}}$ where \hat{H} is at most quadratic in the mode operators, namely

$$\hat{H} = \sum_{ij} A_{ij} \hat{a}_i^\dagger \hat{a}_j + B_{ij} \hat{a}_i^\dagger \hat{a}_j^\dagger + \gamma_i \hat{a}_i^\dagger + \text{h.c.}$$

In the Heisenberg picture this translates to a *linear unitary Bogoliubov transformation* of the creation and annihilation operators

$$\begin{aligned} \hat{a}_k &\rightarrow \hat{U}^\dagger \hat{a}_k \hat{U} = \sum_j \alpha_{jk} \hat{a}_j + \beta_{jk} \hat{a}_j^\dagger + \gamma_k \\ \hat{a}_k^\dagger &\rightarrow \hat{U}^\dagger \hat{a}_k^\dagger \hat{U} = \sum_j \alpha_{jk}^* \hat{a}_j^\dagger + \beta_{jk}^* \hat{a}_j + \gamma_k^* \end{aligned} \quad (1.33)$$

or in matrix form

$$\hat{U} \begin{pmatrix} \hat{\mathbf{a}} \\ \hat{\mathbf{a}}^\dagger \end{pmatrix} \hat{U}^\dagger = \begin{pmatrix} \alpha & \beta \\ \beta^* & \alpha^* \end{pmatrix} \begin{pmatrix} \hat{\mathbf{a}} \\ \hat{\mathbf{a}}^\dagger \end{pmatrix} + \begin{pmatrix} \gamma \\ \gamma^* \end{pmatrix} \quad (1.34)$$

where, due to the unitarity of the transformation, and thus to the need to preserve the commutation relations, the matrices α and β are $N \times N$ matrices that satisfy $\alpha \alpha^\dagger =$

$\beta\beta^\dagger + \mathbb{1}$ and $\alpha\beta^T = \beta\alpha^T$, which are the defining relations of the complex form of the group $\text{Sp}(2N, \mathbb{R})$, that we will briefly illustrate in the next section. We can write more compactly Eq. (1.34) as

$$\hat{U}\hat{\xi}^{(c)}\hat{U}^\dagger = S^{(c)}\hat{\xi}^{(c)} + \mathbf{d}^{(c)} \quad (1.35)$$

where $\hat{\xi}^{(c)} = (\hat{\mathbf{a}}, \hat{\mathbf{a}}^\dagger)^T$. On the quadrature operators this transformation translates to

$$\hat{U}\hat{\xi}\hat{U}^\dagger = S\hat{\xi} + \mathbf{d} \quad (1.36)$$

where $\hat{\xi} = (\hat{q}_1, \dots, \hat{q}_N, \hat{p}_1, \dots, \hat{p}_N)^T$, $\mathbf{d} \in \mathbb{R}^{2N}$ and $S \in \text{Sp}(2N, \mathbb{R})$. We will see in the next subsection how the various terms of Eqs. (1.35) and (1.36) are related.

It is convenient to translate the action of this unitary transformation on the Hilbert space to a transformation acting on the quantum phase space, whose characteristic quantities are the statistical moments. For a Gaussian unitary

$$\begin{aligned} \bar{\xi} &\rightarrow S\bar{\xi} + \mathbf{d} \\ \sigma &\rightarrow S\sigma S^T \end{aligned}$$

holds. Under a symplectic transformation the Wigner function transforms as

$$W(\xi) \rightarrow W'(\xi) = W(S^{-1}(\xi - \mathbf{d})) \quad (1.37)$$

During this dissertation we will mainly neglect the displacement term \mathbf{d} , as we will deal with states with $\mathbf{d} = 0$.

1.4.3 The real symplectic group in quantum optics

The real symplectic group is defined as

$$\text{Sp}(2N, \mathbb{R}) = \{S \text{ real } 2N \times 2N \text{ matrix} \mid S\beta S^T = \beta\}, \quad (1.38)$$

where β is a fixed $2N \times 2N$ non singular, skew-symmetric matrix, a typical choice being

$$\beta = \begin{pmatrix} 0 & \mathbb{1} \\ -\mathbb{1} & 0 \end{pmatrix}.$$

The importance of this group in quantum mechanics lies on the fact that a linear transformation L acting on the vector $\hat{\xi}$ of position and momentum operators preserves the canonical commutation relations if and only if $L \in \text{Sp}(2N, \mathbb{R})$ ¹¹. An extensive description of the relevant properties of this group that emphasizes its role in the fields of quantum optics and quantum mechanics can be found in [31].

From the definition (1.38) many interesting properties arise, as

- 1) $\text{Sp}(2N, \mathbb{R})$ has dimension $N(2N + 1)$

¹¹This holds even for a classical system where the transformation L acts on the canonical variables of the phase space and Poisson brackets are preserved

- 2) $\beta \in \text{Sp}(2N, \mathbb{R})$
 3) $S \in \text{Sp}(2N, \mathbb{R}) \implies \det S = +1$
 4) $S \in \text{Sp}(2N, \mathbb{R}) \implies S^{-1}, S^T \in \text{Sp}(2N, \mathbb{R})$

and if we write S in block-form as

$$S = \begin{pmatrix} A & B \\ C & D \end{pmatrix} \quad (1.39)$$

the definition (1.38) requires

$$\begin{aligned} AB^T, CD^T &\text{ symmetric} \\ AD^T - BC^T &= \mathbb{1} \end{aligned} \quad (1.40)$$

to be satisfied, where A, B, C, D are $N \times N$ matrices¹².

If instead of working with the quadratures \hat{q} and \hat{p} of the field we wish to work with the creation and annihilation operators, we can define S the *complex form* of the real symplectic transformation S , that will act on the vector $\hat{\xi}^{(c)} = (\hat{a}_1, \dots, \hat{a}_N, \hat{a}_1^\dagger, \dots, \hat{a}_N^\dagger)^T$ instead of the quadrature vector $\hat{\xi}$, the two being related by the relation $\hat{\xi}^{(c)} = \Omega \hat{\xi}$, where

$$\Omega = \begin{pmatrix} \mathbb{1}_n & i\mathbb{1}_n \\ \mathbb{1}_n & -i\mathbb{1}_n \end{pmatrix}, \quad \Omega^{-1} = \Omega^\dagger = \begin{pmatrix} \mathbb{1}_n & i\mathbb{1}_n \\ -\mathbb{1}_n & i\mathbb{1}_n \end{pmatrix}$$

trivially from the relations (1.8) and (1.9). Then, the action of S on $\hat{\xi}$ is translated in a transformation $S^{(c)}$ on $\hat{\xi}^{(c)}$ that reads

$$S^{(c)} = \Omega S \Omega^{-1} \quad (1.41)$$

The unitary subgroup We will introduce a subgroup of $\text{Sp}(2N, \mathbb{R})$ that play a central role in quantum optics and that we will often encounter in the next chapters: the *unitary subgroup*, denoted by $K(N)$, of dimension N^2 . If we decompose a unitary matrix U into its real and imaginary parts as $U = X + iY$, we find that the condition for unitarity ($UU^\dagger = U^\dagger U = \mathbb{1}$) translates on the matrices X and Y as $XX^T + YY^T = \mathbb{1}$ and $XY^T = YX^T$. These conditions correspond to the conditions (1.40) with $A = D = X$ and $C = -B = Y$, such that the block-form symplectic matrix of Eq. (1.39) can be rewritten as

$$S = \begin{pmatrix} X & -Y \\ Y & X \end{pmatrix} \quad (1.42)$$

that may be recast in its complex form using Eq. (1.41) to get

$$S^{(c)} = \begin{pmatrix} U & 0 \\ 0 & U^* \end{pmatrix}$$

¹²An equivalent condition requires $A^T C$ and $B^T D$ to be symmetric and $A^T D - C^T B = \mathbb{1}$ to hold

Comparing with Eq. (1.35) we realize that the symplectic transformation $S \in K(N)$ does not mix the creation and annihilation operators with one another, resulting in $\hat{a}_k \rightarrow \sum_j U_{jk} \hat{a}_k$ and $\hat{a}_k^\dagger \rightarrow \sum_j U_{jk}^* \hat{a}_k^\dagger$. These transformations correspond to *linear optical devices*, such as beam splitters and phase shifters¹³.

It's worth to notice that

$$K(N) = \text{Sp}(2N, \mathbb{R}) \cap \text{SO}(2N, \mathbb{R})$$

where $\text{SO}(2N, \mathbb{R})$ is the special orthogonal group of $2N \times 2N$ matrices. Since a symplectic transformation $S \in K(N)$ is also orthogonal, it preserves the trace of the covariance matrix σ , i.e. the mean energy of the system¹⁴, and for this reason we may refer to them as *passive* transformations, as opposed to *active* transformations such as squeezing operations that do not preserve the energy of the system.

Bloch-Messiah decomposition Any element $S \in \text{Sp}(2N, \mathbb{R})$ can be decomposed in several ways. In this section we will describe the *Bloch-Messiah decomposition* (also known as *Euler decomposition*), whereby a symplectic transformation can be decomposed into the product of three factors, namely

$$S = S(X_1, Y_1) D(\mathbf{k}) S(X_2, Y_2)$$

where $S(X_1, Y_1)$ and $S(X_2, Y_2)$ belong to the subgroup $K(n) \subset \text{Sp}(2N, \mathbb{R})$ and $D(\mathbf{k})$ is a diagonal positive-definite matrix such that $D(\mathbf{k}) = \text{diag}(k_1, \dots, k_N, k_1^{-1}, \dots, k_N^{-1})$ [31].

A physical interpretation of the Bloch-Messiah decomposition in a quantum optical framework follows. We saw in Section 1.4.3 how elements of the subgroup $K(N)$ of the real symplectic group are implemented by linear optical devices, while $D(\mathbf{k})$ may be identified as a squeezing transformation if we set $k_i = e^{r_i}$ as we may see by recalling Eq. (1.24). We can draw the following remarkable conclusion: any Gaussian unitary can be decomposed into a multiport linear interferometer, followed by a set of single-mode squeezers and by another multiport linear interferometer [33].

1.4.4 Homodyne detection

Homodyne detection is an essential part in a quantum optics experiment, as it permits us to measure the quadratures of the electric field, which is a crucial point if we are working in a CV framework. In particular, in this Section we will describe the procedure for *balanced* homodyne detection, whose scheme is depicted in Fig. 1.7, in the single-mode case for simplicity.

The *balanced* homodyne detector employs a 50:50 beam splitter and two photon detectors in both output arms. In one input port we have the field that we want to

¹³Some confusion may arise when we talk about *linear transformations* in quantum optics. Eqs. (1.33) are mathematically linear, but usually when in quantum optics we talk about *linear (optical) transformations* we refer to those transformations generated by linear optical devices. Squeezing is excluded, being generated by non-linear dielectric media [32]

¹⁴The mean energy of the system is proportional to the mean number of photons $\langle n \rangle = \frac{1}{m} \sum_k \langle \hat{a}_k^\dagger \hat{a}_k \rangle = \text{Tr} \sigma / m - 1$, with m number of modes.

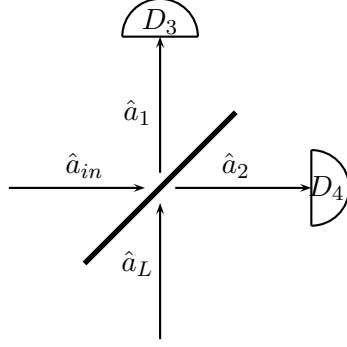


Figure 1.7: Scheme for balanced homodyne detection. D_1 and D_4 represent photon detectors.

measure while in the other we have a strong coherent light beam, the *local oscillator*, which is characterized by a negligible deviation from the mean value, namely $\delta a_L = \hat{a}_L - \langle \hat{a}_L \rangle \ll \langle \hat{a}_L \rangle$, where $\langle \hat{a}_L \rangle = \langle \alpha | \hat{a}_L | \alpha \rangle = |\alpha_L| e^{i\theta}$. The balanced homodyne detection measures the difference between the number of photons detected in the two output ports, $\hat{n}_4 - \hat{n}_3$, that will permit us to get information about the quadratures of the field. Being the beam splitter a Gaussian unitary, its action on the creation and annihilation operators is carried out by a symplectic transformation, as in Eq. (1.35), whose complex form $S^{(c)}$ is given by

$$S_{BS}^{(c)} = \frac{1}{\sqrt{2}} \begin{pmatrix} 1 & -1 \\ 1 & 1 \end{pmatrix}$$

and the output operators thus read

$$\hat{a}_1 = \frac{\hat{a}_{in} - \hat{a}_L}{\sqrt{2}}, \quad \hat{a}_2 = \frac{\hat{a}_{in} + \hat{a}_L}{\sqrt{2}}$$

The difference between the number of photons detected in the two output ports reads

$$\hat{n}_2 - \hat{n}_1 = \hat{a}_2^\dagger \hat{a}_2 - \hat{a}_1^\dagger \hat{a}_1 = \hat{a}_{in}^\dagger \hat{a}_L + \hat{a}_L^\dagger \hat{a}_{in}$$

and since we assumed that the quantum fluctuations of the local oscillator were negligible we can replace \hat{a}_L with its mean value and obtain

$$\hat{n}_2 - \hat{n}_1 = |\alpha_L| (\hat{a}_{in}^\dagger e^{i\theta} + \hat{a}_{in} e^{-i\theta}) = |\alpha_L| \hat{q}_{in}^\theta$$

where the last equality is obtained by remembering the definition of the rotated quadratures given in Eqs. (1.23) and (1.22). With balanced homodyne detection we can thus measure the quadrature \hat{q}^θ , where the angle θ is the phase of the local oscillator and can be adjusted experimentally.

Chapter 2

CV quantum information

Nowadays, we follow mostly two different approaches for the encoding of quantum information: one exploits discrete variables (DV), mainly belonging to a two dimensional space (qubits)¹ [29, 30], while the other one is a continuous variables (CV) approach that employs variables with a continuous spectrum of values (qumodes) [10]. During this section we will recall the basics of DV information theory and we will establish the correspondence with CV information theory.

2.1 From DV quantum Information to CV quantum information

A *qubit* is a quantum state belonging to a two-dimensional Hilbert space that can be defined as

$$|\psi\rangle = \cos \frac{\theta}{2} |0\rangle + e^{i\phi} \sin \frac{\theta}{2} |1\rangle$$

where $(\theta, \phi) \in \mathbb{R}^2$ and where we can identify the two basis vectors $\{|0\rangle, |1\rangle\}$ as the *computational basis* of the space, that can be written in matrix notation as

$$|0\rangle = \begin{pmatrix} 0 \\ 1 \end{pmatrix}, \quad |1\rangle = \begin{pmatrix} 1 \\ 0 \end{pmatrix}$$

Such a state can be represented in the so-called *Bloch sphere*, depicted in Figure 2.1, where the north and south pole are identified with the computational basis states $|0\rangle$ and $|1\rangle$ respectively and where opposite points on the Bloch Sphere correspond to orthogonal states.

¹We mention that the qubits approach is not the only approach on discrete variables, as we may use a d -dimensional space (qudits)

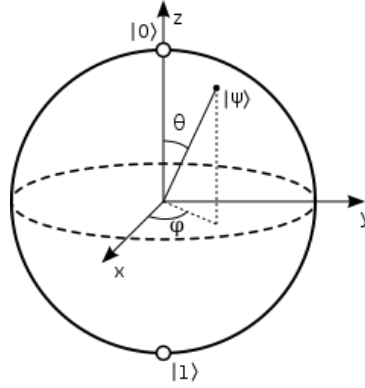


Figure 2.1: Bloch sphere

We can alternatively define the *conjugate basis* $\{|+\rangle, |-\rangle\}$, where

$$\begin{aligned} |+\rangle &= \frac{1}{\sqrt{2}}(|0\rangle + |1\rangle) \\ |-\rangle &= \frac{1}{\sqrt{2}}(|0\rangle - |1\rangle) \end{aligned} \quad (2.1)$$

We call *quantum gate* a linear unitary transformation on a quantum state. In the DV formalism a single-qubit quantum gate corresponds to a rotation in the Bloch Sphere multiplied for a phase and it can be represented by a 2×2 matrix. For example the Hadamard gate is defined as

$$H = \frac{1}{\sqrt{2}} \begin{pmatrix} 1 & 1 \\ 1 & -1 \end{pmatrix}$$

We note that the Hadamard gate maps the computational basis in the conjugate basis and viceversa.

Qubits can be implemented in various ways, with different physical supports. For example we may encode a qubit of quantum information in the spin of an electron or of a nucleus. Optical implementation of the qubit consider different implementation for the qubit degree of freedom, such as photon number, polarization and orbital angular momentum (OAM) states of the photon [34].

In continuous variables the qubit is replaced by a *qumode* and the analogue of the computational basis vectors are the orthogonal states $|s\rangle_q$, such that $\hat{q}|s\rangle_q = s|s\rangle_q$ ², while the conjugate basis is given by $|s\rangle_p$, which satisfies $\hat{p}|s\rangle_p = s|s\rangle_p$. The two basis are complete and normalized such that

$$\begin{aligned} \int_{-\infty}^{+\infty} ds |s\rangle_q \langle s|_q &= \int_{-\infty}^{+\infty} ds |s\rangle_p \langle s|_p = \mathbb{1} \\ {}_p \langle s|r \rangle_p &= {}_q \langle s|r \rangle_q = \delta(r - s) \end{aligned}$$

²This notation is different from the usual one where $\hat{q}|q\rangle = s|q\rangle$ and it will allow us to write the equations in a more compact form

and the basis change is given by

$$|s\rangle_p = \int_{-\infty}^{+\infty} dr |r\rangle_q \langle r|s\rangle_p = \frac{1}{\sqrt{2\pi}} \int_{-\infty}^{+\infty} dr e^{irs} |r\rangle_q$$

In this notation we may write

$$\hat{F} |s\rangle_q = |s\rangle_p$$

where $\hat{F} = \int dr |r\rangle_p \langle r|$. We also have that $\hat{F}^\dagger |s\rangle_p = |s\rangle_q$. Moreover, from the fact that ${}_p\langle s|r\rangle_q = {}_q\langle r|-s\rangle_p$, we may conclude that $F^\dagger |s\rangle_q = |-s\rangle_p$ (and $F |s\rangle_p = |-s\rangle_q$). The unitary operator \hat{F} is the analogous of the Hadamard gate in the DV formalism, as it is used to map the position basis into the momentum basis and viceversa.

During the present dissertation we will use mainly the CV formalism, identifying our CV variables as the quadratures of the electromagnetic field.

2.2 Entanglement and the EPR state

Entanglement is a fascinating quantum phenomenon with no classical analogue that has been and is intensively studied by physicists all over the world and gives rise to many interesting applications, such as quantum teleportation and quantum computation. During our studies as physicists, we usually get familiar with entanglement in the DV formalism, in the form of the Bell states, for example

$$|\phi^+\rangle = \frac{1}{\sqrt{2}}(|00\rangle + |11\rangle)$$

However, historically, the concept of quantum entanglement was introduced in continuous variables in the so-called ‘‘EPR paper’’ by Einstein, Podolsky and Rosen [1], who presented a CV entangled state known as *EPR state*. In this section we will introduce the concept of CV entanglement.

2.2.1 The EPR paradox

With the paper ‘‘Can Quantum-Mechanical Description of Physical Reality Be Considered Complete?’’, Einstein, Podolsky and Rosen questioned the completeness of quantum mechanics, under the assumption of the validity of *local realism*. Local realism is the combination of the principle of locality, that forbids any instantaneous ‘‘action at a distance’’, and the principle of realism, that is formulated in the EPR in the following way:

If, without in any way disturbing a system, we can predict with certainty the value of a physical quantity, then there exist an element of physical reality corresponding to this quantity.

To show the inconsistency between local realism and quantum mechanics, Einstein, Podolsky and Rosen presented a system of two distant particles characterized by the following unnormalized wavefunction in the position representation

$$\psi(q_1, q_2) = \delta(q_1 - q_2 - q_0)$$

In the momentum representation the same state reads

$$\tilde{\psi}(p_1, p_2) = \delta(p_1 + p_2)$$

Measuring the position observable \hat{q}_1 of the first particle, it can be predicted with certainty that a measurement of the position of the second particle will give $q_1 + q_0$ as a result. Equivalently, measuring \hat{p}_1 will lead to the value $-p_1$ for the momentum of the second particle. Since these values are predicted “without disturbing the system” we conclude that both the position and the momentum of the second particle, that correspond to two non-commuting observables, are elements of physical reality. Assuming local realism, we are obliged to conclude that the measurement outcomes are deterministic, and they appear probabilistic because due to lack of knowledge of some degrees of freedom. *Local hidden variable theories* were formulated to make the features of the EPR pair consistent with local realism.

John Bell in 1964 [2] mathematically demonstrated that local realism leads to the celebrated Bell’s inequality that is violated by the quantum-mechanical predictions for an EPR experiment involving several measurement settings. The violation of Bell’s inequality means that the correlations among the two particles of the EPR pair cannot be regarded as classical correlations and the two particles cannot be thought as separated particles: they are *entangled* [4, 35].

2.2.2 Bipartite entanglement

Bipartite entanglement, i.e. the entanglement shared by two systems, is the first type of entanglement that has been investigated and it’s relatively easy to characterize for pure states. A pure state $|\psi\rangle \in \mathcal{H}_A \otimes \mathcal{H}_B$ is called *separable* if it can be expressed as the direct product of pure states belonging to \mathcal{H}_A and \mathcal{H}_B , i.e. as

$$|\psi\rangle = |\phi\rangle_A \otimes |\chi\rangle_B \quad (2.2)$$

otherwise it’s *entangled*. If we are provided with a separable state of the form (2.2) and we compute the reduced density operator for a subsystem, performing a partial trace of the density operator of the combined system over the other subsystem, we obtain density operator of pure states, $\hat{\rho}_A = |\phi\rangle \langle\phi|$ and $\hat{\rho}_B = |\chi\rangle \langle\chi|$ respectively for systems A and B . This is no longer true when the state $|\psi\rangle$ is an entangled state. To show this it is useful to introduce the *Schmidt decomposition*, according to which a bipartite pure state can be expressed in the form

$$|\psi\rangle_{AB} = \sum_i |u_i\rangle_A |v_i\rangle_B \quad (2.3)$$

where $\{u_i\}_{i \in \mathbb{N}}$ and $\{v_i\}_{i \in \mathbb{N}}$ are respectively two orthonormal basis of \mathcal{H}_A and \mathcal{H}_B and c_i are real and non negative numbers such that $\sum_i c_i = 1$. We define the *Schmidt number* as the number of terms in the Schmidt decomposition (2.3) and recalling Eq. (2.2) it is evident that a separable state has a Schmidt number equal to one, while an entangled state has a Schmidt number greater than one.

A state of two d-dimensional systems is *maximally entangled* when all its Schmidt coefficients are non-zero and equal, i.e.

$$|\psi\rangle_{AB} = \frac{1}{\sqrt{d}} \sum_{i=1}^d |u_i\rangle_A |v_i\rangle_B$$

Performing a partial trace on one of the two subsystems, leaves the other in a maximally mixed state. As an example, we may trace out system B, and the reduced density operator for system A reads

$$\hat{\rho}_A = \text{Tr}_B (|\psi\rangle \langle \psi|) = \frac{1}{d} \mathbb{1}$$

Entanglement destroys the coherence of the individual subsystem. This means we cannot observe quantum interference locally, only measuring the subsystem A, and the quantum effects are transferred to the system as a whole [30].

It's important to identify a criterion to establish if a CV system is entangled or not. It can be shown [36] that in the infinite dimensional limit, the violation of a lower bound, determined by the uncertainty relation, is a sufficient condition for the inseparability of the state. Considering the EPR operators $\hat{q}_1 - \hat{q}_2$ and $\hat{p}_1 + \hat{p}_2$, for any separable CV quantum state the following inequality holds

$$\Delta^2(q_1 - q_2) + \Delta^2(p_1 + p_2) \geq 4$$

A state that violates this condition is an entangled state.

2.2.3 Bipartite entanglement: the two-mode squeezed vacuum

The EPR state described in Section 2.2.1 can be approximated by a *two-mode squeezed vacuum state*, of which the EPR state constitutes a limiting case [37]. The two-mode squeezed vacuum state (TMSV) is generated by acting on the vacuum with the two-mode squeezing operator

$$\hat{S}_2(\zeta) = \exp \left[-\zeta \hat{a}_1 \hat{a}_2 + \zeta^* \hat{a}_1^\dagger \hat{a}_2^\dagger \right]$$

where $\zeta = r e^{2i\theta}$. Assuming $\theta = 0$ for simplicity and recalling that the creation and annihilation operators for different modes of the field commute, we find that the corresponding transformation of the annihilation operators in the Heisenberg picture is

$$\begin{aligned} \hat{a}_1(r) &= \hat{a}_1^{(0)} \cosh r + \hat{a}_2^{(0)\dagger} \sinh r \\ \hat{a}_2(r) &= \hat{a}_2^{(0)} \cosh r + \hat{a}_1^{(0)\dagger} \sinh r \end{aligned}$$

where the superscript “0” denotes vacuum modes. The two-mode vacuum state generated by the action of the operator $\hat{S}_2(\zeta)$ on the vacuum, can be physically implemented by a non-degenerate parametric down conversion process [38]. Equivalently, it can be realized by using single-mode squeezed states and combining them by linear optics, as shown in Fig. 2.2 [10].

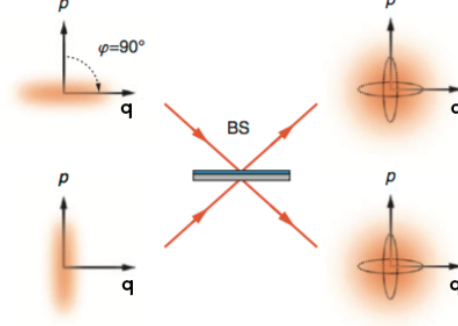


Figure 2.2: Generation of a two-mode squeezed state by sending two single-mode squeezed states into the input ports of a 50:50 beam splitter.

We start from two single-mode squeezed states, one squeezed in the momentum quadrature and the other one squeezed in the position quadrature and we mix them with a 50:50 beam splitter, whose transformation in the quadrature representation is given by

$$S_{BS} = \begin{pmatrix} \frac{1}{\sqrt{2}} & \frac{1}{\sqrt{2}} & 0 & 0 \\ \frac{1}{\sqrt{2}} & -\frac{1}{\sqrt{2}} & 0 & 0 \\ 0 & 0 & \frac{1}{\sqrt{2}} & \frac{1}{\sqrt{2}} \\ 0 & 0 & \frac{1}{\sqrt{2}} & -\frac{1}{\sqrt{2}} \end{pmatrix}$$

The quadratures of the resulting state are $\hat{\xi}_{out} = S_{BS}\hat{\xi}_{in}$, where $\hat{\xi}_{out} = (\hat{q}_1, \hat{q}_2, \hat{p}_1, \hat{p}_2)^T$ and $\hat{\xi}_{in} = (\hat{q}_1^s, \hat{q}_2^s, \hat{p}_1^s, \hat{p}_2^s)^T$, where with the superscript “s” we denote the quadrature of a squeezed state and by recalling Eq. (1.24) we get

$$\begin{aligned} \hat{q}_1 &= (e^{+r}\hat{q}_1^{(0)} + e^{-r}\hat{q}_2^{(0)})/\sqrt{2} \\ \hat{q}_2 &= (e^{+r}\hat{q}_1^{(0)} - e^{-r}\hat{q}_2^{(0)})/\sqrt{2} \\ \hat{p}_1 &= (e^{-r}\hat{p}_1^{(0)} + e^{+r}\hat{p}_2^{(0)})/\sqrt{2} \\ \hat{p}_2 &= (e^{-r}\hat{p}_1^{(0)} - e^{+r}\hat{p}_2^{(0)})/\sqrt{2} \end{aligned} \tag{2.4}$$

While the factor e^r pushes the variances of the single quadratures to infinity as r increases, we note that

$$\begin{aligned} \hat{q}_1 - \hat{q}_2 &= \sqrt{2}e^{-r}\hat{q}_2^{(0)} \\ \hat{p}_1 + \hat{p}_2 &= \sqrt{2}e^{-r}\hat{p}_1^{(0)} \end{aligned}$$

such that

$$\Delta^2(\hat{q}_1 - \hat{q}_2) = 2e^{-2r} \Delta^2 \hat{q}_2^{(0)} = 2e^{-2r} \quad (2.5)$$

$$\Delta^2(\hat{p}_1 + \hat{p}_2) = 2e^{-2r} \Delta^2 \hat{p}_1^{(0)} = 2e^{-2r} \quad (2.6)$$

i.e. as $r \rightarrow \infty$ the noise of the relative position and of the sum of the momenta decreases and we retrieve the behavior of an ideal EPR state.

A more general description of the state is given by the Wigner function. As the state is a Gaussian state, the Wigner function is derived from the covariance matrix as shown in Eq. (1.31). From Eqs. (2.5) and (2.6) and calculating as well $\Delta^2(\hat{q}_1 + \hat{q}_2) = \Delta^2(\hat{p}_1 - \hat{p}_2) = 2e^{2r}$ we are able to write the Wigner function for the two-mode squeezed vacuum as

$$W_{EPR}(q, p) = \frac{1}{4\pi^2} \exp \left\{ -\frac{[(q_1 + q_2)^2 + (p_1 - p_2)^2]}{4e^{2r}} - \frac{[(q_1 - q_2)^2 + (p_1 + p_2)^2]}{4e^{-2r}} \right\} \quad (2.7)$$

which is plotted in Figure 2.3. It can be shown that the TMSV state exhibit correlations

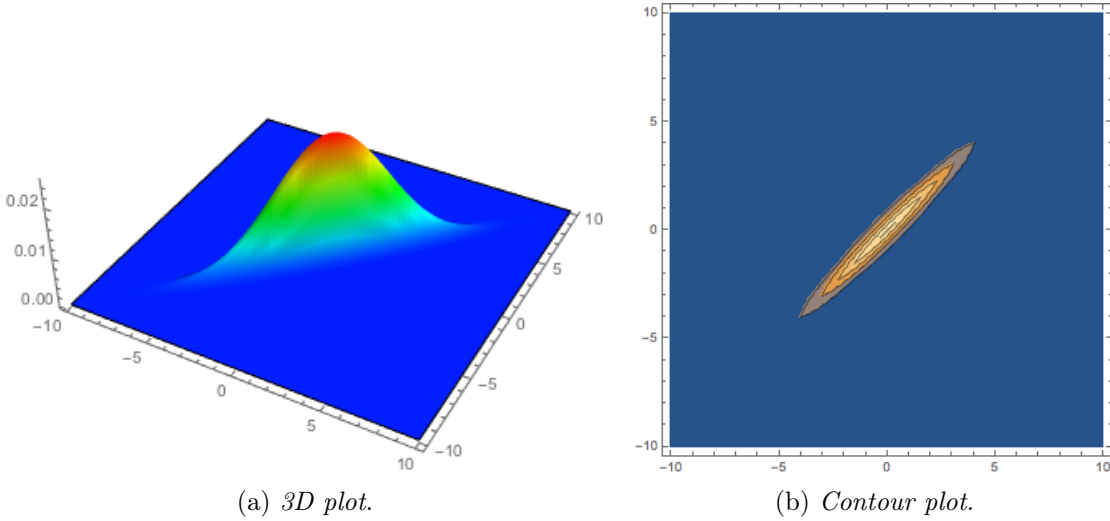


Figure 2.3: Plot of the section $p_1 = p_2 = 0$ of the Wigner function for the EPR state for the squeezing values $\{-10, +10\}$ dB which shows the correlation of the quadratures q_1 and q_2 .

not only in position and momentum, but also in photon number. Indeed, in the Fock basis, the TMSV is written as³

$$\hat{S}_2(r) |00\rangle = \frac{1}{\cosh r} \sum_{n=0}^{\infty} (\tanh r)^n |n\rangle |n\rangle$$

³To obtain this result we use the disentangling theorem for $SU(1,1)$ Lie Algebra [39]

which shows that the TMSV state can be written as a superposition of states with the same photon number [40].

2.3 Quantum teleportation

Entangled states are a useful resource for quantum communication, that allows us to exceed the limits of the classical world. Via *quantum teleportation* we are able to send a quantum state by using two bits of classical information (sent using a classical channel) and a quantum channel (an EPR state). Quantum teleportation has been proposed and realized in DV [41–43] and then translated and implemented in the CV regime [44, 45]. In this section we will concentrate on quantum teleportation with continuous variables.

2.3.1 Quantum teleportation in the Heisenberg representation

Suppose that Alice and Bob share an EPR state. Alice is then given an unknown quantum state $|\phi\rangle_{in}$ that has to be sent to Bob. In order for this quantum teleportation process to be successful, we have to beat the classical scheme⁴. Alice combines her mode of the EPR state (mode 1) with the input state $|\phi\rangle_{in}$ on a 50:50 beamsplitter, such that in the Heisenberg representation we obtain

$$\begin{aligned}\hat{q}_- &= \frac{1}{\sqrt{2}}\hat{q}_{in} - \frac{1}{\sqrt{2}}\hat{q}_1, & \hat{q}_+ &= \frac{1}{\sqrt{2}}\hat{q}_{in} + \frac{1}{\sqrt{2}}\hat{q}_1 \\ \hat{p}_- &= \frac{1}{\sqrt{2}}\hat{p}_{in} - \frac{1}{\sqrt{2}}\hat{p}_1, & \hat{p}_+ &= \frac{1}{\sqrt{2}}\hat{p}_{in} + \frac{1}{\sqrt{2}}\hat{p}_1\end{aligned}$$

and Bob's quadratures can be written as

$$\hat{q}_2 = \hat{q}_{in} - (\hat{q}_1 - \hat{q}_2) - \sqrt{2}\hat{q}_- \quad (2.8)$$

$$\hat{p}_2 = \hat{p}_{in} + (\hat{p}_1 + \hat{p}_2) - \sqrt{2}\hat{p}_+ \quad (2.9)$$

where the relative position $(\hat{q}_1 - \hat{q}_2)$ and the total momentum $(\hat{p}_1 + \hat{p}_2)$ of the EPR state, that vanish in the limit of infinite squeezing, in the general case of finite squeezing can be obtained by Eqs. (2.4). Eqs. (2.8) and (2.9) can thus be rewritten as

$$\begin{aligned}\hat{q}_2 &= \hat{q}_{in} - \sqrt{2}e^{-r}\hat{q}_2^{(0)} - \sqrt{2}\hat{q}_- \\ \hat{p}_2 &= \hat{p}_{in} + \sqrt{2}e^{-r}\hat{p}_1^{(0)} - \sqrt{2}\hat{p}_+\end{aligned}$$

Alice performs a homodyne detection on the quadratures \hat{q}_- and \hat{p}_+ and she sends the measurement results to Bob, who can displace his mode accordingly, obtaining, for a unitary gain,

$$\begin{aligned}\hat{q}_{tel} &= \hat{q}_{in} - \sqrt{2}e^{-r}\hat{q}_2^{(0)} \\ \hat{p}_{tel} &= \hat{p}_{in} + \sqrt{2}e^{-r}\hat{p}_1^{(0)}\end{aligned} \quad (2.10)$$

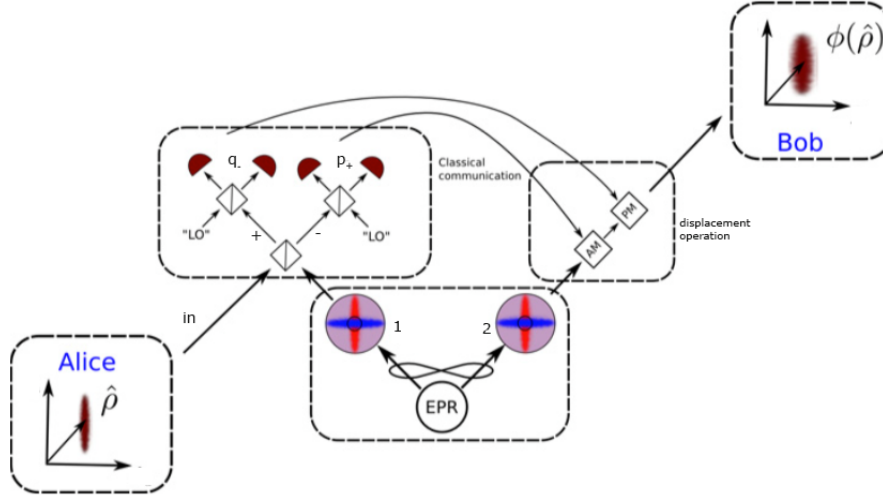


Figure 2.4: Schema of the CV teleportation protocol. Alice to Bob exploit an EPR state and a classical communication channel to teleport an unknown quantum state $\hat{\rho}$. The teleportation is achieved by classically communicating the results of Alice's homodyne measurements to Bob, who will displace his quadratures accordingly [47].

The whole procedure of the CV teleportation is schematized in Fig. 2.4.

From (2.10) we immediately see that in the case of infinite squeezing $r \rightarrow \infty$ the input state is perfectly teleported. In the case of finite squeezing we have to add noise to the variance of the output state:

$$\Delta^2 q_{tel} = \Delta^2 q_{in} + 2e^{-2r} \Delta^2 \hat{q}_2^{(0)} = \Delta^2 q_{in} + 2e^{-2r} \quad (2.11)$$

$$\Delta^2 p_{tel} = \Delta^2 p_{in} + 2e^{-2r} \Delta^2 \hat{p}_1^{(0)} = \Delta^2 p_{in} + 2e^{-2r} \quad (2.12)$$

It's interesting to note that in the classical case (i.e. no entanglement, which corresponds to the condition $r = 0$) we get

$$\Delta^2 q_{tel} = \Delta^2 q_{in} + \Delta^2 \hat{q}^{(0)}$$

$$\Delta^2 p_{tel} = \Delta^2 p_{in} + \Delta^2 \hat{p}^{(0)}$$

so we have to add two units of vacuum noise to the quadratures of the teleported state. These are called *quduties*, duties to pay every time we cross the border between the quantum and the classical world. One is paid when Alice performs a heterodyne detection (simultaneous measure) of q_{in} and p_{in} and the other one is paid when Bob uses this information to construct the teleported state [44].

2.3.2 Quantum teleportation in the Wigner representation

In the previous section we presented the CV teleportation protocol using the Heisenberg representation. However, it is useful to introduce CV teleportation also using the

⁴The classical scheme sets the best average fidelity obtainable for the classical teleportation of a coherent state to $F_{class} = 1/2$ [46], as explained in Section 2.3.3

Wigner representation, as it was originally introduced in [44]. The teleportation procedure is the same that has been explained in Section 2.3.1, where Alice and Bob are provided with an EPR pair described by the Wigner function of Eq. (2.7) and Alice is provided with an unknown input state described by $W_{in}(\alpha_{in})$, with $\alpha_{in} = (q_{in} + ip_{in})/2$. The Wigner function of the composite system after the beam splitter operation performed on the input mode and on Alice mode 1 can be written as⁵

$$\begin{aligned} W(q_+, q_-, q_2, p_+, p_-, p_2) &= W_{in}\left(\frac{q_+ + q_-}{\sqrt{2}}, \frac{p_+ + p_-}{\sqrt{2}}\right) W_{EPR}\left(\frac{q_+ + q_-}{\sqrt{2}}, q_2, \frac{p_+ + p_-}{\sqrt{2}}, p_2\right) \\ &= \int dq_{in} dp_{in} W_{in}(q_{in}, p_{in}) W_{EPR}\left(\frac{q_+ + q_-}{\sqrt{2}}, q_2, \frac{p_+ + p_-}{\sqrt{2}}, p_2\right) \times \\ &\quad \times \delta\left(\frac{q_+ + q_-}{\sqrt{2}} - q_{in}\right) \delta\left(\frac{p_+ + p_-}{\sqrt{2}} - p_{in}\right) \end{aligned}$$

Re-expressing the two deltas as

$$\begin{aligned} \delta\left(\frac{q_+ + q_-}{\sqrt{2}} - q_{in}\right) &= \delta\left(q_+ - (\sqrt{2}q_{in} - q_-)\right) \\ \delta\left(\frac{p_+ + p_-}{\sqrt{2}} - p_{in}\right) &= \delta\left(p_- - (\sqrt{2}p_{in} - p_+)\right) \end{aligned}$$

and knowing that Alice's homodyne detection on q_- and p_+ is carried out by integrating out q_+ and p_- we obtain the resulting Wigner function

$$\begin{aligned} W(q_-, q_2, p_+, p_2) &= \int dq_+ dp_- W(q_+, q_-, q_2, p_+, p_-, p_2) = \int dq_{in} dp_{in} W_{in}(q_{in}, p_{in}) \times \\ &\quad \times W_{EPR}(q_{in} - \sqrt{2}q_-, q_2, \sqrt{2}p_+ - p_{in}, p_2) \end{aligned}$$

Bob displacement transformations $q'_2 = q_2 + \sqrt{2}q_-$ and $p'_2 = p_2 + \sqrt{2}p_+$ are implemented by rewriting the Wigner function with the quadratures transformed with the inverse symplectic transformation as explained in Eq. (1.37) and we obtain

$$\begin{aligned} W(q_-, q'_2, p_+, p'_2) &= \int dq_{in} dp_{in} W_{in}(q_{in}, p_{in}) \times \\ &\quad \times W_{EPR}(q_{in} - \sqrt{2}q_-, q'_2 - \sqrt{2}q_-, \sqrt{2}p_+ - p_{in}, p'_2 - \sqrt{2}p_+) \end{aligned}$$

By recalling Eq. (2.7) we may now explicitly write W_{EPR} as

$$W_{EPR} = \frac{1}{4\pi^2} \exp \left[-\frac{(q_{in} + q'_2 - 2\sqrt{2}q_-)^2 + (2\sqrt{2}p_+ - p_{in} - p'_2)^2}{4e^{2r}} - \frac{(q_{in} - q'_2)^2 + (p'_2 - p_{in})^2}{4e^{-2r}} \right]$$

⁵We note that the beam splitter is a linear optical operation, i.e. a symplectic transformation of the quadratures, and we recall Eq. (1.37)

where we omitted the argument of W_{EPR} for brevity. The integration over q_- and p_+ gives a factor of $e^{2r}\pi/2$ leading us to the Wigner function of the teleported state

$$W_{tel}(q'_2, p'_2) = \frac{1}{8\pi e^{-2r}} \int dq_{in} dp_{in} W_{in}(q_{in}, p_{in}) e^{-\frac{(q_{in}-q'_2)^2 + (p_{in}-p'_2)^2}{4e^{-2r}}}$$

from which is evident that, up to normalization⁶, the Wigner function of the teleported state can be expressed as

$$W_{tel} = W_{in} * G_\sigma \quad (2.13)$$

i.e. as the convolution of the input Wigner function with a Gaussian function of width $\sigma_q = \sigma_p = 2e^{-2r}$. The convolution operation adds thus $2e^{-2r}$ units of noise to each quadrature, which is consistent with what we showed in Eqs. (2.11) and (2.12) in the Heisenberg representation.

2.3.3 Fidelity

Quantum teleportation is a tricky issue: it's not only about the results of measurement of the quadratures, there's so much more to it. We can have, for example, two orthogonal states $|\psi^+\rangle$ and $|\psi^-\rangle$ that give rise to the same q and p statistics. Suppose that Alice sends the $|\psi^+\rangle$ state and Bob receives the $|\psi^-\rangle$ state. If we rely only on the q and p measurements to evaluate the faithfulness of a teleportation protocol we may conclude that the teleportation was successful. But the overlap of the two states tells a different story, showing that the two states are indeed as different as they may possibly be. It is useful then to define the ‘‘similarity’’ between the input state and the output state of a teleportation protocol by the fidelity

$$F = \langle \psi_{in} | \hat{\rho}_{out} | \psi_{in} \rangle$$

When we teleport a quantum state with a given experimental setting we cannot expect our state to be perfectly teleported. The first CV teleportation experiment using optical modes was carried out by Furusawa et al., who in [45] managed to teleport an optical coherent state using a two-mode squeezed state, achieving a fidelity $F_{exp} = 0.58 \pm 0.02$. It is then natural to ask ourselves which criteria we should apply to conclude that our state has been successfully teleported in the laboratory.

In general, it's possible to achieve a non zero fidelity even without using entanglement, i.e. by a cheating Alice and Bob, if they have some knowledge about the set of the input states, which is managed by a third part, Victor. For example, if the set \mathcal{S} of all the possible input states consists of given orthogonal states, then Alice may perform a measurement of a suitable observable \mathcal{O} whose eigenstates coincide with Victor's orthogonal set. Then, after reading her measurement, she will know everything about the input state and she will send this (classical) information to Bob, who will prepare a state identical to the input state. So there is no way to know if Alice and Bob have used or not the entanglement if \mathcal{S} consists of orthogonal states.

⁶To normalize we have to multiply by a factor 2

In constructing this theory we assume that Alice and Bob actually know the set \mathcal{S} used by Victor, but they have no knowledge of the state Victor chose from this set. It is straightforward to define an average fidelity which is calculated over all the possible input states

$$F_{av} = \int_{\mathcal{S}} P(|\psi_{in}\rangle) F d|\psi_{in}\rangle$$

and it serves as a "test" for the quantum protocol to see if Alice and Bob are cheating.

If \mathcal{S} consists of every normalized vector in a Hilbert space of dimension d with a uniform probability distribution then we get

$$F_{av} = \frac{2}{d+1}$$

If we are not constrained by the dimension, so our quantum state is completely unknown, we should work in the limit $d \rightarrow \infty$. But a reasonable assumption is that Victor creates optical single mode coherent states $|\alpha\rangle$ with a Gaussian distribution centered on the vacuum state. It can be shown [46] that in the limit of an infinite variance of the Gaussian distribution, i.e. in the limit of a uniform distribution, if Alice and Bob are cheating they can get at most

$$F_{av} = \frac{1}{2}$$

which is the upper bound for a classical teleportation. If, teleporting our quantum state, we achieve $F > F_{av} = 1/2$ we may conclude that we had to use an entanglement-based teleportation scheme to teleport our state.

2.3.4 The Q-function

To calculate the fidelity of a teleportation protocol involving coherent states it is useful to introduce another quasiprobability function: the Husimi Q distribution or Q-function [48]. The Q-function can be obtained by smoothening the Wigner function, convolving it with a Gaussian distribution with vacuum width

$$Q(q, p) = \frac{1}{2\pi} \iint dq' dp' W(q', p') e^{-\frac{(q-q')^2}{2} - \frac{(p-p')^2}{2}}$$

and recalling the expression 1.3.2 for the Wigner function of a coherent state and the overlap formula 1.3.1 we obtain⁷

$$Q(\alpha, \alpha^*) = \frac{1}{\pi} \langle \alpha | \hat{\rho} | \alpha \rangle$$

where $\alpha = (q + ip)/2$. The Q-function gives us the probability to find $\hat{\rho}$ in the state $|\alpha\rangle$ [28].

⁷Note that $Q(\alpha, \alpha^*) = 4Q(q, p)$

Having introduced this quasi-probability distribution, the calculation of the fidelity for the teleportation of coherent states, and for coherent states only, is extremely simplified, as $F = \langle \alpha_{in} | \hat{\rho}_{tel} | \alpha_{in} \rangle$, where $|\alpha_{in}\rangle$ is the input coherent state and $\hat{\rho}_{tel}$ is the teleported state, can be expressed as⁸

$$F = \pi Q_{tel}(\alpha_{in}) \quad (2.14)$$

Note that $Q_{tel}(\alpha_{in})$ is the Q-function of the teleported state but it's evaluated on the input variables q_{in}, p_{in} .

We can calculate the Q-function of the teleported state from its Wigner function W_{tel} , which is simply the Wigner function of the input state W_{in} convolved with vacuum, as explained in Section 2.3.2, that can be experimentally reconstructed via quantum state tomography. We remark that W_{tel} is a Gaussian function when the input state is a Gaussian function, because it's the convolution of the Wigner at the input with a Gaussian. We see from the transformation of the quadratures that the mean of the teleported state is $\mu_{tel} = \alpha_{tel} = \alpha_{in}$ and the variances are as well calculated from the relations and we obtain $\sigma_{q,tel}, \sigma_{p,tel}$ where $\sigma_{q,tel} = \sigma_0 + \sigma_{q,tel} = \sigma_{q,in} + 1$. To obtain the Q-function we have to convolute a vacuum Gaussian with such a Wigner function and this adds vacuum noise to $\sigma_{q,tel}$. We obtain a bipartite Gaussian function

$$Q_{tel}(q, p) = \frac{1}{2\pi\sqrt{\sigma_q\sigma_p}} \exp \left[-\frac{(q - q_{in})^2}{2\sigma_q} - \frac{(p - p_{in})^2}{2\sigma_p} \right]$$

where $\sigma_q = \sigma_0 + \sigma_{q,tel} = \Delta^2 q_0 + \Delta^2 q_{tel}$ and $\sigma_p = \sigma_0 + \sigma_{p,tel} = \Delta^2 p_0 + \Delta^2 p_{tel}$. Evaluating $Q_{tel}(q, p)$ in (q_{in}, p_{in}) , as requested by Eq. (2.14), we get

$$F = \frac{2}{\sqrt{\sigma_q\sigma_p}} \quad (2.15)$$

Recalling Eqs. (2.11) and (2.12) and noting that considering a coherent state as an input we have that the input variances are equal to vacuum variances, we get

$$\begin{aligned} \sigma_q &= 2\Delta^2 q_0 + 2e^{-2r} = 2 + 2e^{-2r} \\ \sigma_p &= 2\Delta^2 p_0 + 2e^{-2r} = 2 + 2e^{-2r} \end{aligned}$$

If we don't use entanglement as a resource, i.e. $r = 0$, we see from Eq. (2.15) that $F = F_{av} = 1/2$. For any value $r > 0$ we obtain a fidelity $F > F_{av} = 1/2$, beating the classical scheme.

2.4 One Way Quantum Computation

Quantum computing employs the rules of the quantum realm to carry out computations, allowing for a faster resolution of specific problems with respect to classical computing. A well-known example consists in the integer factorization resolution, for

⁸Or equivalently as $F = 4\pi Q_{tel}(q_{in}, p_{in})$

which the most efficient classical algorithm works in sub-exponential time, while with *Shor's quantum algorithm* the solution would be found in a polynomial time [49]. Moreover, Quantum Computers would enable *quantum simulation*, as the simulation of a large quantum mechanical system is not achievable by the means of a classical computer, as the time scales exponentially with the size of the system.

Many models of quantum computation have been presented. One of the most popular is the *quantum circuit model*, analogous to the classical model of computation: a series of one and two-qubits (or qumodes) quantum gates are applied to n input states resulting in a final output state [29]. If we are provided with a *universal set of quantum gates* we can implement any desired unitary operation on the input state by combining the elementary gates. Differently the quantum circuit model, which is based on unitary evolution and which employs destructive measurements only as the final step of the computation process, *Measurement Based Quantum Computing* (MBQC) models employs measurements to carry out the computation [50]; this is the case of the *generalized quantum teleportation* [51, 52] and of the *one-way quantum computing* (1WQC) [53].

We will concentrate on the one-way quantum computing model, which involves a series of measurements and feed-forward operations performed on a particular entangled state, a *cluster state*.

2.4.1 Quantum Gates and Universality

Both in DV and in CV, universality is attainable with a finite set of quantum gates, making it possible to implement any given operation on an input state. For example, a set consisting of displacement operations, squeezing operations, the Fourier transform and a C_Z gate permits us to apply any desired multi-mode Gaussian operation. Adding any kind of non-Gaussian operation (for example a cubic phase gate) allows us to attain universality [54, 55].

Quadrature displacements can be both in momentum and in position. We will identify as $Z(s) = e^{is\hat{q}}$ a displacement by s in momentum and as $X(s) = e^{-is\hat{p}}$ a displacement by s in position, so that

$$X(s) |r\rangle_q = |r + s\rangle_q \quad (2.16)$$

$$Z(s) |r\rangle_p = |r + s\rangle_p \quad (2.17)$$

In the Heienberg picture this translates as

$$\begin{aligned} \begin{pmatrix} \hat{q} \\ \hat{p} \end{pmatrix} &\xrightarrow{X(s)} \begin{pmatrix} \hat{q} \\ \hat{p} \end{pmatrix} + \begin{pmatrix} 0 \\ s \end{pmatrix} \\ \begin{pmatrix} \hat{q} \\ \hat{p} \end{pmatrix} &\xrightarrow{Z(s)} \begin{pmatrix} \hat{q} \\ \hat{p} \end{pmatrix} + \begin{pmatrix} s \\ 0 \end{pmatrix} \end{aligned}$$

Note that the conjugate basis vectors are eigenstates of the $X(s)$ operator, and the same can be said for $Z(s)$ with respect to the position basis vector⁹.

⁹This is analogous to the DV case where the $\{|+\rangle, |-\rangle\}$ basis vectors are eigenstates of X and the $\{|0\rangle, |1\rangle\}$ basis vectors are eigenstates of Z .

A two-qumode gate which is a good theoretical candidate¹⁰, to represent the interaction between modes in an universal gate set, as mentioned above, is the C_Z gate, which is responsible for entangling two qumodes. The C_Z operator reads $C_Z = e^{i\hat{q}_1\hat{q}_2}$ and in a quantum circuit it's represented, as in the DV formalism, as a vertical line connecting two qumodes. To show its action on two quantum states, it's sufficient to recall Eqs. (2.16) and (2.17) of the displacement operators and to proceed step by step. We will label with 1 and 2 respectively the first and the second qumode, such that \hat{q}_1 and \hat{q}_2 act respectively on the first and second mode. In the Schroedinger picture the C_Z gate acts as

$$e^{i\hat{q}_1\hat{q}_2}(|s\rangle_{1,q} \otimes |r\rangle_{2,p}) = e^{is\hat{q}_2}(|s\rangle_{1,q} \otimes |r\rangle_{2,p}) = (|s\rangle_{1,q} \otimes |r+s\rangle_{2,p}) \quad (2.18)$$

where to get the first equality we used the fact that $|s\rangle_{1,q}$ is an eigenstate of \hat{q}_1 with eigenvalue s and that $e^{is\hat{q}_2}$ is a momentum displacement operator for the second mode. This translates in the Heisenberg picture as

$$C_Z^\dagger \hat{p}_i C_Z = e^{-i\hat{q}_i\hat{q}_j} \hat{p}_i e^{i\hat{q}_i\hat{q}_j} = \hat{p}_i + \hat{q}_j \quad (2.19)$$

$$C_Z^\dagger \hat{q}_i C_Z = e^{-i\hat{q}_i\hat{q}_j} \hat{q}_i e^{i\hat{q}_i\hat{q}_j} = \hat{q}_i \quad (2.20)$$

We will now show how these gates will be used to propagate and manipulate quantum information [55, 56].

2.4.2 Teleportation gate

The most elementary component for One-Way Quantum Computing is the teleportation gate, shown in Fig. 2.5. In the DV case a generic state $|\psi\rangle$ expanded in the

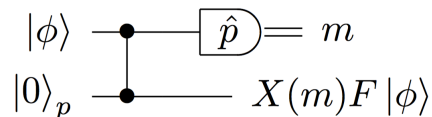


Figure 2.5: Circuitual representation of the teleportation gate [56].

computational basis is entangled with the conjugate basis state $|+\rangle$ via C_Z gate¹¹. The analogous case in CV is applying the C_Z to a generic $|\psi\rangle$, expanded in the position basis, and to the conjugate basis vector $|0\rangle_p$. Our input state is thus in the form

$$|\psi\rangle_1 |0\rangle_{2,p} = \int ds \psi(s) |s\rangle_{1,q} |0\rangle_{2,p}$$

¹⁰As we will mention later, the C_Z gate is a good theoretical tool, as it permits simple calculations, but is difficult to implement experimentally. Another possibility to attain universality is a beam splitter interaction.

¹¹A state $|\psi\rangle = \alpha|0\rangle + \beta|1\rangle$ is entangled via C_Z gate with a state $|+\rangle$. The state after the gate is $|\psi\rangle|+\rangle \rightarrow \alpha|+\rangle|0\rangle + \beta|-\rangle|1\rangle \equiv \frac{1}{\sqrt{2}}(|+\rangle \otimes H|\psi\rangle + |-\rangle \otimes XH|\psi\rangle)$ so that measuring in the conjugate basis $\{|+\rangle, |-\rangle\}$ the first qubit we know that the second qubit is $X^m H|\psi\rangle$, where m is the result of the measure of the first qubit ($m=0$ if we got $|+\rangle$ and $m=1$ if we got $|-\rangle$) [57].

where $\psi(s) = {}_{1,q}\langle s|\psi\rangle$ and after the entanglement operation, whose action on the input states is given by Eq. (2.18), we obtain

$$C_Z(|\psi\rangle_1 |0\rangle_{2,p}) = \int ds \psi(s) |s\rangle_{1,q} |s\rangle_{2,p}$$

We now measure the first mode in the momentum basis p , obtaining the output m . Thus the state of the second mode collapses as

$$|\psi\rangle_{out} \propto {}_{1,p}\langle m| \int ds \psi(s) |s\rangle_{1,q} |s\rangle_{2,p} \propto \int ds \psi(s) e^{-ims} |s\rangle_p$$

where in the end we neglected the label of the second mode and we neglected normalization constants. Given the fact that e^{-ims} is an eigenvalue of the $X(m) = e^{-im\hat{p}}$ operator acting on the eigenstate $|s\rangle_p$, we may rewrite the output state of the second mode as

$$|\psi\rangle_{out} = e^{-im\hat{p}} \int ds \psi(s) |s\rangle_p = X(m) \int ds \psi(s) |s\rangle_p$$

Now we recall that $\psi(s)$ were the coefficient of the expansion of the input state $|\psi\rangle$ in the momentum basis. We can easily switch basis using the Fourier operator such that $|s\rangle_p = F |s\rangle_q$ and

$$|\psi\rangle_{out} = X(m)F \int ds \psi(s) |s\rangle_q = X(m)F |\psi\rangle$$

which is the normalized output state that results from the teleportation circuit. The effect of the teleportation gate is then to teleport the input state modulo a Fourier transformation and a quadrature displacement that depends on the measurement outcome.

2.4.3 Universal Quantum Computation

Given an operator $D_{\hat{q}} = e^{if(\hat{q})}$, diagonal in the computational basis state, a transformed input state $D_{\hat{q}}|\psi\rangle$ will obviously have the output $X(m)FD_{\hat{q}}|\psi\rangle$. Being the operator $D_{\hat{q}}$ a function only of the momentum operator, it commutes with the C_Z gate, so that circuitwise, starting from an input state $|\psi\rangle$, the unitary operation $D_{\hat{q}}$ can also be implemented after the entanglement. The action of the unitary operator $D_{\hat{q}}$ followed by a momentum measurement is equivalent to measuring the first mode in the rotated basis $\hat{p}_{f(\hat{q})} = D^\dagger \hat{p} D$, so that the circuit of Fig 2.6 gives the desired output.

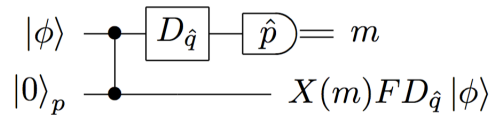


Figure 2.6: Circuitual representation for the implementation of $D_{\hat{q}}$ on an input state [56].

It is to stress out that the operator $D_{\hat{q}}$ doesn't represent an observable, as it's unitary and not self-adjoint, but being a function of the observable \hat{q} , it evolves accordingly to

\hat{q} when other unitary transformations take place¹². Evolving the ket with the transformation $X(m)$ followed by $D_{\hat{q}} = f(\hat{q})$ corresponds in the Heisenberg picture to evolving $D_{\hat{q}}$ according to $X(m)^\dagger D_{\hat{q}} X(m) = X(m)^\dagger f(\hat{q}) X(m) = f(X(m)^\dagger \hat{q} X(m)) = f(\hat{q} + m) = D_{\hat{q}+m}$. By taking advantage of the above considerations, we note that, for example

$$\begin{aligned} D_{\hat{q}} X(m) &= X(m) D_{\hat{q}+m} \\ D_{\hat{q}} F &= F D_{-\hat{p}} \end{aligned}$$

and by using these relations we may implement the desired unitary transformation on the input state $|\psi\rangle$, by choosing a suitable measurement basis, as we are about to explain.

Let's imagine that we have another ancilla state $|0\rangle_p$ (mode 3) entangled with the first ancilla (mode 2) of Fig. 2.6 and that we measure the first two qumodes in the basis $\hat{p}_{f(\hat{q})} = D_{\hat{q}}^\dagger \hat{p} D_{\hat{q}}$, obtaining the outcomes m_1 and m_2 for the two measurements. The output state will be

$$\begin{aligned} |\psi\rangle_{out} &= X(m_2) F D_{\hat{q}} X(m_1) F D_{\hat{q}} |\psi\rangle = X(m_2) F X(m_1) D_{\hat{q}+m_1} F D_{\hat{q}} |\psi\rangle \\ &= X_{m_2} F X_{m_1} F D_{-\hat{p}+m_1} D_{\hat{q}} |\psi\rangle \end{aligned}$$

so we see that, up to a Gaussian operation $X_{m_2} F X_{m_1} F$, we perform the unitary operations $D_{-\hat{p}+m_1} D_{\hat{q}}$ on the input state $|\psi\rangle$. We see that by choosing a different measurement basis for the second mode we can get different results. For example by choosing the measurement basis $\hat{p}_{f(-\hat{q}-m_1)}$, dependent of the measurement outcome, for the second mode and following the same steps, we obtain the result

$$|\psi\rangle_{out} = X_{m_2} F X_{m_1} F D_{\hat{p}} D_{\hat{q}} |\psi\rangle$$

We may then conclude that being able to adapt our measurement according to the previous measurement results allows us to deterministically implement any given single-mode unitary transformation, modulo a measurement dependent Gaussian operation.

Adding nodes, i.e. entangling sequentially more momentum eigenstates to the circuit, allows us to propagate the computation via homodyne detection in a suitable basis down this linear entangled state that we can identify as a “quantum wire”. The creation of a link of entanglement between two nodes belonging to different wires permits us to implement any multi-mode operation via single-mode measurements. Universal computation is thus attainable if we are able to prepare a highly entangled state with the required shape to implement the desired multi-mode operation. We will call this state a *cluster state*.

¹²In general, if we have a self-adjoint operator \hat{A} and a unitary operator \hat{U} , it can be demonstrated that $\hat{U} f(\hat{A}) \hat{U}^\dagger = f(\hat{U} \hat{A} \hat{U}^\dagger)$.

Chapter 3

Cluster states

Cluster states have been introduced for the first time in discrete variables (DV) as a special class of multipartite entangled states which can be depicted as a graph $G = (V, E)$, where V denotes a set of vertices and E a set of edges. Physically, we identify the vertices as qubits and the edges as entanglement connections among them. A distinctive feature of cluster states is a large *persistency of entanglement* [53, 58], i.e. the fact that they are difficult to disentangle: the measure of at least half of the qubits is required to completely disentangle the state. We may refer to them also as *graph states*¹ [59], a term that reflects the fact that cluster states may be represented by a graph.

In DV to prepare a cluster state described by a graph G we adopt the following procedure:

1. We prepare each qubit in the $|+\rangle$ state, as defined in Eq. (2.1)
2. We apply a C_Z gate² to qubits that are connected by an edge in G

Such graph states have been originally introduced to be used as a substrate for *one-way quantum computing* [53], but they can also be considered as a general paradigm of multipartite entangled resources for quantum communication protocols.

During this dissertation we will investigate cluster states with different topologies: *regular* clusters, usually considered as a physical support for MBQC, and *complex* clusters, the quantum equivalent of the classical complex networks used in classical communication, that we want to use as a tool for Quantum Communication protocols.

¹In the beginning cluster states were introduced as graph states where G consisted in a 2D or 3D lattice useful for quantum computation. This notion has been subsequently generalized to any graph G , such that now the two terms are substantially equivalent [29]

²We recall that the action of the C_Z (or Controlled-PHASE) gate on two qubits is the following: $|i\rangle|j\rangle \rightarrow (-1)^{ij}|i\rangle|j\rangle$ with $i, j \in \{0, 1\}$. It can be easily demonstrated that the C_Z gate entangles two qubits initialized in the state $|+\rangle$.

3.1 Continuous variable cluster states via C_Z gate

3.1.1 Definition

The cluster state model can be extended to the continuous variable (CV) formalism [56]. In CV the qubit is replaced by a qumode, the state of the conjugate basis $|+\rangle$ by a momentum eigenstate $|0\rangle_p$ and the DV C_Z gate by the interaction $C_Z = e^{i\hat{q}_i\hat{q}_j}$, which entangles the nodes i and j , and whose action has been shown in Eqs. (2.19) and (2.20). Applying repeatedly the C_Z gate on momentum eigenstates $|0\rangle_p$, according to the shape we want to give to the graph, results in a CV cluster state.

A generic n -mode cluster state described by the *unweighted* graph G is written in the Schrödinger picture as

$$|G\rangle = C_Z(V) |0\rangle_p^{\otimes n} \quad (3.1)$$

where

$$C_Z(V) = \prod_{1 \leq i < j \leq n} e^{iV_{ij}\hat{q}_i\hat{q}_j}$$

and where V is the *adjacency matrix* of the graph G , whose entries read $V_{ij} = V_{ji} = 1$ if the modes i and j are connected by an edge and $V_{ij} = 0$ otherwise. We use the concept of *unweighted* graph as opposed, obviously, to the one of *weighted* graph, where we have weighted edges implemented by the operation $C_Z = e^{ig\hat{q}_i\hat{q}_j}$, where g represents the strength of the interaction. We will mainly restrict our dissertation to unweighted graphs, if not specified otherwise.

In the Heisenberg picture, acting on the input modes repeatedly with the C_Z gate to obtain a graph with the covariance matrix V , we get, according to the Eqs. (2.19) and (2.20),

$$\begin{pmatrix} \hat{\mathbf{q}}^c \\ \hat{\mathbf{p}}^c \end{pmatrix} = C_Z(V)^\dagger \begin{pmatrix} \hat{\mathbf{q}} \\ \hat{\mathbf{p}} \end{pmatrix} C_Z(V) = \begin{pmatrix} \mathbb{1} & 0 \\ V & \mathbb{1} \end{pmatrix} \begin{pmatrix} \hat{\mathbf{q}} \\ \hat{\mathbf{p}} \end{pmatrix} \quad (3.2)$$

where $\hat{\mathbf{q}}^c$ and $\hat{\mathbf{p}}^c$ represent the quadratures of the cluster state.

3.1.2 Stabilizers and Nullifiers

An operator \hat{O} is a *stabilizer* for a state $|\psi\rangle$ if $\hat{O}|\psi\rangle = |\psi\rangle$, i.e. if $|\psi\rangle$ is an eigenstate of \hat{O} with eigenvalue $+1$. For example $X(s)$ stabilizes a zero-momentum eigenstate $|0\rangle_p$ for every s and, generalizing to a multimode setting, $X_i(s) = e^{-is\hat{p}_i}$ stabilizes $|0\rangle_p^{\otimes n}$. In general if an operator \hat{O} stabilizes the state $|\psi\rangle$, $\hat{U}\hat{O}\hat{U}^\dagger$, with \hat{U} unitary operator, stabilizes $\hat{U}|\psi\rangle$. Moreover, reversing the sign of the time evolution of Eq. (2.19) and Eq. (2.20) we get to the relations

$$C_Z\hat{p}_iC_Z^\dagger = e^{i\hat{q}_i\otimes\hat{q}_j}\hat{p}_ie^{-i\hat{q}_i\otimes\hat{q}_j} = \hat{p}_i - \hat{q}_j \quad (3.3)$$

$$C_Z\hat{q}_iC_Z^\dagger = e^{i\hat{q}_i\otimes\hat{q}_j}\hat{q}_ie^{-i\hat{q}_i\otimes\hat{q}_j} = \hat{q}_i \quad (3.4)$$

These considerations allow us to write the stabilizers for the cluster state defined in Eq. (3.1) as

$$\hat{K}_i(s) = C_Z(V)X_i(s)C_Z(V)^\dagger = X_i(s) \prod_{j \in N(i)} Z_j(s), \quad i = 1, \dots, n \quad (3.5)$$

where $N(i)$ denotes the set of nodes connected to the node labeled by i . To get to the last equation we used the fact that if \hat{A} is a self-adjoint operator and \hat{U} is a unitary operator $\hat{U}f(\hat{A})\hat{U}^\dagger = f(\hat{U}\hat{A}\hat{U}^\dagger)$, so that, using the relation (3.3)

$$e^{i\hat{q}_i\hat{q}_j} e^{-is\hat{p}_i} e^{-i\hat{q}_i\hat{q}_j} = e^{-is(\hat{p}_i - \hat{q}_j)} = X_i(s)Z_j(s)$$

and reiterating the process according to the adjacency matrix V we get to Eq. (3.5), which can indeed be rewritten as

$$\hat{K}_i(s) = e^{-is\hat{\delta}_i}$$

where

$$\hat{\delta}_i = \hat{p}_i - \sum_{j \in N(i)} \hat{q}_j$$

are Hermitian operators called *nullifiers*, that correspond to the generators of the Lie Algebra of the stabilizers Lie group. Being Hermitian operators, nullifiers are observables [15].

If we write the Eqs. (3.3) and (3.4) in a more compact form

$$C_Z(V) \begin{pmatrix} \hat{\mathbf{q}} \\ \hat{\mathbf{p}} \end{pmatrix} C_Z(V)^\dagger = \begin{pmatrix} \mathbb{1} & 0 \\ -V & \mathbb{1} \end{pmatrix} \begin{pmatrix} \hat{\mathbf{q}} \\ \hat{\mathbf{p}} \end{pmatrix} \quad (3.6)$$

from the definition of the cluster state given in Eq (3.1) we may conclude that

$$(\hat{\mathbf{p}} - V\hat{\mathbf{q}}) |G\rangle = (C_Z(V)\hat{\mathbf{p}}C_Z(V)^\dagger)C_Z(V) |0\rangle_p^{\otimes n} = 0 \quad (3.7)$$

i.e. cluster states are eigenvectors of the nullifiers with null eigenvalue. We want to stress again that Eq. (3.6) does not “build” the cluster state: indeed, the quadratures of the cluster are provided by Eq. (3.2).

From Eq. (3.7) it's evident that for an *ideal* cluster state, i.e. a cluster state which is effectively implemented starting with momentum eigenstates as in Eq. (3.1), $\Delta^2\hat{\delta}_i = 0$, must hold. Since momentum eigenstates are unphysical states, we can't have ideal cluster states $|G\rangle$. We demand, however, to be as close as possible to the defining property $(\hat{\mathbf{p}} - V\hat{\mathbf{q}}) |G\rangle = 0$, and we demand that

$$\Delta^2\hat{\delta}_i \rightarrow 0$$

Thus nullifiers provide a multipartite entanglement generalization of the entanglement relations of the EPR state and they give an efficient description of the graph, as it's shown in Table 3.1.

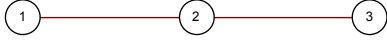
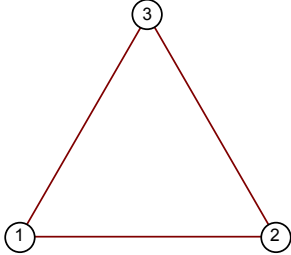
Graph	Nullifiers
	$\begin{aligned}\hat{\delta}_1 &= \hat{p}_1 - \hat{q}_2 \\ \hat{\delta}_2 &= \hat{p}_2 - \hat{q}_1 - \hat{q}_3 \\ \hat{\delta}_3 &= \hat{p}_3 - \hat{q}_2\end{aligned}$
	$\begin{aligned}\hat{\delta}_1 &= \hat{p}_1 - \hat{q}_2 - \hat{q}_3 \\ \hat{\delta}_2 &= \hat{p}_2 - \hat{q}_1 - \hat{q}_2 \\ \hat{\delta}_3 &= \hat{p}_3 - \hat{q}_1 - \hat{q}_2\end{aligned}$

Table 3.1: Example of two 3-mode graphs with the corresponding nullifiers

3.1.3 Wigner representation of Cluster States

As already noted, momentum eigenstates are unphysical states. Their Wigner function can be viewed as a Gaussian with infinitely small width on the momentum quadrature, i.e. a delta function $\delta(p - p_0)$, and an infinitely large width on the position quadrature, i.e. an infinite uniform distribution $\epsilon(q)$. We may then write, for a momentum eigenstate with zero eigenvalue,

$$W_{|0\rangle_p} = \epsilon(q)\delta(p)$$

To evaluate the Wigner function of the cluster, we recall that the Wigner function under a symplectic transformation of the quadratures transforms as (1.37), so that given the symplectic transformation of Eq. (3.6) we straightforwardly evaluate

$$W(\mathbf{q}, \mathbf{p}) = \prod_{i=1}^n \epsilon(q_i)\delta(\delta_i) \quad (3.8)$$

as the Wigner function of an ideal, thus unphysical, cluster state.

3.1.4 The effect of finite squeezing

Since we can't be provided with eigenstates of momentum, we have to rely on highly squeezed states in the momentum quadrature to obtain the approximate cluster state $|\tilde{G}\rangle$

$$|\tilde{G}\rangle = C_Z(V)(\hat{S}(r)|0\rangle)^{\otimes n} \quad (3.9)$$

where $\hat{S}(r)$ identifies the squeezing operator.

Recalling the Wigner function for a squeezed state from Eq. (1.30) it is easy to see that the Wigner function for a finitely squeezed cluster state reads

$$W(\mathbf{q}, \mathbf{p}) = \prod_i G_s(q_i) G_{1/s}(\delta_i)$$

where $G_s(q)$ is a Gaussian distribution with variance $s = e^{2r}$. By sending the squeezing r to infinity we retrieve the Wigner function of the perfect cluster state of Eq.(3.8).

Using non-ideal cluster states will give rise to distortions in quantum computation outputs. As an example, consider the teleportation gate of Section 2.4.2, where the momentum eigenstate $|0\rangle_p$ is replaced by a momentum-squeezed state $\hat{S}(r)|0\rangle$, as shown in Fig. 3.1. Before the entangling operation the Wigner of the composite system reads

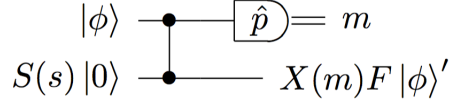


Figure 3.1: Circuitual representation of the teleportation gate employing a finitely squeezed state [56].

$W_{in}(q_1, p_1)G_s(q_2)G_{1/s}(p_2)$ such that after the C_Z operation we get

$$W_{in}(q_1, p_1 - q_2)G_s(q_2)G_{1/s}(p_2 - q_1)$$

according to Eq. (1.37) and Eq. (3.6). Recalling the transformation of the Wigner function after a measurement from Eq. (1.29), we see that after a p-measurement with outcome m on mode 1, the Wigner transforms as

$$\begin{aligned} p(m)W_{out}(q_2, p_2) &\propto \int dq_1 dp_1 W_{in}(q_1, p_1 - q_2)G_s(q_2)G_{1/s}(p_2 - q_1)\delta(p_1 - m) = \\ &= G_s(q_2) \int dq_1 W_{in}(q_1, m - q_2)G_{1/s}(p_2 - q_1) = G_s(q_2)(W_{in} *_{1} G_{1/s})(p_2, m - q_2) \end{aligned}$$

To have access to the Wigner W'_{in} of the teleported state $|\phi'\rangle$ we need to undo the $X(m)F$ corrections that we have at the output, by applying in sequence $X^\dagger(m)$ and F^\dagger . The effect of these operations on the Wigner function is

$$W(q, p) \xrightarrow{X^\dagger(m)} W(q + m, p) \xrightarrow{F^\dagger} W(-p + m, q)$$

and this allows us to write the Wigner function W'_{in} of the state $|\psi'\rangle$ as

$$p(m)W'_{in} = G_s(m - p)(W_{in} *_{1} G_{1/s})(q, p)$$

The effect of finite squeezing is thus that of convolving the input Wigner function in the position variable with a Gaussian filter and applying a Gaussian envelope modulation, centered on the measurement result m . This means that the success of the teleportation

will depend strongly on the measurement value, as for certain values of m the Gaussian envelope will be strongly shifted such that most of the W_{in} will be cut off.

We can also decide to look at the average value of the teleported function, averaging over the possible measurement outcomes, obtaining

$$\langle W'_{in} \rangle = \int dm \quad p(m) W'_{in}(q, p) = (W_{in} *_{1} G_{1/s})(q, p)$$

The average effect we expect when we teleport a state $|\phi\rangle$ using finitely squeezed states is to add $1/s$ of noise on the q quadrature. Repeating the process to propagate the state down a linear cluster we obtain

$$\langle W'_{in} \rangle = (W_{in} *_{1} G_{1/s} *_{2} G_{1/s} *_{1} G_{1/s} *_{2} \dots)(q, p)$$

such that noise is added, on average, in alternating quadratures throughout the propagation.

To note the difference with the Wigner function of the teleported state of Eq. (2.13) obtained by using the teleportation protocol to teleport a state via two-mode squeezed state.

3.2 Implementation via multimode squeezing and linear optics

As we already mentioned in Section 1.4.3, symplectic transformations involving *linear optical devices*, such as beam splitters and phase shifters, are such that the complex representation of the symplectic transformation acting on the operators vector $\hat{\xi}^{(c)} = (\hat{\mathbf{a}}, \hat{\mathbf{a}}^\dagger)^T$ is

$$S_{(c)} = \begin{pmatrix} U & 0 \\ 0 & U^* \end{pmatrix}$$

We can see that we can decompose the matrix U into its real and imaginary parts as $U = X + iY$, such that the corresponding symplectic matrix on the quadrature operators is given by Eq. (1.42), that we rewrite here for clarity:

$$S = \begin{pmatrix} X & -Y \\ Y & X \end{pmatrix}$$

where, due to the symplecticity of S , the relations $XX^T + YY^T = \mathbb{1}$ and $XY^T = YX^T$. During the present dissertation we will allow only symplectic transformations of the form (1.42) as, experimentally, the implementation of the C_Z gate is difficult and costly, requiring online squeezing. We will now see how to implement cluster states using only linear optics and single-mode squeezers.

Since we can't be provided with eigenstates of momentum, we have to rely on highly squeezed states in the momentum quadrature to obtain the approximate cluster state $|\tilde{G}\rangle$ of Eq. (3.9):

$$|\tilde{G}\rangle = C_Z(V)(\hat{S}(r)|0\rangle)^{\otimes n}$$

We may use the *Bloch-Messiah reduction* (also known as Euler decomposition) [31] [33], that allows us to decompose an element of the symplectic group into a product of three factors, to decompose the operation $U_S = C_Z(V)\hat{S}(r)^{\otimes n}$ as

$$\hat{U}_S = \hat{U}_V \left[\otimes_{k=1}^n \hat{S}(r_k^{BM}) \right] \hat{U}_W$$

where \hat{U}_V and \hat{U}_W are multiport linear interferometers³ (that in general represent basis change) and $\otimes_k(\hat{S}r_k^{BM})$ is a set of single-mode squeezers that in general employs different squeezing parameters with respect to the ones of Eq. (3.9). Since a passive element⁴ leaves the vacuum state invariant, the state $|\tilde{G}\rangle$ of Eq. (3.9) can be equivalently obtained by

$$|\tilde{G}\rangle = \hat{U}_V \left[\otimes_{k=1}^n \hat{S}(r_k) \right] |0\rangle^{\otimes n}$$

i.e. by acting on the multi-mode vacuum state with single-mode squeezers, to obtain a set of momentum squeezed states, and then applying a linear optical transformation \hat{U}_V on the state, that corresponds to a suitable symplectic transformation of the form (1.42) on the quadratures in the Heisenberg picture.

In particular, to obtain the approximate graph state $|\tilde{G}\rangle$ characterized by the adjacency matrix V , we have to fulfill the relation

$$Y - VX = 0$$

where X and Y are the matrices that characterize the symplectic transformation of Eq. (1.42). On the quadrature formalism this translates as

$$\begin{pmatrix} \hat{\mathbf{q}}^c \\ \hat{\mathbf{p}}^c \end{pmatrix} = \begin{pmatrix} X & -Y \\ Y & X \end{pmatrix} \begin{pmatrix} \hat{\mathbf{q}}^s \\ \hat{\mathbf{p}}^s \end{pmatrix}$$

where $(\hat{\mathbf{q}}^c, \hat{\mathbf{p}}^c)^T$ contains the quadratures of the cluster state $|\tilde{G}\rangle$ while $(\hat{\mathbf{q}}^s, \hat{\mathbf{p}}^s)^T$ are vacuum squeezed states quadratures, obtained by acting on the multimode vacuum with the n single-mode squeezers identified with the Bloch-Messiah decomposition. In the end we obtain

$$X = (\mathbb{1} + V^2)^{-1/2}O \tag{3.10}$$

$$Y = V(\mathbb{1} + V^2)^{-1/2}O \tag{3.11}$$

where O can be any real orthogonal matrix [60].

³In the symplectic representation acting on quadratures the action of a multiport linear interferometer is carried out by an orthogonal symplectic matrix $O_V^{-1} = O_V^T$

⁴By definition we call a passive element an element which preserves the number of photons. A passive element preserves the trace of the covariance matrix of a state

3.3 Building cluster states

We saw in Section 3.2 how we cannot physically obtain a perfect cluster and how we have to rely on an approximation of an ideal state where we demand that

$$\Delta^2 \hat{\delta} \rightarrow 0$$

Mathematically, we can interpret $\hat{\delta}_i$ as the quadrature of a mode, with operators \hat{a}_i^{null} . This allows us to view the transformation

$$\hat{\delta} = \hat{\mathbf{p}}^c - V\hat{\mathbf{q}}^c = (\mathbb{1} + V^2)^{1/2} O \hat{\mathbf{p}}^s$$

which relates the nullifier operator to the input squeezed quadrature, as an optical transformation between quadratures and we can interpret $(\mathbb{1} + V^2)^{1/2} O$ as the symplectic transformation $\hat{\xi} \rightarrow S\hat{\xi}$, which acts on the covariance matrix as $\sigma \rightarrow S\sigma S^T$. We thus have the transformation

$$\sigma^{null} = S\sigma^{sqz,p}S^T \quad (3.12)$$

where $\sigma^{sqz,p}$ is the reduced covariance matrix of the input squeezed states that contains the information on the squeezing of the momentum and σ^{null} is the covariance matrix that contains the quadratures of the nullifiers, where

$$S = (\mathbb{1} + V^2)^{1/2} O \quad (3.13)$$

The importance of σ^{null} lies on the fact that it contains the second statistical moments of the nullifiers, thus also the values of our interest $\Delta^2 \hat{\delta}_i$ that we aim to minimize to have a cluster which is the closest possible to the ideal cluster state.

3.3.1 Shot noise

If we start with the vacuum state $|0\rangle$ we work with $\sigma^s = \mathbb{1}$.

$$\sigma^{null} = (\mathbb{1} + V^2)$$

These nullifiers are not normalized quadratures. This means we have to define a new covariance matrix $\bar{\sigma}^{null}$ with physical, i.e. normalized with the vacuum, nullifiers such that $\Delta^2 \bar{\delta}_i^0 = 1$. The *shot noise* $\Delta^2 \hat{\delta}_i^0$ can be easily calculated by noticing the fact that $V_{ij} = 1$ iff i and j are connected by an edge, leading us to $\Delta^2 \hat{\delta}_i^0 = (\mathbb{1} + V^2)_{ii} = 1 + n_i$. Thus the new matrix $\bar{\sigma}^{null}$ of the physical nullifiers can be obtained by

$$\bar{\sigma}^{null} = D\sigma^{null}D \quad (3.14)$$

where $D = \text{diag} \left[(\mathbb{1} + V^2)_{ii}^{-1/2} \right]$ and

$$\Delta^2 \bar{\delta}_i = \frac{\Delta^2 \hat{\delta}_i}{\Delta^2 \hat{\delta}_i^0}$$

3.3.2 Optimization protocol

The O matrix that appears in Eqs. (3.10) and (3.11) is not unique and it can be chosen with the aim to optimize a specific function of the nullifiers variances. From Eqs. (3.12) and (3.13) we can see that $\Delta^2 \hat{\delta}_i = \Delta^2 \hat{\delta}_i(O, \sigma^{sqz})$. In [61] it's shown that the matrix O that optimizes a given function $f(\Delta^2 \hat{\delta}_i(O))$ is the matrix that diagonalizes \mathcal{M}

$$\mathcal{M} = (\mathbb{1} + V^2)^{1/2} \text{diag}[\partial_i f(\Delta^2 \hat{\delta}(O))] (\mathbb{1} + V^2)^{1/2}$$

We stress out that the matrix O of interest depends on the choice of the function $f(\Delta^2 \hat{\delta}_i(O))$ we want to minimize. What about the squeezing values? They play a role in determining $\Delta^2 \hat{\delta}_i$. The more the input states are squeezed, the smaller $\Delta^2 \hat{\delta}_i$ is, and the better the approximation of the cluster state is.

We saw that a suitable choice of O permits us to reach an extremum of the function $f(\Delta^2 \hat{\delta}_i(O))$. How do we know if it's a maximum or a minimum? In [61] it's shown that we can rewrite the function f as

$$f(\Delta^2 \hat{\delta}_i(O)) = \text{Tr}(O^T \mathcal{M} O \sigma^{sqz,p}) = \sum_i k_i d_i$$

where k_i are the eigenvalues of $\sigma^{sqz,p}$ and d_i are the eigenvalues of the diagonal matrix $O^T \mathcal{M} O$. Thus, if we order the eigenvalues k_i as $k_j < k_l$ for $j < l$, the ordering of the eigenvalues m_i determines the nature of the extremum, i.e. if we order the m_i as $m_1 < m_2 < \dots$ we reach the global minimum and if we order as $m_1 > m_2 > \dots$ we reach the global maximum.

Depending on the task we want to perform with our cluster, we choose different $f(\Delta^2 \hat{\delta}_i)$. For example, if we want a cluster which is, globally, as close as possible to an ideal cluster we may choose to minimize the function $f(\Delta^2 \hat{\delta}_i) = \sum_i \Delta^2 \bar{\delta}_i$. Let's imagine we want a cluster that will allow us, in the future, to teleport a state between two nodes or to implement a quantum secret sharing protocol among six given nodes [15]. In that case we may want to have the best nullifiers on the corresponding nodes, not caring about the others, to achieve the best result possible, minimizing the function $f(\Delta^2 \hat{\delta}_i) = \sum_k \Delta^2 \bar{\delta}_k$, where the sum is over the k nodes that are involved in the protocol.

3.3.3 Implementation of regular clusters

We will give some examples the implementation of a 6-mode cluster with different shapes and average degree $\langle k \rangle = \sum_i k_i / N$, where k_i is the node's degree, i.e. the number of edges connected to the node itself. In the trivial case of equal squeezing values, according to Eqs. (3.12) and (3.14), due to the fact that $\sigma^{sqz,p}$ is the identity matrix, we get

$$\text{diag}(\bar{\sigma}^{null}) = \text{diag}(\sigma^{sqz,p}),$$

i.e. the variances $\Delta^2 \bar{\delta}_i$ are equal to the squeezing values. In this scenario, we cannot force any optimization on the nullifiers variances.

We will thus start from squeezed vacuum modes, with the following list of squeezing values, in dB, which corresponds to a series of realistic values that can be obtained via the experiment described in [15]:

$$\{-6.27, -5.56, -4.16, -3.21, -2.41, -1.56\}$$

We proceed to build the cluster using the optimization protocol of Section 3.3.2 using two different optimization functions:

$$f_1(\Delta^2 \hat{\delta}_i) = \sum_i \Delta^2 \bar{\delta}_i \quad (3.15)$$

$$f_2(\Delta^2 \hat{\delta}_i, n_1, n_2) = \sum_i A_i(n_1, n_2) \Delta^2 \bar{\delta}_i \quad (3.16)$$

where $A_i(n_1, n_2) = 10^5$ if $i = n_1, n_2$, with n_1, n_2 two given modes, and $A_i(n_1, n_2) = 1$ otherwise. When we minimize f_1 we implement a cluster with a better overall quality. As we saw in Section 3.2, a good cluster should have $\Delta^2 \hat{\delta}_i \rightarrow 0$, and we can take the mean of the variance of the nullifiers $\mu = f_1/N$ as a measure for the overall quality of the cluster. Differently, minimizing f_2 permits us to “concentrate” the quality on two given nodes, with the future aim of teleporting a state between them following a suitable protocol.

As we will see in the next paragraphs, implementing the clusters with the optimization protocol effectively led to the desired results. We also anticipate that clusters with a higher average degree $\langle k \rangle$, when we implement them minimizing f_1 , exhibit a better overall quality.

6-mode linear cluster

Linear clusters allow for universal single-mode quantum computing [54].



Figure 3.2: 6-mode linear cluster

The 6-mode linear cluster shown in Figure 3.2 is implemented by the following adjacency matrix

$$V = \begin{pmatrix} 0 & 1 & 0 & 0 & 0 & 0 \\ 1 & 0 & 1 & 0 & 0 & 0 \\ 0 & 1 & 0 & 1 & 0 & 0 \\ 0 & 0 & 1 & 0 & 1 & 0 \\ 0 & 0 & 0 & 1 & 0 & 1 \\ 0 & 0 & 0 & 0 & 1 & 0 \end{pmatrix}$$

in 4 different ways: without optimization, optimizing the function f_1 of Eq. (3.15), optimizing the function f_2 of Eq. (3.16) first on the nodes 1 and 2 and then on the nodes 3 and 4. The results are shown in Table 3.2.

function	$\Delta^2 \bar{\delta}_i$ (dB)	μ
no opt.	{ -6.12, -5.46, -4.16, -3.19, -2.45, -1.64 }	-3.84
f_1	{ -4.18, -3.85, -4.20, -5.04, -4.18, -4.21 }	-4.28
$f_2(1, 2)$	{ -6.27, -5.56, -3.26, -3.31, -3.02, -3.41 }	-
$f_2(3, 4)$	{ -3.31, -3.09, -5.56, -6.27, -3.46, -2.88 }	-

Table 3.2: Evaluation of the variances of the nullifiers and their mean μ using two different optimization functions f_1 and f_2 defined in (3.15) and (3.16) for the implementation of the linear 6-mode cluster with average degree $\langle k \rangle = 1.67$.

6-mode grid cluster

We move now towards 2D structures, as they are necessary for universal quantum computing [62].

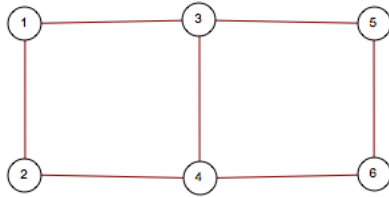


Figure 3.3: 6-mode grid cluster

The 6-mode grid cluster shown in Figure 3.3 is implemented by the following adjacency matrix

$$V = \begin{pmatrix} 0 & 1 & 1 & 0 & 0 & 0 \\ 1 & 0 & 0 & 1 & 0 & 0 \\ 1 & 0 & 0 & 1 & 1 & 0 \\ 0 & 1 & 1 & 0 & 0 & 1 \\ 0 & 0 & 1 & 0 & 0 & 1 \\ 0 & 0 & 0 & 1 & 1 & 0 \end{pmatrix}$$

in 4 different ways: without optimization, optimizing the function f_1 of Eq. (3.15), optimizing the function f_2 of Eq. (3.16) first on the nodes 1 and 2 and then on the nodes 3 and 4. The results are shown in Table 3.3.

function	$\Delta^2 \bar{\delta}_i$ (dB)	μ
no opt.	$\{-5.76, -5.30, -3.99, -3.30, -2.52, -1.80\}$	-3.78
f_1	$\{-4.43, -4.95, -4.93, -4.62, -4.43, -4.95\}$	-4.72
$f_2(1, 2)$	$\{-5.56, -6.27, -4.19, -3.33, -3.14, -4.05\}$	-
$f_2(3, 4)$	$\{-3.54, -3.56, -5.72, -6.08, -3.54, -3.56\}$	-

Table 3.3: Evaluation of the variances of the nullifiers and their mean μ using two different optimization functions f_1 and f_2 defined in (3.15) and (3.16) for the implementation of the grid 6-mode cluster, with average degree $\langle k \rangle = 2.33$.

6-mode “secret sharing” cluster

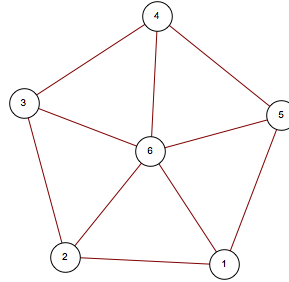


Figure 3.4: 6-mode “secret sharing” cluster

Quantum secret sharing is a protocol that permits to share a secret among many “players”, which can be recovered only through the collaboration of a given number of players. The 6-mode “secret sharing” cluster shown in Figure 3.4, proposed in [63], which allows to recover a shared quantum secret via the collaboration of at least three nodes, is implemented by the following adjacency matrix

$$V = \begin{pmatrix} 0 & 1 & 0 & 0 & 1 & 1 \\ 1 & 0 & 1 & 0 & 0 & 1 \\ 0 & 1 & 0 & 1 & 0 & 1 \\ 0 & 0 & 1 & 0 & 1 & 1 \\ 1 & 0 & 0 & 1 & 0 & 1 \\ 1 & 1 & 1 & 1 & 1 & 0 \end{pmatrix}$$

in 2 different ways: without optimization and optimizing the function f_1 of Eq. (3.15)⁵. The results are shown in Table 3.4.

⁵We didn’t optimize the function f_2 because when we are provided a “secret-sharing” cluster our purpose is to run a secret-sharing protocol and we have no interest in teleportation between two nodes.

function	$\Delta^2 \bar{\delta}_i$ (dB)	μ
n opt	{ -5.60, -4.95, -4.01, -3.36, -2.59, -1.79 }	-3.72
f_1	{ -5.15, -4.74, -4.68, -4.58, -4.89, -4.58 }	-4.77

Table 3.4: Evaluation of the variances of the nullifiers and their mean μ using the optimization function f_1 defined in Eq. (3.15) for the implementation of the “secret sharing” 6-mode cluster, with average degree $\langle k \rangle = 3.33$.

6-mode fully connected cluster

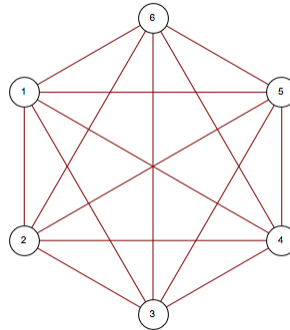


Figure 3.5: 6-mode fully connected cluster

The 6-mode fully connected cluster, which can be for example used in quantum repeaters protocols [64], shown in Figure 3.5 is implemented by the following adjacency matrix

$$V = \begin{pmatrix} 0 & 1 & 1 & 1 & 1 & 1 \\ 1 & 0 & 1 & 1 & 1 & 1 \\ 1 & 1 & 0 & 1 & 1 & 1 \\ 1 & 1 & 1 & 0 & 1 & 1 \\ 1 & 1 & 1 & 1 & 0 & 1 \\ 1 & 1 & 1 & 1 & 1 & 0 \end{pmatrix}$$

in 4 different ways: without optimization, optimizing the function f_1 of Eq. (3.15), optimizing the function f_2 of Eq. (3.16) first on the nodes 1 and 2 and then on the nodes 3 and 4. The results are shown in Table 3.5.

Comments

Implementing the clusters with the optimization protocol of Section 3.3.2 using the fitness function f_1 effectively led to clusters with a better quality than the ones implemented without optimization. We note that the quality of the clusters improves with the quantity of edges, i.e. the quantity of entanglement links. Indeed, the best quality

function	$\Delta^2 \bar{\delta}_i$ (dB)	μ
no opt.	{-5.04, -4.67, -3.92, -3.33, -2.80, -2.21}	-3.66
f_1	{-4.72, -5.21, -5.14, -5.17, -5.26, -5.52}	-5.17
$f_2(1, 2)$	{-6.14, -6.14, -4.43, -4.43, -4.36, -4.79}	-
$f_2(3, 4)$	{-4.42, -4.40, -6.14, -6.14, -4.70, -4.49}	-

Table 3.5: Evaluation of the variances of the nullifiers and their mean μ using two different optimization functions f_1 and f_2 defined in (3.15) and (3.16) for the implementation of the fully connected 6-mode cluster, with average degree $\langle k \rangle = 5$.

cluster is the fully connected one, having an average degree of $\langle k \rangle = 5$, while the worst quality cluster is the linear one, with an average degree of $\langle k \rangle = 1.67$. The results show indeed that the highest the average degree is, the better the cluster is, in terms of the quality of nullifiers.

When we use the fitness function f_2 to implement the cluster state, the variances of the nullifiers of the two selected nodes reach smaller values with respect to the variances of the other nodes, as we required. In general they reach values that lay between the two highest squeezing values, as in the case of the fully connected cluster, or they correspond perfectly to the two, as with a linear cluster. In any case they exceed the highest squeezing value.

3.3.4 Implementation of complex clusters

By implementing complex clusters we want to study models that can reproduce real-world networks, investigating their behavior under Quantum Communication protocols. We will investigate different complex topologies, namely

- Barabási-Albert
- Erdős–Rényi
- Watts-Strogatz

These models have different features and properties: the Barabási-Albert model generates a scale-free complex network, such as the World Wide Web, the Erdős–Rényi is a model of purely random graphs, while the Watts-Strogatz model lies between the regular graph and the random graph and it exhibits *small-world* properties⁶.

In this Section we will present some implementation of a 48-mode complex cluster with the above-mentioned network topologies. We will start from squeezed vacuum modes, with the following list of squeezing values in dB, which corresponds to a series of

⁶Among the properties characterizing a small-world network there is a high clustering coefficient and the fact that most pair of nodes are connected through a short path.

realistic values that can be obtained via the experiment described in [15]:

$$\{-6.51, -6.51, -6.50, -6.50, -6.49, -6.48, -6.46, -6.43, -6.34, -6.35, \\ -6.30, -6.23, -6.15, -6.06, -5.95, -5.83, -5.70, -5.56, -5.40, -5.23, \\ -5.06, -4.87, -4.67, -4.47, -4.27, -4.06, -3.84, -3.63, -3.42, -3.21, \\ -3.00, -2.80, -2.60, -2.41, -2.22, -2.05, -1.88, -1.71, -1.56, -1.41, \\ -1.27, -1.13, -1.01, -0.89, -0.76, -0.59, -0.44, -0.31\}$$

Due to the fact that the graphs with the aforementioned topologies are a class of graphs with specific statistical properties, we will implement $N = 100$ graphs for each case. Considering the high number of modes, we may consider the value

$$\mu_j = \frac{1}{48} \sum_i \Delta^2 \bar{\delta}_{i,j} \quad (3.17)$$

i.e. the mean of the variance of the nullifiers of a graph, where $\Delta^2 \bar{\delta}_{i,j}$ identifies variance of the i -th nullifier of the j -th graph. We will indicate as μ and σ respectively the mean and the standard deviation of the μ_j values. Instead, we will indicate as $\mu_{n1=i}$ and $\sigma_{n1=i}$ the mean and the variance of the set of values $\Delta^2 \bar{\delta}_{i,j}$ and as μ_{all} the mean of

$$\mu_j = \frac{1}{46} \sum_{i \neq n_1, n_2} \Delta^2 \bar{\delta}_{i,j} \quad (3.18)$$

Barabási-Albert complex network

The Barabási-Albert model generates *scale-free* complex networks. A scale-free network is characterized by a power-law degree distribution⁷

$$P(k) \sim k^{-\gamma}$$

where $P(k)$ is the probability that a node has k links, representing its ‘‘popularity’’ and γ its a parameter that depends on the network [65]. Scale-free networks exhibit two important properties that are common in most real networks: growth and preferential attachment. Indeed, as most random networks models (as the ER and the Small-World model) start with a fixed number of nodes and then proceed to connect or rewire them with a certain probability, in the BA model we start with a small number of nodes and we add new nodes as time increases, describing a variety of existing situations such as the World Wide Web. Moreover, taking into account *preferential attachment*, i.e. the fact that new nodes attach preferentially to nodes that already have a high node’s degree, we describe a characteristic feature of most of the social networks. *Hubs*, heavily linked nodes, arise spontaneously from the preferential attachment property.

The Barabási-Albert algorithm is characterized by a parameter m_{BA} and it works in the following way:

⁷At least asymptotically

1. We start with a small number of nodes m_0 and at each step we add a new node with m_{BA} links to other nodes of the graph, where $m_{BA} \leq m_0$
2. The probability that the new node is connected with the node i is

$$P_{att}(k_i) = \frac{k_i}{\sum_j k_j}$$

where k_i is the node's degree, reflecting the property of preferential attachment [14].

Following this model, we implemented 48-nodes Barabási-Albert networks with different values of the m_{BA} parameter, using the protocol presented in Section 3.3.2, optimizing the two functions of Eq. (3.15) and Eq. (3.16) already used for regular clusters. The results are shown in Tables 3.6 and 3.7.

m_{BA}	μ (dB)	$[\mu \pm \sigma]$ (dB)	$\langle k \rangle$
1	-4.70	$[-4.73, -4.67]$	1.96
5	-5.55	$[-5.58, -5.53]$	9.38
10	-5.82	$[-5.84, -5.80]$	17.71
20	-6.15	$[-6.16, -6.14]$	31.25
47	-6.33	$[-6.33, -6.33]$	47

Table 3.6: Mean μ and standard deviation σ of the values μ_j of Eq. (3.17), which represent the mean of the variance of the nullifiers of the graph j , evaluated on $N = 100$ Barabási-Albert graphs with different parameter m_{BA} and consequently different average degrees $\langle k \rangle$, optimized using the function f_1 of Eq. (3.15)

We will see that the same result that we found in regular clusters hold: increasing with the quantity of entanglement connections among the nodes, the cluster built by minimizing f_1 with the optimization protocol exhibit a better quality. Moreover, we will show that the topology of the graph plays a role: indeed, regular graphs are optimized better than random graphs

Erdős–Rényi complex network

The Erdős–Rényi model generates *random graphs*. Differently from the Barabási-Albert model, whose characteristic property is the concept of growth, in the random graph theory we start with a fixed number of nodes n and we assign a probability p_{ER} for two nodes to be connected by an edge. The distribution of the degree of any vertex reads

$$P(k) = \binom{n-1}{k} p^k (1-p)^{n-1-k}$$

which is Poissonian in the limit of large n . Most nodes have a comparable degree and for this reason we don't observe hubs.

m_{BA}	$\mu_{n_1=12}$ (dB)	$[\mu_{n_1=12} \pm \sigma_{n_1=12}]$ (dB)	$\mu_{n_2=13}$	$[\mu_{n_1=13} \pm \sigma_{n_1=13}]$ (dB)	μ_{all} (dB)	$[\mu_{all} \pm \sigma_{all}]$ (dB)
1	-6.51	$[-6.51, -6.51]$	-6.51	$[-6.51, -6.51]$	-4.61	$[-4.64, -4.59]$
5	-6.51	$[-6.51, -6.51]$	-6.51	$[-6.51, -6.51]$	-5.48	$[-5.50, -5.46]$
10	-6.51	$[-6.51, -6.51]$	-6.51	$[-6.51, -6.51]$	-5.76	$[-5.78, -5.74]$
20	-6.51	$[-6.51, -6.51]$	-6.51	$[-6.51, -6.51]$	-6.10	$[-6.12, -6.09]$
47	-6.51	$[-6.51, -6.51]$	-6.51	$[-6.51, -6.51]$	-6.32	$[-6.32, -6.32]$

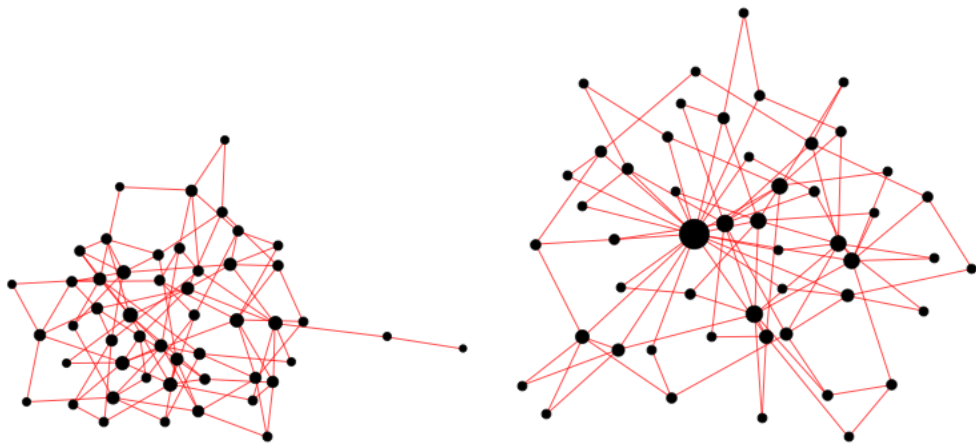
Table 3.7: Means $\mu_{n_1=12}$, $\mu_{n_1=13}$ and μ_{all} and standard deviation $\sigma_{n_1=12}$, $\sigma_{n_2=13}$ and σ_{all} of the nullifiers of the nodes 12 and 13 and of the value μ_j of Eq. (3.18), which represent the mean of the variance of the nullifiers of the graph j , evaluated on $N = 100$ Barabási-Albert graphs with different parameter m_{BA} , optimized using the function f_2 of Eq. (3.16)

p_{ER}	$\mu_{n_1=12}$ (dB)	$[\mu_{n_1=12} \pm \sigma_{n_1=12}]$ (dB)	$\mu_{n_2=13}$	$[\mu_{n_1=13} \pm \sigma_{n_1=13}]$ (dB)	μ_{all} (dB)	$[\mu_{all} \pm \sigma_{all}]$ (dB)
0.2	-6.51	$[-6.51, -6.51]$	-6.51	$[-6.51, -6.51]$	-5.42	$[-5.46, -5.39]$
0.4	-6.51	$[-6.51, -6.51]$	-6.51	$[-6.51, -6.51]$	-5.74	$[-5.77, -5.71]$
0.6	-6.51	$[-6.51, -6.51]$	-6.51	$[-6.51, -6.51]$	-5.97	$[-5.99, -5.95]$
0.8	-6.51	$[-6.51, -6.51]$	-6.51	$[-6.51, -6.51]$	-6.20	$[-6.21, -6.18]$
1	-6.51	$[-6.51, -6.51]$	-6.51	$[-6.51, -6.51]$	-6.32	$[-6.32, -6.32]$

Table 3.8: Means $\mu_{n_1=12}$, $\mu_{n_1=13}$ and μ_{all} and standard deviation $\sigma_{n_1=12}$, $\sigma_{n_2=13}$ and σ_{all} of the nullifiers of the nodes 12 and 13 and of the value μ_j of Eq. (3.18), which represent the mean of the variance of the nullifiers of the graph j , evaluated on $N = 100$ Erdős-Rényi graphs with different parameter p_{ER} , optimized using the function f_2 of Eq. (3.16) and setting $n_1 = 12$ and $n_2 = 13$.

We implemented 48-nodes Erdős–Rényi networks with different values of the p_{ER} parameter, using the protocol presented in Section 3.3.2, optimizing the two functions of Eq. (3.15) and Eq. (3.16) already used for regular clusters. The results are shown in Tables 3.9 and 3.8.

The average degree of a graph may represent an useful characteristic to compare different models of complex networks. In Figure 3.6 we may see the difference between a scale-free graph and a random graph with the same average degree. As we see in Figure 3.6b, the Barabási–Albert network exhibits highly connected nodes (*hubs*) that are absent in the Erdős–Rényi model (Figure 3.6a).



(a) Erdős–Rényi model with $p_{ER} = 4/49$, graph with a maximum degree of $k=8$. (b) Barabási–Albert model with $m_{BA} = 2$, graph with a maximum degree of $k=21$.

Figure 3.6: Comparison between two models of complex networks, both with an average degree of $\langle k \rangle \sim 4$. The size of the dots increases with the number of links.

p_{ER}	μ (dB)	$[\mu \pm \sigma]$ (dB)	$\sum_i \langle k_i \rangle$
0.2	-5.50	$[-5.54, -5.46]$	9.35
0.4	-5.80	$[-5.83, -5.76]$	18.83
0.6	-6.02	$[-6.04, -6.00]$	28.29
0.8	-6.22	$[-6.23, -6.21]$	37.58
1	-6.33	$[-6.33, -6.33]$	47

Table 3.9: Mean μ and standard deviation σ of the values μ_j of Eq. (3.17), which represent the mean of the variance of the nullifiers of the graph j , evaluated on $N = 100$ Erdős–Rényi graphs with different parameter p_{ER} and consequently different average degrees $\langle k \rangle$, optimized using the function f_1 of Eq. (3.15). In the Erdős–Rényi graph the average degree $\langle k \rangle$ changes slightly with the graph, so we considered the mean of the average degree over the 100 graphs.

Watts-Strogatz complex network

A model of graph that lies between the regular graph and the random graph model was proposed by Watts and Strogatz [66]. The main idea of the Watts-Strogatz model is to start with a regular network and then “rewire” it, to increase randomness and disorder. We thus start with a ring lattice with n nodes and k edges per node, which connect it to the closest neighbors, and then we randomly rewire each edge with probability p_{WS} , as it’s shown in Figure 3.7.

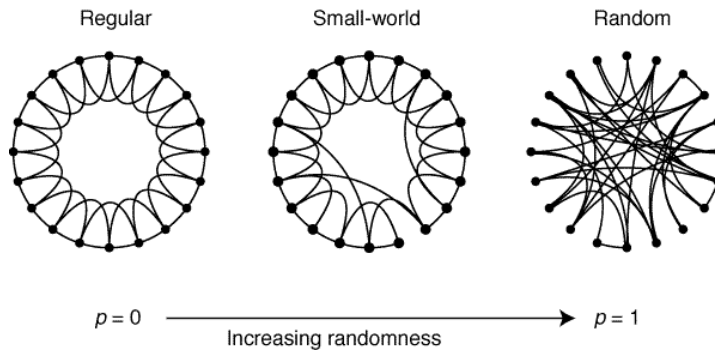


Figure 3.7: Rewiring of a regular network for the construction of a “small world” network as shown in [66]

We implemented 48-nodes Watts-Strogatz network with different values of the p_{WS} parameter, using the protocol presented in Section 3.3.2, optimizing the two functions of Eq. (3.15) and Eq. (3.16) already used for regular clusters. The results are shown in Tables 3.10a and 3.11a for $k = \langle k \rangle = 4$ and in Table 3.10b and 3.11a for $k = \langle k \rangle = 8$.

p_{WS}	μ (dB)	$[\mu \pm \sigma]$ (dB)	p_{WS}	μ (dB)	$[\mu \pm \sigma]$ (dB)
0	-5.19	$[-5.19, -5.19]$	0	-5.79	$[-5.79, -5.79]$
0.1	-5.16	$[-5.17, -5.14]$	0.1	-5.69	$[-5.71, -5.66]$
0.4	-5.10	$[-5.12, -5.07]$	0.4	-5.49	$[-5.51, -5.46]$
0.7	-5.09	$[-5.11, -5.07]$	0.7	-5.43	$[-5.46, -5.40]$
1	-5.09	$[-5.12, -5.06]$	1	-5.43	$[-5.46, -5.41]$

(a) $k = \langle k \rangle = 4$ (b) $k = \langle k \rangle = 8$

Table 3.10: Mean μ and standard deviation σ of the values μ_j of Eq. (3.17), which represent the mean of the variance of the nullifiers of the graph j , evaluated on $N = 100$ Watts-Strogatz graphs with different parameter p_{WS} and different k , optimized using the function f_1 of Eq. (3.15)

p_{WS}	$\mu_{n_1=12}$ (dB)	$[\mu_{n_1=12} \pm \sigma_{n_1=12}]$ (dB)	$\mu_{n_2=13}$	$[\mu_{n_1=13} \pm \sigma_{n_1=13}]$ (dB)	μ_{all} (dB)	$[\mu_{all} \pm \sigma_{all}]$ (dB)
0	-6.51	$[-6.51, -6.51]$	-6.51	$[-6.51, -6.51]$	-5.10	$[-5.10, -5.10]$
0.1	-6.51	$[-6.51, -6.51]$	-6.51	$[-6.51, -6.51]$	-5.07	$[-5.09, -5.05]$
0.4	-6.51	$[-6.51, -6.51]$	-6.51	$[-6.51, -6.51]$	-5.00	$[-5.03, -4.98]$
0.7	-6.51	$[-6.51, -6.51]$	-6.51	$[-6.51, -6.51]$	-4.99	$[-5.02, -4.96]$
1	-6.51	$[-6.51, -6.51]$	-6.51	$[-6.51, -6.51]$	-4.99	$[-5.02, -4.97]$

(a) $k = \langle k \rangle = 4$

p_{WS}	$\mu_{n_1=12}$ (dB)	$[\mu_{n_1=12} \pm \sigma_{n_1=12}]$ (dB)	$\mu_{n_2=13}$	$[\mu_{n_1=13} \pm \sigma_{n_1=13}]$ (dB)	μ_{all} (dB)	$[\mu_{all} \pm \sigma_{all}]$ (dB)
0	-6.51	$[-6.51, -6.51]$	-6.51	$[-6.51, -6.51]$	-5.73	$[-5.73, -5.73]$
0.1	-6.51	$[-6.51, -6.51]$	-6.51	$[-6.51, -6.51]$	-5.62	$[-5.65, -5.59]$
0.4	-6.51	$[-6.51, -6.51]$	-6.51	$[-6.51, -6.51]$	-5.41	$[-5.44, -5.38]$
0.7	-6.51	$[-6.51, -6.51]$	-6.51	$[-6.51, -6.51]$	-5.35	$[-5.38, -5.32]$
1	-6.51	$[-6.51, -6.51]$	-6.51	$[-6.51, -6.51]$	-5.35	$[-5.37, -5.32]$

(b) $k = \langle k \rangle = 8$

Table 3.11: Means $\mu_{n_1=12}$, $\mu_{n_1=13}$ and μ_{all} and standard deviation $\sigma_{n_1=12}$, $\sigma_{n_2=13}$ and σ_{all} of the nullifiers of the nodes 12 and 13 and of the value μ_j of Eq. (3.18), which represent the mean of the variance of the nullifiers of the graph j , evaluated on $N = 100$ Watts-Strogatz graphs with different parameter p_{WS} , optimized using the function f_2 of Eq. (3.16) and setting $n_1 = 12$ and $n_2 = 13$.

Comments

As we expected from the results of Section 3.3.3 on regular clusters, the implementation of quantum complex networks following the Barabási-Albert model or the Erdős-Rényi model shows that the quality of the cluster increases with the quantity of entanglement connections among the nodes. Indeed, as the parameters m_{BA} and p_{ER} increase, so do the number of edges between nodes, thus the average degree $\langle k \rangle$, and the results show clearly that the quality of the cluster increases with these parameters, until the limiting case of the fully connected graph is reached, corresponding to the parameters $m_{BA} = n - 1$, with n number of nodes for the Barabási-Albert model and $p_{ER} = 1$ for the Erdős-Rényi model. Moreover, clusters with a similar average degree $\langle k \rangle$ have a comparable overall quality. The degree $\langle k \rangle$ in complex graphs could thus be used as a benchmark for the quality of the state.

Following the same reasoning, we would expect for a Watts-Strogatz quantum network to have the same quality, independently from the parameter p_{WS} . Indeed, in the Watts-Strogatz model, p_{WS} is a rewiring parameter and we don't lose nor create connections by changing it. Instead, as the p_{WS} parameter approaches 1, the quality of the cluster gets worse, i.e. regular graphs are optimized better than random graphs.

Moreover, as in the regular cluster case, the optimization of the nullifiers of two given nodes with the fitness function of Eq. 3.16 shows that, as expected, the corresponding nullifiers reach the two highest squeezing values.

3.3.5 Comparison of complex graphs

The results we found in the previous sections, especially the ones from Table 3.10, show a dependence between the topology of the graph and the quality of the optimization, for a fixed degree $\langle k \rangle$. Wanting to explore further this dependence, we compared the different topologies of complex graphs, evaluating the overall quality of the cluster as a function of the degree $\langle k \rangle$.

To do that, we calculated the mean value of squeezing and the degree $\langle k \rangle$ of a set of 10 complex graphs of 1000 nodes, with fixed topology and fixed parameters. This way, we average out the fluctuations due to the randomness of the complex shape. We repeated the same calculations changing the parameters and the topology of the complex network. The list of squeezing values that has been used has been generated by using a pseudorandom number generator that created uniformly distributed random numbers in the range $[-14, -3]$. The results are reported in Fig. 3.8.

The data show that, as already anticipated by the results of Table 3.10, the regular cluster converges very fast to its optimal overall quality. On the other hand, the difference in complex topology of the Barabási-Albert, Erdős-Rényi and Watts-Strogatz $p_{WS} = 0.5$ complex graphs doesn't play a significant role. The Erdős-Rényi is found to be the one with the worst overall quality, differing only slightly⁸ from the Barabási-Albert behavior, while the Watts-Strogatz graph with $p_{WS} = 0.5$ converges to the behavior of the Erdős-Rényi for $\langle k \rangle > 300$.

⁸The difference is, on average, 0.26 dB

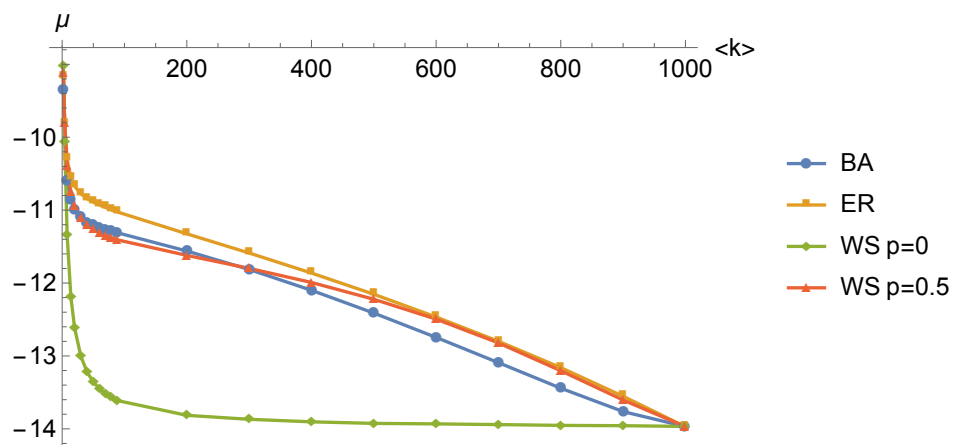


Figure 3.8: Plot of the mean squeezing value of the nullifiers of the cluster as a function of its average degree $\langle k \rangle$ for the different topologies of complex graphs. In the legend, “BA”=Barabási-Albert, “ER”=Erdős-Rényi, “WS p=0” = Watts-Strogatz with $p_{WS} = 0$, “WS p=0.5” = Watts-Strogatz with $p_{WS} = 0.5$

Chapter 4

Transformations on Cluster States

In this chapter we consider some basic task that could be useful in multipartite Quantum Communication. We will concentrate mainly on *entanglement percolation*, i.e. the establishment of a maximally entangled state between two arbitrary nodes of a network which are partially entangled. The entanglement percolation has already been considered for DV networks [67, 68]. Here we consider a similar CV protocol for our complex networks. Given a multipartite entangled resource, we consider the case in which a quantum communication protocol has to be performed between specific nodes after the generation or even the distribution of the multipartite state, so that the entanglement connections have to be modified accordingly. We will see how this can be done via global or local transformation and, particularly, if this can be done via simple linear optical transformations. In the last Section we will see also how measurements can be implemented to re-shape the cluster.

4.1 Global transformations for entanglement percolation

We consider in this section global operations, i.e. operation that involve and are simultaneously applied to all the nodes of the cluster, which can be performed to make an efficient protocol. Later, in Section 4.2, we will generalize to local operations, i.e. operations that different parties can apply independently on subsets of nodes.

4.1.1 Global transformation from cluster to cluster

We consider a scenario in which we are given a particular cluster A and we want to modify it to get to a different cluster B . The problem can be tackled in the following way: we search for the symplectic transformation S_A that bring us from a given set of squeezed vacuum states to a cluster with a given adjacency matrix V_A . We repeat the procedure using a transformation S_B that implements the cluster B with the adjacency

matrix V_B .

$$\begin{pmatrix} \hat{\mathbf{q}}_A^c \\ \hat{\mathbf{p}}_A^c \end{pmatrix} = S_A \begin{pmatrix} \hat{\mathbf{q}}^s \\ \hat{\mathbf{p}}^s \end{pmatrix} \quad (4.1)$$

$$\begin{pmatrix} \hat{\mathbf{q}}_B^c \\ \hat{\mathbf{p}}_B^c \end{pmatrix} = S_B \begin{pmatrix} \hat{\mathbf{q}}^s \\ \hat{\mathbf{p}}^s \end{pmatrix} \quad (4.2)$$

What we want to find is the matrix S such that

$$\begin{pmatrix} \hat{\mathbf{q}}_B^c \\ \hat{\mathbf{p}}_B^c \end{pmatrix} = S \begin{pmatrix} \hat{\mathbf{q}}_A^c \\ \hat{\mathbf{p}}_A^c \end{pmatrix} \quad (4.3)$$

From (4.1) we can re-express Eq. (4.3) as

$$\begin{pmatrix} \hat{\mathbf{q}}_B^c \\ \hat{\mathbf{p}}_B^c \end{pmatrix} = S \cdot S_A \begin{pmatrix} \hat{\mathbf{q}}^s \\ \hat{\mathbf{p}}^s \end{pmatrix}$$

and, taking into account Eq. (4.2), we immediately see that

$$S = S_B \cdot S_A^{-1}$$

Such a matrix always exists, because symplectic matrix are always invertible. We conclude that it is always possible to find a global transformation that leads us from a given cluster to a cluster with a desired adjacency matrix.

Does the covariance matrix of the cluster B gets affected if we obtain it acting on a cluster A instead of obtaining it starting from vacuum modes? The covariance matrix σ_B obtained acting with a symplectic transformation S on a cluster with a covariance matrix σ_A reads

$$\sigma_B = S \sigma_A S^T$$

Given the fact that $\sigma_A = S_A \sigma_{sqz} S_A^T$ we obtain

$$\sigma_B = S S_A \sigma_{sqz} S_A^T S^T$$

but since $S S_A = S_B$ this equation reduces to

$$\sigma_B = S_B \sigma_{sqz} S_B^T$$

which is exactly the covariance matrix that we obtain for the cluster B if we decide to act directly on vacuum modes.

We conclude that any cluster can be obtained from any other cluster, no matter its complexity or shape. Given the same initial squeezing, if we want to obtain a given cluster B there is no optimal choice and every cluster A is equivalent, from a theoretical point of view. This holds for every general symplectic matrix

4.1.2 EPR vs two-mode cluster state with equal squeezing

We build a two-mode linear cluster state using linear optics as explained in Section 3.2. The adjacency matrix of the cluster state is trivial, reading

$$V = \begin{pmatrix} 0 & 1 \\ 1 & 0 \end{pmatrix}$$

and the transformation we need to implement on the momentum-squeezed modes to obtain such a cluster is

$$S = \begin{pmatrix} \frac{1}{\sqrt{2}} & 0 & 0 & -\frac{1}{\sqrt{2}} \\ 0 & \frac{1}{\sqrt{2}} & -\frac{1}{\sqrt{2}} & 0 \\ 0 & \frac{1}{\sqrt{2}} & \frac{1}{\sqrt{2}} & 0 \\ \frac{1}{\sqrt{2}} & 0 & 0 & \frac{1}{\sqrt{2}} \end{pmatrix}$$

The covariance matrix of the resulting finite-squeezed cluster state is given by $\sigma_{cluster} = S\sigma_{sqz}S^T$, where σ_{sqz} is the covariance matrix for the squeezed states, that reads

$$\sigma_{sqz} = \begin{pmatrix} s & 0 & 0 & 0 \\ 0 & s & 0 & 0 \\ 0 & 0 & \frac{1}{s} & 0 \\ 0 & 0 & 0 & \frac{1}{s} \end{pmatrix}$$

where $s = e^{2r}$, which permits us to get a covariance matrix

$$\sigma_{cluster} = \begin{pmatrix} \frac{1}{2s} + \frac{s}{2} & 0 & 0 & -\frac{1}{2s} + \frac{s}{2} \\ 0 & \frac{1}{2s} + \frac{s}{2} & -\frac{1}{2s} + \frac{s}{2} & 0 \\ 0 & -\frac{1}{2s} + \frac{s}{2} & \frac{1}{2s} + \frac{s}{2} & 0 \\ -\frac{1}{2s} + \frac{s}{2} & 0 & 0 & \frac{1}{2s} + \frac{s}{2} \end{pmatrix} \quad (4.4)$$

and using Eq. (1.31) we get the Wigner function

$$W(q_1, q_2, p_1, p_2) = \frac{1}{4\pi^2} \exp \left\{ -(q_1^2 + q_2^2 + p_1^2 + p_2^2) \left(\frac{1}{4s} + \frac{s}{4} \right) + (p_2q_1 + p_1q_2) \left(-\frac{1}{2s} + \frac{s}{2} \right) \right\} \quad (4.5)$$

which can be written exactly as Eq.(2.7) by exchanging q_2 with p_2 and p_2 with $-q_1$, so that it exhibit correlation between q_1 and p_2 and between q_2 and p_1 , approximating the behavior $\delta(q_1 - p_2)\delta(q_2 - p_1)$ for $r \rightarrow \infty$. This state can be used to perform quantum teleportation protocols as described in Section 2.3, by opportunely changing the quadrature measurement done by Alice and the quadrature displacement done by Bob.

4.1.3 Is the 3-modes cluster an EPR channel?

We just showed that we get an EPR state from two modes that are disconnected from the rest of the graph. What happens if the two modes out of which we want to create

a teleportation channel are entangled with a third mode? Does this connection with another mode affects the correlation between the two? If the third connection does not affect the two modes, in fact we wouldn't even need to perform the global transformation explained above in order to disconnect the third node.

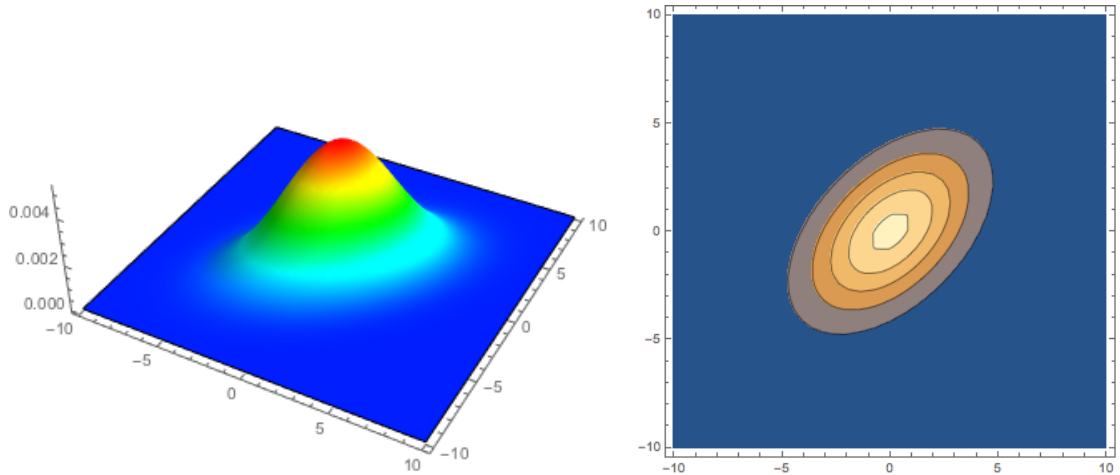
We start from squeezed vacuum states with the same level of squeezing and we implement a linear 3-mode cluster. We get the following covariance matrix

$$\sigma_{cluster} = \begin{pmatrix} \frac{1}{3s} + \frac{2s}{3} & 0 & \frac{1}{3s} - \frac{s}{3} & 0 & -\frac{1}{3s} + \frac{s}{3} & 0 \\ 0 & \frac{2}{3s} + \frac{s}{3} & 0 & -\frac{1}{3s} + \frac{s}{3} & 0 & -\frac{1}{3s} + \frac{s}{3} \\ \frac{1}{3s} - \frac{s}{3} & 0 & \frac{1}{3s} + \frac{2s}{3} & 0 & -\frac{1}{3s} + \frac{s}{3} & 0 \\ 0 & -\frac{1}{3s} + \frac{s}{3} & 0 & \frac{2}{3s} + \frac{s}{3} & 0 & -\frac{1}{3s} + \frac{s}{3} \\ -\frac{1}{3s} + \frac{s}{3} & 0 & -\frac{1}{3s} + \frac{s}{3} & 0 & \frac{1}{3s} + \frac{2s}{3} & 0 \\ 0 & -\frac{1}{3s} + \frac{s}{3} & 0 & -\frac{1}{3s} + \frac{s}{3} & 0 & \frac{2}{3s} + \frac{s}{3} \end{pmatrix}$$

If we look only at the subsystem of the nodes 1 and 2, by performing the partial trace over the mode 3, we obtain the following Wigner function

$$W_{1,2} \propto \exp \left\{ -\frac{\frac{s}{4} \left(s^2 + \frac{1}{2} \right)}{s^2 + \frac{1}{2}} (p_1^2 + q_2^2) + \frac{s^2 + \frac{1}{2}}{s(s^2 + 2)} (p_2^2 + q_1^2) \right. \\ \left. \frac{s^2 - 1}{s(s^2 + 2)} p_2 q_1 + \frac{\frac{s}{2} (s^2 - 1)}{s^2 + \frac{1}{2}} p_1 q_2 \right\} \quad (4.6)$$

plotted in Figure 4.1 for $s = 10$, i.e. for -10 dB of squeezing in the p-quadrature. Even if



(a) Plot of the Wigner function for $p_1 = q_2 = 0$.

(b) Contour plot of the Wigner function for $p_1 = q_2 = 0$.

Figure 4.1: Plot of the section $p_1 = q_2 = 0$ of the reduced Wigner of Eq. (4.6) which shows the correlation of the quadratures q_1 and p_2 for $s = 10$.

some correlation is present, we see that the Wigner function of Eq. (4.6) differs from the one obtained in Eq. (4.5) and thus the reduced state of the modes 1 and 2 cannot even

approximate the behavior $\delta(q_1 - p_2)\delta(q_2 - p_1)$ typical of an ideal EPR state, even if we started with states with a high level of squeezing. Moreover, correlations are present also between the mode 3 and the other nodes (we can find the same kind of Wigner function of Eq.(4.6) for nodes 2 and 3, by tracing out the node 1. This means that any operation made by using node 1 and 2 will have some effect on node 3, which will then have some information on the protocol. The teleportation is still possible without making any global or local transformation in a connected cluster but in a MBQC framework and/or adding measurements to our procedure, which effectively disconnect the third node of the cluster..

4.1.4 Global linear optics transformations on Quantum Network to get an EPR state

We ask ourselves a question: given a cluster, or more generally a quantum network, whose adjacency matrix will be denoted by V_{in} , is it possible to implement a linear optics transformation to get an EPR state, disconnected from the rest of the graph, with the aim of creating a good teleportation channel? So we are working in the frame introduced above in Section 4.1.1, considering: i) the particular case of linear optics transformation and ii) a transformation that will result in modifying the correlations of two specific nodes of the final cluster. For the moment we will restrict ourselves to global transformations, later we will see what is going to happen if we add other constrains, for example in the case where only local transformations on a set of modes are allowed.

In the following we will consider V_{in} to be the adjacency matrix of a 6-mode grid cluster (shown in Section 3.3.3) and we want to act on it with a linear optics transformation to obtain an EPR channel out of two given modes, say 1 and 4, thus creating a connection between them and disconnecting them from the other modes. These actions will result in a graph state with adjacency matrix V_{out} that reads

$$V_{out} = \begin{pmatrix} 0 & 0 & 0 & 1 & 0 & 0 \\ 0 & 0 & 0 & 0 & 0 & 0 \\ 0 & 0 & 0 & 0 & 1 & 0 \\ 1 & 0 & 0 & 0 & 0 & 0 \\ 0 & 0 & 1 & 0 & 0 & 1 \\ 0 & 0 & 0 & 0 & 1 & 0 \end{pmatrix}$$

In Section 4.1.1 we saw that the covariance matrix of a cluster with a given adjacency matrix V_{out} is independent of the transformations implemented to obtain it and it can be found by simply acting on a set of given vacuum modes with a symplectic matrix S . To obtain the graph state with adjacency matrix V_{out} we will thus build the cluster via linear optics as explained in Section 3.2 acting directly on the vacuum squeezed modes. Moreover, we will use the optimization of Section 3.3.2 using the function f_2 of Eq. (3.16) to optimize the nullifiers of two given modes, say 1 and 4. The set of squeezing values we will use is $\{-10, -10, -5, -4, -2, -2\}$, where for simplicity and without loss of generality we set the two highest squeezing values to the same value. The covariance matrix of the

cluster with adjacency matrix V_{out} reads

$$\sigma_{out} = \begin{pmatrix} \underline{5.05} & 0. & 0. & 0. & 0. & 0. & 0. & 0. & 0. & \underline{4.95} & 0. & 0. \\ 0. & 3.98107 & 0. & 0. & 0. & 0. & 0. & 0. & 0. & 0. & 0. & 0. \\ 0. & 0. & 2.7724 & 0. & 0. & 0.777142 & 0. & 0. & 0. & 0. & 0.731163 & 0. \\ 0. & 0. & 0. & \underline{5.05} & 0. & 0. & \underline{4.95} & 0. & 0. & 0. & 0. & 0. \\ 0. & 0. & 0. & 0. & 0.251289 & 0. & 0. & 0. & 0.0517624 & 0. & 0. & 0.0517624 \\ 0. & 0. & 0.777142 & 0. & 0. & 2.7724 & 0. & 0. & 0. & 0. & 0.731163 & 0. \\ 0. & 0. & 0. & \underline{4.95} & 0. & 0. & \underline{5.05} & 0. & 0. & 0. & 0. & 0. \\ 0. & 0. & 0. & 0. & 0. & 0. & 0. & 0.251189 & 0. & 0. & 0. & 0. \\ 0. & 0. & 0. & 0. & 0.0517624 & 0. & 0. & 0. & 0.402119 & 0. & 0. & -0.0990681 \\ \underline{4.95} & 0. & 0. & 0. & 0. & 0. & 0. & 0. & 0. & 0. & \underline{5.05} & 0. \\ 0. & 0. & 0.731163 & 0. & 0. & 0.731163 & 0. & 0. & 0. & 0. & 4.28071 & 0. \\ 0. & 0. & 0. & 0. & 0.0517624 & 0. & 0. & 0. & -0.0990681 & 0. & 0. & 0.402119 \end{pmatrix}$$

If we look at the numbers in the covariance matrix we see that the reduced matrix obtained by considering modes 1 and 4 looks exactly as the EPR cluster state covariance matrix we found in Subsection 4.1.2 for $s = 10$. In addition, there is no correlation between the nodes 1 and 4 and the other nodes.

However, to be rigorous, we will verify this fact by using again the Wigner function formalism. From the covariance matrix $\sigma_{cluster}$ it's possible to obtain the Wigner function of the cluster state, being the cluster state a Gaussian state. The reduced Wigner function for the modes 1 and 4, which is the equivalent of the partial trace for the density operator, can be obtained by integrating out the other modes, as

$$W_{1,4}(x_1, x_4, p_1, p_4) = \int \prod_{i \neq 1,4} dx_i dp_i W(\mathbf{x}, \mathbf{p})$$

where $\mathbf{x} = (x_1, \dots, x_6)$ and $\mathbf{p} = (p_1, \dots, p_6)$.

Carrying out the computation we obtain

$$W_{1,4} = \frac{1}{4\pi^2} e^{\frac{1}{2}(-\alpha q_4^2 + \beta p_1 q_4 - \alpha p_1^2 - \alpha q_1^2 + \beta q_1 p_4 - \alpha p_4^2)}$$

where $\alpha = 5.05$ and $\beta = 9.9$, which is exactly equivalent to the Wigner function of Eq. (4.5) found in Subsection 4.1.2 for a 2-mode cluster state for $s = 10$. We conclude that via an optimized global transformation on a cluster state it is possible to obtain an EPR-like state out of two desired nodes.

4.2 Local linear optics transformations for entanglement percolation

We saw that it's always possible, given a cluster, to implement a global transformation on it with the aim of creating an EPR channel out of two given nodes. Now let's try to complicate this scenario. We imagine to distribute the modes of the cluster to two spatially separated parties, such that each party is allowed to perform *local* linear optical transformations only on its set of nodes. This scenario is interesting because we want to check the versatility of a complex cluster as a resource to distribute, with the hope that it could be easily re-shaped according to the protocol the two parties would like to perform.

4.2.1 Local transformations for two parties

Let's say n and p are the number of nodes of party A and B respectively. In [69] is shown how a local transformation is implemented. Let's imagine we want to act with a local linear optical transformation $S_{n-local}$ on the n modes and with a local linear optical transformation $S_{p-local}$ on the p modes, namely

$$S_{n-local} = \begin{pmatrix} X_1 & -Y_1 \\ Y_1 & X_1 \end{pmatrix}, \quad S_{p-local} = \begin{pmatrix} X_2 & -Y_2 \\ Y_2 & X_2 \end{pmatrix} \quad (4.7)$$

where X_1 and Y_1 are $n \times n$ matrices while X_2 and Y_2 are $p \times p$ matrices. The transformation acting on the whole set of modes then reads

$$S = \begin{pmatrix} X_1 & 0 & -Y_1 & 0 \\ 0 & X_2 & 0 & -Y_2 \\ Y_1 & 0 & X_1 & 0 \\ 0 & Y_2 & 0 & X_2 \end{pmatrix} \quad (4.8)$$

where the 0 on the first and third line represents a $n \times p$ null matrix while the 0 on the second and fourth line represents a $p \times n$ null matrix. We already saw in Section 3.2 that a linear transformation on the quadrature operators of the kind represented in Eq (4.7) corresponds to a unitary operator $U = X + iY$ acting on the annihilation operators. We can thus rewrite Eq (4.8) in terms of the unitary matrices as

$$S = \begin{pmatrix} \text{Re}(U_1) & 0 & -\text{Im}(U_1) & 0 \\ 0 & \text{Re}(U_2) & 0 & -\text{Im}(U_2) \\ \text{Im}(U_1) & 0 & \text{Re}(U_1) & 0 \\ 0 & \text{Im}(U_2) & 0 & \text{Re}(U_2) \end{pmatrix} \quad (4.9)$$

where U_1 and U_2 are two unitary matrices parametrized respectively by n^2 and p^2 parameters. A method for the generation of numerically random unitary matrices is presented in [70], making use of n^2 angular parameters. It is to note that some of these parameters are constrained to lie in the interval $[0, \pi/2]$.

If we define $\sigma_{cluster1}$ as the covariance matrix of the cluster we are given and $\sigma_{cluster2}$ as the covariance matrix of the cluster we obtain after the transformation, it holds

$$\sigma_{cluster2} = S\sigma_{cluster1}S^T$$

where S is defined in Eq. (4.9). Our goal is to find the two matrices U_1 and U_2 , whose real and imaginary parts define S , such that $\sigma_{cluster2}$ is of the desired form. In our case we want $\sigma_{cluster2}$ to be such that, for two given nodes, we get an EPR channel. For this purpose we will use a Derandomized Evolution Strategy (DES) algorithm, presented in the next section.

4.2.2 Derandomized Evolution Strategy (DES)

The main idea underlying a Derandomized Evolutionary Strategies (DES) is the following. We start our ‘‘evolutionary journey’’ from a point of a *parameter landscape*,

where we indicate \mathbf{x} as the parameter of a given function $f(\mathbf{x})$ we want to optimize. We then proceed to “mutate” this point \mathbf{x}^{old} by generating λ new points (*offspring*) as

$$\mathbf{x}_k^{new} = \mathbf{x}^{old} + \Delta\mathbf{x}_k, \text{ where } k = 1, \dots, \lambda$$

where $\Delta\mathbf{x}_k$ is drawn from a multivariate normal distribution $\mathcal{N}(0, \sigma)$. The λ new points are then evaluated with respect to the chosen fitness function f and sorted. The μ “mutants” that provide the best result¹, after the evaluation, are chosen to generate a new parent as

$$\mathbf{x}^{new} = \sum_k w_k \mathbf{x}_k^{new}$$

where $\sum_k w_k = 1$.

We will use a DES presented in [16] as $(\mu-\lambda)$ *iso-CMA algorithm*, which is provided with a learning component.

Initialization of variables

This algorithm searches for *local* extremal points, moving in the direction of maximal ascent if we search for a maximum or descent if we search for a minimum. We may thus not find the global maximum we aim to search, thus the function may not be optimized at its best. On the other side DES algorithms have a high convergence speed.

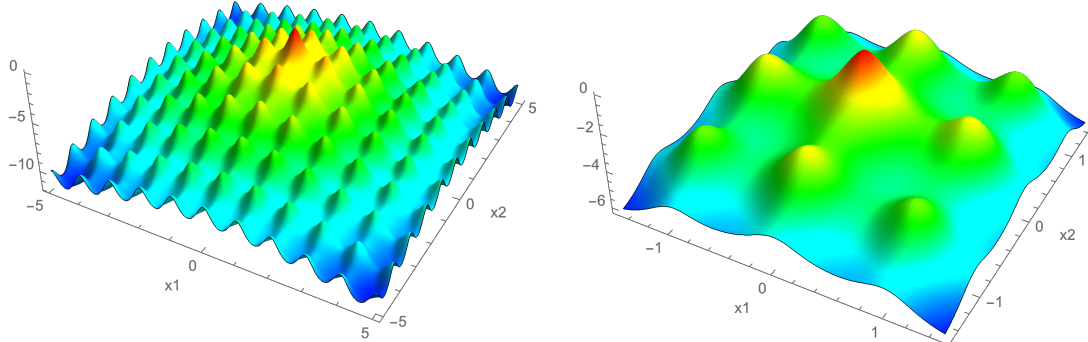
The local extremum \mathbf{x}^{best} we find generally may depend on the starting point on the parameter landscape, which we have to choose. To better understand this let’s pick a “test function” with a high number of local extrema, such as the Ackley function. We will see how the result of the single run of the algorithm may depend on the initialization of the variables, i.e. the starting point on our landscape but how in most of the cases, even if there is no guarantee to always find a global maximum, if we deal with a not strongly irregular function, running the algorithm multiple times it converges to the global maximum independently from the starting point, as we will see in the following example. Let’s pick the 2-dimensional Ackley function

$$f_{Ackley}(x_1, x_2) = 20 - 20 \cdot \exp\left(-0.2\sqrt{\frac{x_1^2}{2} + \frac{x_2^2}{2}}\right) \\ + e - \exp\left(\frac{\cos(2\pi x_1)}{2} + \frac{\cos(2\pi x_2)}{2}\right)$$

and let’s search for the minima of the Ackley function or, equivalently, for the maxima of $-f_{Ackley}$, which is plotted in Figure 4.2.

Let’s work a bit on the initializations. Firstly, we initialized our variables with $\mathbf{x}^{(0)} = (0.3, 0.3)$, we set the number of generations n_{gen} to 100 and we ran the algorithm 10 times: we always got to the result $\mathbf{x}^{best} = (0.0, 0.0)$, which corresponds to the global maximum. Let’s see what happens when we initialize to different starting points. We

¹If we search for a minimum we will choose the μ mutants that will result in a lower value of the function with respect to the other $\lambda - \mu$ mutants, viceversa if we search for a maximum



(a) Plot in the range $[-5, +5] \times [-5, +5]$. (b) Plot in the range $[-1.5, +1.5] \times [-1.5, +1.5]$.

Figure 4.2: Plot of $-f_{Ackley}$

see from the results of Table 4.1 that by choosing a different starting point the algorithm finds in general a different local maximum at every run, local maxima that are shown in Figure 4.2, and in general the function is not optimized at its best, i.e. we are not guaranteed to have found the global maximum. Moreover, we see the algorithm in general doesn't make "big jumps" to maxima that are far away but it finds the maxima which in the neighborhood of the starting point $\mathbf{x}^{(0)}$, except for the case of the global maximum. We see indeed that the global maximum can be found even we begin our search "far away" from it.

Constraints on variables

In some problems we may want to give constraints to the variables, for example we may want to accept variables that lay in the interval $[a, b]$. We may achieve this result by adding a penalty term to our fitness function.

For example, let's say that in the case of f_{Ackley} we want to select only variables such that each variable belongs to the interval $[-0.8, 0.8]$. This means that if we start from $\mathbf{x}^{(0)} = (0.75, 0.75)$ as before we should only find the $\mathbf{x}^{best} = (0.0, 0.0)$ result. A suitable choice could be for example the ramp function². We will thus evaluate the function

$$f(x_1, x_2) = f_{Ackley}(x_1, x_2) + 10000 \cdot [R(|x_1| - 0.8) + R(|x_2| - 0.8)]$$

Initializing the variables as $\mathbf{x}^{(0)} = (0.75, 0.75)$ and running the algorithm 30 times with $n_{gen} = 200$, we find only the $\mathbf{x}^{best} = (0.0, 0.0)$ solution now.

Luckily, there was a local maxima in our selected region $[-0.8, 0.8] \times [-0.8, 0.8]$. We want to check what happens if there are no local maxima of the function. Ideally, we want the algorithm to stop in the maximal value it encounters without exceeding the

²An attempt has been made with the Heaviside step function but the discontinuity sometimes brings the algorithm to "fall off" the step and to search outside the boundaries.

$\mathbf{x}^{(0)}$	\mathbf{x}^{best}	$-f_{Ackley}$	N
	(0.0, 0.0)	0.0	3
(0.75, 0.75)	(0.976714, 0.976714)	-2.60915	3
	(0, 0.965488)	-1.87233	3
	(0.965488, 0)	-1.87233	1
	(0.0, 0.0)	0.0	4
(4.7, 4.7)	(4.98692, 4.98692)	-10.1295	4
	(4.98454, 3.98764)	-9.44704	3
	(3.98491, 3.98491)	-8.6285	1
	(0.0, 0.0)	0.0	8
(9.5, 8.5)	(8.99162, 7.99255)	-13.9978	2

Table 4.1: Results obtained running the DES algorithm 10 times for the fitness function $-f_{Ackley}$ for $n_{gen} = 100$ and for different starting points $\mathbf{x}^{(0)}$, where N indicates the number of times the corresponding value \mathbf{x}^{best} was found

boundaries of the region. We will check that this is what happens. Let's for example pick the function

$$f_{sin}(x_1, x_2) = \sin(x_1) + \sin(x_2)$$

Without putting constraints on the variables, starting from the values of $\mathbf{x}^{(0)} = (0.75, 0.75)$

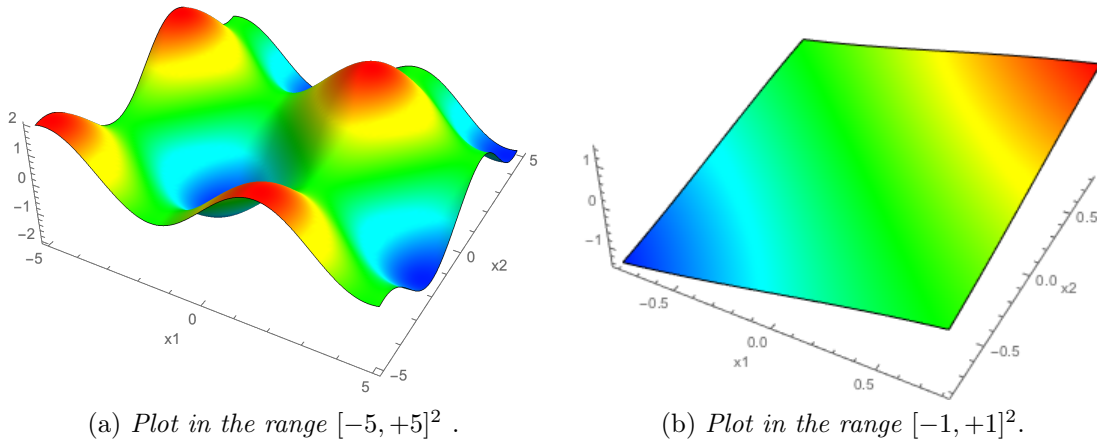


Figure 4.3: Plot of f_{sin}

and running the algorithm 30 times with $n_{gen} = 200$, we always get to the value $\{1.5708, 1.5708\}$, a maxima we can clearly see in Figure 4.3a. Now assume we want to constrain our parameters to the region $[-0.8, 0.8] \times [-0.8, 0.8]$, shown in Figure 4.3b, from which it's evident that . We will run the algorithm on the fitness function

$$f_{sin}(x_1, x_2) = \sin(x_1) + \sin(x_2) - 10000 \cdot R(|x_1| - 0.8) + R(|x_2| - 0.8)]$$

Running the algorithm 30 times with $n_{gen} = 200$, we always get a value which exceeds only slightly the value $\mathbf{x}^{max} = (0.8, 0.8)$, “only slightly” meaning that we get values $\mathbf{x}^{best} = (0.8 + a, 0.8 + b)$ with $a, b \sim 10^{-5}$. If we want to remain strictly inside the boundaries we can modify the ramp function accordingly as $R(|x| - 0.8 - \epsilon)$, with $\epsilon \ll 1$ but $\epsilon > a, b$.

4.2.3 Fitness function for the creation of an EPR channel via local transformations

From Subsection 4.2.1 we saw that our goal is to find two suitable unitary matrices U_1 and U_2 with n^2 and p^2 parameters respectively. Then $n^2 + p^2$ will be the dimension of the parameter space of the algorithm, i.e. the number of parameters the algorithm has to “work with” to optimize the function.

We note that in the implementation of our optimization function, $\sigma_{cluster1}$ is a fixed matrix as it corresponds to the resource we are given. $\sigma_{cluster2}$, which depends on the parametrization of U_1 and U_2 should reflect the fact that 2 chosen nodes represent an EPR state, and it should be as close as possible to an ideal result for our aim, a covariance matrix σ_{ideal} . We can for example impose that, if the nodes N_1 and N_2 are the nodes out of which we want to obtain an EPR state, we can define

$$\sigma_{cluster2,red}(N_1, N_2) = \begin{pmatrix} \sigma_{cluster2, N_1} \\ \sigma_{cluster2, N_2} \\ \sigma_{cluster2, N_2+n+p} \\ \sigma_{cluster2, N_2+n+p} \end{pmatrix}$$

as the reduced $4 \times 2(n + p)$ matrix obtained by selecting only the rows of $\sigma_{cluster2}$ we want to fix as an EPR. We thus define the $4 \times 2(n + p)$ matrix σ_{ideal} as the matrix with null entries except for

$$\begin{aligned} \sigma_{1, N_1} = \sigma_{2, N_2} = \sigma_{3, N_1+n+p} = \sigma_{4, N_2+n+p} &= \lambda \\ \sigma_{1, N_2+p+n} = \sigma_{2, N_1+p+n} = \sigma_{3, N_2} = \sigma_{4, N_1} &= \mu \end{aligned}$$

given a fixed value of squeezing s , $\lambda = 1/2s + s/2$ and $\mu = -1/2s + s/2$, according to the covariance matrix of a two-modes cluster of Eq.(4.4). We thus will search for the minimal value of the function

$$f_{opt} = \|\sigma_{ideal,red} - \sigma_{cluster2,red}(N_1, N_2)\| \quad (4.10)$$

where $\|\cdot\|$ indicates the Frobenius norm.

We stress out the fact that to get a good EPR channel we need $f_{opt} \sim 0$, i.e. a global minimum. Since the algorithm described in 4.2.2 searches for local extrema, the algorithm may converge but we may not reach the desired value $f_{opt} \sim 0$.

4.2.4 Creation of an EPR channel via local transformations on given graphs

A well-known case

Let's give an example with a well-known case [71], namely a 4-mode *weighted* cluster, i.e. a cluster whose adjacency matrix has elements which can be different from 1 and 0, described by the adjacency matrix

$$V = \begin{pmatrix} 0 & 0 & \frac{1}{\sqrt{2}} & -\frac{1}{\sqrt{2}} \\ 0 & 0 & \frac{1}{\sqrt{2}} & \frac{1}{\sqrt{2}} \\ \frac{1}{\sqrt{2}} & \frac{1}{\sqrt{2}} & 0 & 0 \\ -\frac{1}{\sqrt{2}} & \frac{1}{\sqrt{2}} & 0 & 0 \end{pmatrix}$$

We implemented the cluster with equal values of squeezing on the vacuum modes set to -10 dB. Let's suppose we want an EPR state out of the modes 1 and 3: we thus minimize the function of Eq. (4.10) with $N_1 = 1$ and $N_2 = 3$. We run the algorithm setting $n_{gen} = 600$ and we get to a value $f_{opt} \sim 10^{-10}$, concluding that we have indeed found a suitable transformation for the construction of an EPR channel. The linear optical transformation that has to be performed locally on each set of nodes is of the form (1.42) with

$$X_{1,2} = \begin{pmatrix} 0.157242 & 0.157242 \\ -0.353826 & 0.353826 \end{pmatrix}, \quad Y_{1,2} = \begin{pmatrix} 0.689402 & 0.689402 \\ -0.612215 & 0.612215 \end{pmatrix}$$

for the local transformation performed on the modes 1 and 2 and

$$X_{3,4} = \begin{pmatrix} 0.222379 & -1.9 \cdot 10^{-6} \\ -8.8 \cdot 10^{-7} & 0.222379 \end{pmatrix}, \quad Y_{3,4} = \begin{pmatrix} -0.97496 & 1.9 \cdot 10^{-6} \\ -2.5 \cdot 10^{-6} & -0.97496 \end{pmatrix}$$

These matrices are not unique. We found indeed other linear optical transformation that led to the same result.

Successful establishment of an EPR link

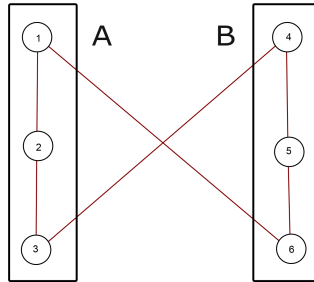


Figure 4.4: 6-mode cluster distributed among two players A and B.

We implemented a 6-mode cluster and we distributed its modes as shown in Figure 4.4, setting $n_{gen} = 5000$. We then used the algorithm to create an EPR channel out of modes 1 and 6. The linear optical transformation both teams have to perform on their set of nodes is of the form (1.42) with

$$X = X_A = \begin{pmatrix} 0.28259 & 0.28259 & \mathcal{O}(10^{-9}) \\ -0.618453 & 0.618453 & \mathcal{O}(10^{-9}) \\ \mathcal{O}(10^{-9}) & \mathcal{O}(10^{-9}) & 0.859636 \end{pmatrix}$$

$$Y = Y_A = \begin{pmatrix} 0.648184 & 0.648184 & \mathcal{O}(10^{-9}) \\ 0.342806 & -0.342806 & \mathcal{O}(10^{-9}) \\ \mathcal{O}(10^{-9}) & \mathcal{O}(10^{-9}) & 0.510906 \end{pmatrix}$$

for “team A” and

$$X = X_B = \begin{pmatrix} 0.618454 & -1.8 \cdot 10^{-6} & -0.618452 \\ -0.707085 & \mathcal{O}(10^{-7}) & -0.707089 \\ \mathcal{O}(10^{-8}) & 0.9672 & 1.1 \cdot 10^{-6} \end{pmatrix}$$

$$Y = Y_B = \begin{pmatrix} 0.342807 & 2.9 \cdot 10^{-6} & -0.342803 \\ -0.00532526 & 1.3 \cdot 10^{-6} & -0.0053229 \\ 1.6 \cdot 10^{-6} & 0.254018 & -3.1 \cdot 10^{-6} \end{pmatrix}$$

for “team B”. It is also possible, using linear optics, to create an EPR channel between the nodes 1 and 4 and between the nodes 1 and 5, as the results reported in Appendix A show.

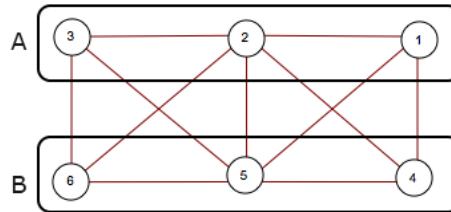


Figure 4.5: 6-mode cluster distributed among two players A and B.

We tried also to establish an EPR link between the nodes 1 and 6 of the graph of Figure 4.5, setting $n_{gen} = 5000$. We found it is indeed possible, if “team A” performs the transformation characterized by

$$X_A = \begin{pmatrix} -0.0388494 & \mathcal{O}(10^{-10}) & 0.0388494 \\ -0.0711785 & -0.340491 & -0.0711785 \\ -0.684642 & -0.0595105 & -0.684642 \end{pmatrix}$$

$$Y_A = \begin{pmatrix} -0.706039 & \mathcal{O}(10^{-10}) & 0.706039 \\ -0.0517365 & 0.931976 & -0.0517365 \\ 0.153369 & -0.109291 & 0.153369 \end{pmatrix}$$

and “team B” performs

$$X_B = \begin{pmatrix} -0.374838 & 0.817445 & -0.374838 \\ -0.575589 & -0.54852 & -0.575589 \\ -0.0388494 & \mathcal{O}(10^{-10}) & 0.0388494 \end{pmatrix}$$

$$Y_B = \begin{pmatrix} 0.159338 & \mathcal{O}(10^{-9}) & 0.159338 \\ 0.0529694 & -0.175812 & 0.0529694 \\ 0.706039 & \mathcal{O}(10^{-10}) & -0.706039 \end{pmatrix}$$

It was also possible to find the transformations for the creation of an EPR channel between the nodes 1 and 4 and between the nodes 1 and 5. The results are found in Appendix A.

Lastly, the so-called “grid” topology was investigated, for 6, 8 and 10 nodes. We tried to establish an EPR link between a belonging to Alice, and all the nodes belonging to Bob and we could always find a suitable transformation for this specific task. For example, for the 10-nodes grid of Fig. 4.6, setting $n_{gen} = 8000$, the transformations to establish an EPR link between the nodes 1 and 9 of Alice and Bob are

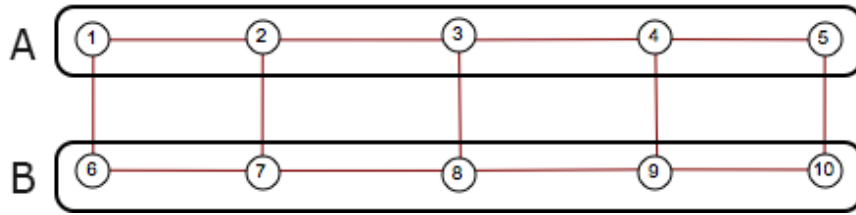


Figure 4.6: 10-mode cluster distributed among two players A and B.

$$X_A = \begin{pmatrix} \mathcal{O}(10^{-17}) & \mathcal{O}(10^{-16}) & \mathcal{O}(10^{-16}) & \mathcal{O}(10^{-16}) & \mathcal{O}(10^{-16}) \\ 0.403474 & -0.0870331 & 0.166897 & \mathcal{O}(10^{-17}) & -0.236577 \\ -0.0643617 & -0.906976 & 0.16927 & \mathcal{O}(10^{-17}) & 0.233632 \\ 0.0572625 & -0.347792 & -0.144588 & \mathcal{O}(10^{-16}) & -0.20185 \\ \mathcal{O}(10^{-17}) & \mathcal{O}(10^{-17}) & \mathcal{O}(10^{-16}) & 0.955786 & \mathcal{O}(10^{-17}) \end{pmatrix}$$

$$Y_A = \begin{pmatrix} 0.57735 & \mathcal{O}(10^{-16}) & -0.57735 & \mathcal{O}(10^{-16}) & 0.57735 \\ 0.502183 & -0.126409 & -0.168164 & \mathcal{O}(10^{-17}) & -0.670347 \\ -0.173667 & 0.0831156 & -0.224432 & \mathcal{O}(10^{-16}) & -0.0507651 \\ 0.462716 & 0.16116 & 0.714566 & \mathcal{O}(10^{-17}) & 0.25185 \\ \mathcal{O}(10^{-16}) & \mathcal{O}(10^{-16}) & \mathcal{O}(10^{-18}) & 0.294062 & \mathcal{O}(10^{-16}) \end{pmatrix}$$

for Alice and

$$X_B = \begin{pmatrix} 0.00619455 & 0.208494 & -0.135882 & 0.0903469 & -0.142077 \\ 0.673557 & -0.12453 & 0.00171553 & 0.163035 & -0.671842 \\ 0.103711 & 0.491517 & -0.0277931 & -0.806682 & -0.131504 \\ 0.417499 & 0.13029 & 0.796662 & 0.023899 & 0.379164 \\ \mathcal{O}(10^{-17}) & \mathcal{O}(10^{-17}) & \mathcal{O}(10^{-16}) & \mathcal{O}(10^{-17}) & \mathcal{O}(10^{-16}) \end{pmatrix}$$

$$Y_B = \begin{pmatrix} 0.0336493 & -0.8152 & 0.0854874 & -0.483736 & 0.0518381 \\ 0.0179886 & -0.0216224 & 0.028614 & 0.22613 & 0.0106254 \\ -0.162267 & -0.0229788 & 0.00478799 & 0.155128 & 0.167055 \\ -0.0100478 & -0.130045 & -0.0678698 & -0.0689169 & -0.057822 \\ -0.57735 & \mathcal{O}(10^{-16}) & 0.57735 & 0 & -0.57735 \end{pmatrix}$$

for Bob. Additional results for the “grid” clusters are reported in Appendix A.

For all the graphs implemented in above it was possible to find an entanglement link between nodes belonging to the two parties. It was not possible, however, to find a linear optical transformation to create an EPR channel out of nodes belonging to the same team, for example 1 and 3 or 1 and 2. This was instead possible with the fully connected cluster of Fig. 3.5³, as it can be seen in Appendix A. This suggests that, in most cases, a player cannot disconnect some of his nodes from the portion that belong to the other player via linear optical transformation. We need either a global transformation, or to introduce some projective measurement.

We remark that using this method the correlations between the nodes of the EPR channel and the other nodes are not identically zero, but they depend on the value of f_{opt} of Eq. (4.10), thus in general they decrease if we increase the number of generations n_{gen} . In the results presented in this Section, these correlations take values at most of the order of 10^{-15} , being f_{opt} of the same order. Moreover, while for these clusters it was possible to create EPR links between two nodes belonging to different parties, we couldn’t find a suitable transformation to establish an EPR link between nodes of the same party. This was instead possible with the fully connected cluster of Figure 3.5. We remark that, however, for the fully connected cluster, it wasn’t possible to find transformations for the creation of an EPR link between two different parties.

Unsuccessful establishment of an EPR link

We tried to establish an EPR link between Alice and Bob for the clusters of Fig. 4.7 and for the fully connected cluster of Fig. 3.5 (for which we considered nodes 1, 2, 3 belonging to Alice and nodes 4, 5, 6 belonging to Bob) but the desired solution wasn’t found.

³We remark that, however, for the fully connected cluster it wasn’t possible to find transformation connecting two nodes of separate teams, as we will see shortly.

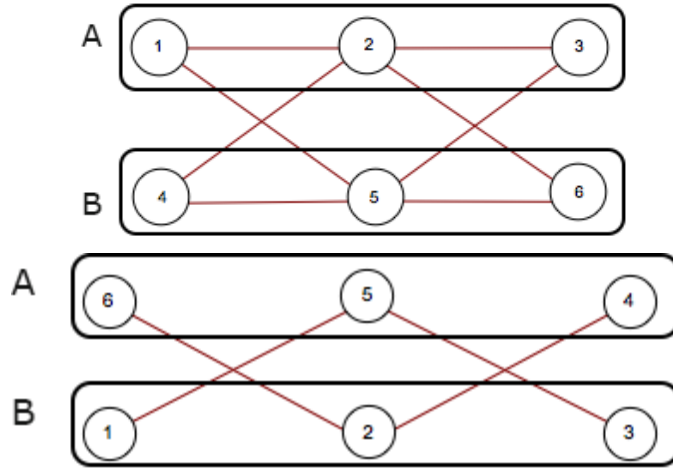


Figure 4.7: 6-mode cluster distributed among two players A and B.

We remark that this doesn't exclude the fact that the solution exists.

Comments

The DES can be used with a suitable fitness function to find the desired local operations to implement on the quantum network with the aim of reshaping it to perform specific tasks. In the case of the creation of an EPR channel the use of the fitness function of Section 4.2.3 effectively brings results.

A disadvantage of this approach is that with the DES we find in general the local extrema, while for the specific task of the creation of an EPR channel we need the global extremum, as we search for the specific value $f_{opt} \sim 0$ of a non-negative function. Running the algorithm various times and changing the starting point in the parameter space may help to tackle this problem. Moreover, even if we don't find the desired solution $f_{opt} \sim 0$ we cannot be sure that it doesn't exist, so we cannot conclude with certainty that there is no way to create an EPR channel with a given quantum resource.

4.3 Measurement of nodes in cluster states

In this section we will show how the statistical moments of our quantum system change if we measure one or multiple nodes. In particular, we will see how to re-shape our cluster with *node removal* or *wire-shortening* operations via homodyne measurements.

4.3.1 Measurements in the characteristic function formalism

We define the vector $\hat{\mathbf{R}} = (\hat{q}_1, \hat{p}_1, \dots, \hat{q}_N, \hat{p}_N)$ such that Eqs. (1.10) and (1.11) can be rewritten as

$$\left[\hat{R}_i, \hat{R}_j \right] = 2i\Omega_{ij}$$

where Ω is the N -symplectic form

$$\Omega = \bigoplus_{k=1}^n \omega, \quad \omega = \begin{pmatrix} 0 & 1 \\ -1 & 0 \end{pmatrix}$$

that satisfies $\Omega^T = \Omega^{-1} = -\Omega$. It is useful to rewrite also the Weyl displacement operator in terms of $\hat{\mathbf{R}}$

$$\hat{D}(\mathbf{x}) = e^{-i\mathbf{x}^T \Omega \hat{\mathbf{R}}}$$

where $\mathbf{x} \in \mathbb{R}^{2N}$. We see indeed that by setting $\mathbf{x} = 2(\text{Re}\alpha, \text{Im}\alpha)$ we recover the form of the Weyl operator of Eq. (1.16).

In Section 1.3 we saw how a quantum system characterized by the density matrix $\hat{\rho}$ can be described with a Wigner function. Equivalently, we may use the *characteristic function*

$$\chi_\rho(\mathbf{x}) = \text{Tr} \left[\hat{\rho} \hat{D}(\mathbf{x}) \right],$$

which is related to the Wigner function via Fourier transform

$$W(\mathbf{x}) = \frac{1}{(2\pi)^{2N}} \int d^{2N} \mathbf{y} e^{-i\mathbf{x}^T \Omega \mathbf{y}} \chi_\rho(\mathbf{x})$$

where $\mathbf{y} \in \mathbb{R}^{2N}$ [72, 73].

The characteristic function for a Gaussian state $\hat{\rho}$ can be written as

$$\chi_\rho(\mathbf{x}) = e^{-\frac{1}{2} \mathbf{x}^T \Omega \sigma \Omega^T \mathbf{x} - i\mathbf{x}^T \Omega \langle \hat{\mathbf{R}} \rangle} \quad (4.11)$$

where $\sigma_{ij} = 1/2 \langle \hat{R}_i \hat{R}_j + \hat{R}_j \hat{R}_i \rangle - \langle \hat{R}_i \rangle \langle \hat{R}_j \rangle$ [72, 74]. Note that this definition of the covariance matrix, as well as the definition for the quadrature operators vector $\hat{\mathbf{R}}$, is different from the one we used in Eq. (1.32). The reason for this change of notation, to which we will stick throughout this whole section, arises from the fact that to implement measurements the covariance matrix will be decomposed in block form corresponding to the set of nodes that will be measured and to the set of nodes that won't be measured, as we will see shortly.

We will use the characteristic function formalism to show how the state of a multimode gaussian system $\hat{\rho}$ changes after some of its modes (subsystem B) are measured by the means of a gaussian measurement while the other modes (subsystem A) are left unchanged. Let's restrict for simplicity, and without loss of generalization, to the case in which subsystem B consists only on one mode. According to Eq. (1.28) the state $\hat{\rho}_A$ of the remaining modes after the measurement is

$$p(m) \hat{\rho}_A = \text{Tr}_B [\hat{\rho} (\mathbb{1}_A \otimes |m\rangle \langle m|)] \quad (4.12)$$

where $\mathbb{1}_A$ has the dimensionality of the subsystem A, so that, following the calculations in Appendix B, it can be expressed in the characteristic function formalism as

$$\chi_{\rho_A}(\mathbf{x}_A) = \frac{1}{p(m)} \frac{1}{2\pi} \int d^2 \mathbf{x}_B \chi_\rho(\mathbf{x}_A, \mathbf{x}_B) \chi_\omega(-\mathbf{x}_B) \quad (4.13)$$

If we are dealing with Gaussian states and Gaussian measurements, the characteristic functions are Gaussian as in Eq. (4.11). We define

$$\Gamma = \Omega\sigma\Omega^T \quad (4.14)$$

$$\mathbf{d} = \Omega\langle\hat{\mathbf{R}}\rangle \quad (4.15)$$

that are still good definition for the statistical momenta of a state as the canonical commutation relations are preserved, since Ω is a symplectic transformation.

Let's consider the covariance matrix of the whole state expressed in block form

$$\Gamma = \begin{pmatrix} A & C \\ C^T & B \end{pmatrix} \quad (4.16)$$

Substituting Γ in Eq.(4.11) and considering a Gaussian measurement, characterized by a projected state with statistical moments Γ_ω and D_ω , the normalized⁴ characteristic function of the system after the measurement reads

$$\chi_{\rho_A}(\mathbf{x}_A) = e^{-\frac{1}{2}\mathbf{x}_A^T[A-C(B+\Gamma_\omega)^{-1}C^T]\mathbf{x}_A - i\mathbf{x}_A^T[\mathbf{D}_A - C(B+\Gamma_\omega)^{-1}(\mathbf{D}_B - \mathbf{D}_\omega)]} \quad (4.17)$$

The calculations are shown in Appendix B. It follows that the statistical moments of the resulting state are

$$\Gamma' = A - C(B + \Gamma_\omega)^{-1}C^T \quad (4.18)$$

$$\mathbf{D}' = \mathbf{D}_A - C(B + \Gamma_\omega)^{-1}(\mathbf{D}_B - \mathbf{D}_\omega) \quad (4.19)$$

We stress out again that Γ and \mathbf{D} differ from the statistical moments σ and $\mathbf{d} = \langle\hat{\mathbf{R}}\rangle$, as we defined in Eqs. (4.14) and (4.15) but the relations of Eqs. (4.18) and (4.19) holds even for the statistical moments σ and d . This can be seen by a straightforward calculation using the definitions (4.14) and (4.15). Indeed, let's express the matrix σ in block matrix form as

$$\sigma = \begin{pmatrix} A_\sigma & C_\sigma \\ C_\sigma^T & B_\sigma \end{pmatrix}$$

then from block-matrix multiplication and the definition (4.14) it follows that

$$A = \Omega_1 A_\sigma \Omega_1^T$$

$$B = \Omega_2 B_\sigma \Omega_2^T$$

$$C = \Omega_1 C_\sigma \Omega_2^T$$

where Ω_1 and Ω_2 have the dimension of A and B respectively. From Eq. (4.18), simple algebraic calculations lead to

$$\sigma' = A_\sigma + C_\sigma[(B + \Gamma_\omega)]^{-1}C_\sigma^T$$

The same calculations can be carried out for the displacement vector.

⁴The normalization condition of the characteristic function is $\chi_\rho(\mathbf{0}) = 1$, that follows from the condition $\text{Tr}\hat{\rho} = 1$

4.3.2 Homodyne detection for node removal or wire-shortening

In the framework of the implementation of quantum teleportation between two given nodes, cluster state shaping via the removal of nodes may be a crucial step for the success of the operation. The removal of a given node is carried out by a measurement of the node in the computational basis, i.e. the position basis. A feedforward operation on the neighboring nodes, that corresponds to phase-space displacement of the quadratures, is then necessary to properly shape the resource state [56, 75].

Since we are given Gaussian resources, if we restrict ourselves to Gaussian measurements, such as the homodyne detection, we can work with the covariance matrix and the displacement vector of the state, analyzing how they change after performing the measurement operation.

Let's consider a $n + m$ mode Gaussian state with zero displacement vector and with covariance matrix

$$\Gamma = \begin{pmatrix} A & C \\ C^T & B \end{pmatrix}$$

where A and B are respectively a $n \times n$ matrix and $m \times m$ matrix describing the n -mode system and the m -mode system and C is a $n \times m$ matrix describing the correlations between them. Suppose that we want to perform a Gaussian measurement on the last m modes, projecting them into a pure Gaussian state with covariance matrix Γ_ω and displacement \mathbf{D}_ω . The resulting n -mode state will be characterized by a covariance matrix Γ' and a displacement vector \mathbf{D}' that, according to Eqs. (4.18) and (4.19) will read

$$\Gamma' = A - C(B + \Gamma_\omega)^{-1}C^T \quad (4.20)$$

$$\mathbf{D}' = C(B + \Gamma_\omega)^{-1}\mathbf{D}_\omega \quad (4.21)$$

[76, 77]. In the case of a homodyne measurement the covariance matrix Γ_ω will represent an infinitely squeezed state for each measured mode, as we will see in the following, and the displacement \mathbf{D}_ω will read $\mathbf{D}_\omega = (\bar{q}, 0)$ for a position measurement and $\mathbf{D}_\omega = (0, \bar{p})$ for a momentum measurement.

Indeed, let's consider the homodyne measurement of a single mode of our given resource, where the aim is to remove a node from the graph state. The covariance matrix Γ_ω is

$$\Gamma_\omega = \begin{pmatrix} \frac{1}{a^2} & 0 \\ 0 & a^2 \end{pmatrix}$$

where the limit $a \rightarrow 0$ represents a state infinitely squeezed in momentum, while the limit $a \rightarrow \infty$ represents a state infinitely squeezed in position, thus, respectively, a momentum measurement and a position measurement. In both cases we can identify the inverse matrix appearing in Eqs. (4.20) and (4.21) as

$$(B + \Gamma_\omega)^{-1} = \frac{1}{(b_1 a^2 + 1)(b_3 + a^2) - b_2^2 a^2} \begin{pmatrix} b_3 a^2 + a^4 & -b_2 a^2 \\ -b_2 a^2 & b_1 a^2 + 1 \end{pmatrix}$$

This is equivalent, in the limit cases where $a \rightarrow 0$ or $a \rightarrow \infty$, to identifying the inverse $(B + \Gamma_\omega)^{-1}$ with the matrix $(\pi B \pi)^{MP}$, where $\pi = \text{diag}(1, 0)$ in the case of a position measurement while $\pi = \text{diag}(0, 1)$ for a momentum measurement, and where the subscript MP denotes the Moore-Penrose inverse⁵ [72, 77].

Example: 3-mode cluster state Our aim is to carry out measurements on our quantum resource to shape it in a suitable way such that it will be possible to perform a given quantum computing or quantum communication task. We will concentrate on the creation of a quantum channel out of two desired nodes: it is thus necessary to analyze the effect of measurements and feed-forward operations on the cluster nodes.

We will consider the paradigmatic case of a 3-modes cluster state with equal squeezing on the 3 nodes. Here we will identify the squeezing degree with the parameter $s = e^{2r}$, such that the covariance matrix of the squeezed multimode vacuum takes the form

$$\sigma_{sqz} = \begin{pmatrix} s & 0 & 0 & 0 & 0 & 0 \\ 0 & \frac{1}{s} & 0 & 0 & 0 & 0 \\ 0 & 0 & s & 0 & 0 & 0 \\ 0 & 0 & 0 & \frac{1}{s} & 0 & 0 \\ 0 & 0 & 0 & 0 & s & 0 \\ 0 & 0 & 0 & 0 & 0 & \frac{1}{s} \end{pmatrix}$$

and, consequently, the covariance matrix of the 3-mode state reads, as a function of the parameter s ,

$$\sigma = \begin{pmatrix} \frac{2s}{3} + \frac{1}{3s} & 0 & 0 & \frac{s^2-1}{3s} & -\frac{s^2-1}{3s} & 0 \\ 0 & \frac{s^2+2}{3s} & \frac{s^2-1}{3s} & 0 & 0 & \frac{s^2-1}{3s} \\ 0 & \frac{s^2-1}{3s} & \frac{s^2+2}{3s} & 0 & 0 & \frac{s^2-1}{3s} \\ \frac{s^2-1}{3s} & 0 & 0 & \frac{2s}{3} + \frac{1}{3s} & \frac{s^2-1}{3s} & 0 \\ -\frac{s^2-1}{3s} & 0 & 0 & \frac{s^2-1}{3s} & \frac{2s}{3} + \frac{1}{3s} & 0 \\ 0 & \frac{s^2-1}{3s} & \frac{s^2-1}{3s} & 0 & 0 & \frac{s^2+2}{3s} \end{pmatrix} \quad (4.22)$$

where it is to stress out again that the covariance matrix is expressed using the convention $(q_1, p_1, \dots, q_N, p_N)$ for the quadratures vector. If we want to remove the third node, to obtain a quantum channel between nodes 1 and 2, we have to perform a q -measurement on the third node. The resulting statistical moments, obtained by using the Eqs. (4.20)

⁵The Moore-Penrose inverse (or pseudoinverse) of a matrix generalizes the notion of an inverse.

and (4.21), are

$$\sigma' = \begin{pmatrix} \frac{s(s^2+2)}{2s^2+1} & 0 & 0 & \frac{s(s^2-1)}{2s^2+1} \\ 0 & \frac{s^2+2}{3s} & \frac{s^2-1}{3s} & 0 \\ 0 & \frac{s^2-1}{3s} & \frac{s^2+2}{3s} & 0 \\ \frac{s(s^2-1)}{2s^2+1} & 0 & 0 & \frac{s(s^2+2)}{2s^2+1} \end{pmatrix} \quad (4.23)$$

$$\mathbf{d} = \begin{pmatrix} \frac{\bar{q}(1-s^2)}{2s^2+1} \\ 0 \\ 0 \\ -\frac{\bar{q}(s^2-1)}{2s^2+1} \end{pmatrix} \quad (4.24)$$

where \bar{q} represent the measured value of the position of the third node, obtained via homodyne detection. From (4.24) we see that measuring the node 3 causes a displacement in the quadratures of the nodes 1 and 2, so that a feed-forward operation, that will depend on the measured value \bar{q} and on the initial squeezing value s , has to be applied to these nodes. From Eq. (4.23) we may see that the resulting state, whose Wigner is depicted in Fig. 4.8 for $s = 10$, exhibits the behavior of a cluster-like EPR state, with correlations between the quadratures \hat{q}_1 and \hat{p}_2 and between the quadratures \hat{q}_2 and \hat{p}_1 . Indeed, after the feedforward operation, we have

$$\Delta^2(\hat{q}_1 - \hat{p}_2) + \Delta^2(\hat{q}_2 - \hat{p}_1) = \frac{6s}{2s^2 + 1} + \frac{2}{s} \xrightarrow{s \rightarrow \infty} 0$$

We point out the fact that the covariance matrix of (4.23) of the 2-mode state obtained

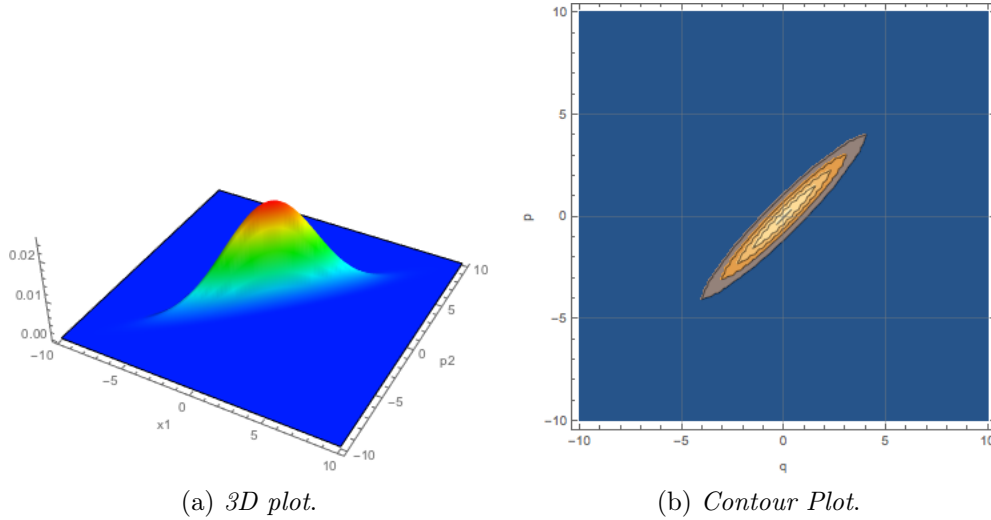


Figure 4.8: Plot of the section $q_2 = p_1 = 0$ of the Wigner function for the cluster state characterized by a covariance matrix given by Eq. (4.23) for $s = 10$.

after the measurement of the third node, in case of finite squeezing, will have different

values with respect to the covariance matrix of Eq. (4.4) of a 2-mode state directly built from two squeezed vacuum states with equal squeezing, which reads, conversely

$$\sigma_{cluster} = \begin{pmatrix} \frac{1}{2s} + \frac{s}{2} & 0 & 0 & -\frac{1}{2s} + \frac{s}{2} \\ 0 & \frac{1}{2s} + \frac{s}{2} & -\frac{1}{2s} + \frac{s}{2} & 0 \\ 0 & -\frac{1}{2s} + \frac{s}{2} & \frac{1}{2s} + \frac{s}{2} & 0 \\ -\frac{1}{2s} + \frac{s}{2} & 0 & 0 & \frac{1}{2s} + \frac{s}{2} \end{pmatrix}$$

and whose inseparability inequality reads

$$\Delta^2(\hat{q}_1 - \hat{p}_2) + \Delta^2(\hat{q}_2 - \hat{p}_1) = \frac{4}{s} \xrightarrow{s \rightarrow \infty} 0$$

exhibiting slightly less noise on the EPR-like quadratures⁶.

Another way of creating a quantum channel in this configuration is *wire shortening*. It consists of measuring the momentum of a node, which causes the node removal but keeps the connections of its neighbors. Thus, being provided with a linear 3-mode cluster, we can create an EPR channel out of the nodes 1 and 2, performing a q -measurement on the third node, but we can equivalently create an EPR channel out of the nodes 1 and 3, by measuring the momentum of the second node. This is done by reorganizing the entries of the covariance matrix of Eq. (4.22), such that it reflects the order $(\hat{q}_1, \hat{p}_1, \hat{q}_3, \hat{p}_3, \hat{q}_2, \hat{p}_2)$, namely

$$\sigma = \begin{pmatrix} \frac{2s}{3} + \frac{1}{3s} & 0 & -\frac{s^2-1}{3s} & 0 & 0 & \frac{s^2-1}{3s} \\ 0 & \frac{s^2+2}{3s} & 0 & \frac{s^2-1}{3s} & \frac{s^2-1}{3s} & 0 \\ -\frac{s^2-1}{3s} & 0 & \frac{2s}{3} + \frac{1}{3s} & 0 & 0 & \frac{s^2-1}{3s} \\ 0 & \frac{s^2-1}{3s} & 0 & \frac{s^2+2}{3s} & \frac{s^2-1}{3s} & 0 \\ 0 & \frac{s^2-1}{3s} & 0 & \frac{s^2-1}{3s} & \frac{s^2+2}{3s} & 0 \\ \frac{s^2-1}{3s} & 0 & \frac{s^2-1}{3s} & 0 & 0 & \frac{2s}{3} + \frac{1}{3s} \end{pmatrix}$$

By using the Eqs. (4.20) and (4.21) it is possible to obtain the resulting statistical moments after a p -measurement of the second node, thus by projecting on a squeezed momentum state with displacement vector $(0, \bar{p})$. The resulting covariance matrix and displacement vector are

$$\sigma' = \begin{pmatrix} \frac{s(s^2+2)}{2s^2+1} & 0 & \frac{s(1-s^2)}{2s^2+1} & 0 \\ 0 & \frac{s^2+2}{3s} & 0 & \frac{s^2-1}{3s} \\ \frac{s(1-s^2)}{2s^2+1} & 0 & \frac{s(s^2+2)}{2s^2+1} & 0 \\ 0 & \frac{s^2-1}{3s} & 0 & \frac{s^2+2}{3s} \end{pmatrix}$$

$$\mathbf{d} = \begin{pmatrix} \frac{\bar{p}(s^2-1)}{2s^2+1} \\ 0 \\ \frac{\bar{p}(s^2-1)}{2s^2+1} \\ 0 \end{pmatrix}$$

⁶For $s = 10$ the inseparability condition reads $\Delta^2(\hat{q}_1 - \hat{p}_2) + \Delta^2(\hat{q}_2 - \hat{p}_1) = 0.49$ for the 2-mode cluster resulting from a node-removal and $\Delta^2(\hat{q}_1 - \hat{p}_2) + \Delta^2(\hat{q}_2 - \hat{p}_1) = 0.4$ for the EPR-like cluster state directly built from two squeezed states.

We may see that the values in the covariance matrix are the same we obtained in Eq. (4.23) for node-removal, but in the case of wire shortening, the resulting quantum channel exhibits correlations between the momentum quadratures of the modes and anticorrelations between the position quadratures, such that

$$\Delta^2(\hat{q}_1 + \hat{q}_3) + \Delta^2(\hat{p}_1 - \hat{p}_3) = \frac{6s}{2s^2 + 1} + \frac{2}{s} \xrightarrow{s \rightarrow \infty} 0$$

We conclude that, if our aim is to create an EPR-channel out of a 3-mode cluster, we can equivalently perform an operation of node-removal or wire-shortening, which will result in a 2-mode state with EPR-like correlations between specific quadratures, depending on the operation we chose. The resulting state will be slightly more noisy than a state directly built from squeezed resources.

We could then add measurements to linear optics operations to manipulate cluster states to solve the specific task of creating an EPR-channel out of two given nodes of an entangled resource. In particular, operations of node-removal or wire-shortening will be useful in the cases we couldn't find a suitable transformation to create an EPR-link between two nodes, disconnecting them from all the other nodes of the cluster.

Conclusions

During the present dissertation we studied the implementation of cluster states, either regular or with a complex topology, in a linear optical framework following an optimization protocol. The results showed that the quality of the implemented cluster, measured as the mean of the variance of its nullifiers, increases with the quantity of entanglement links. We have analysed different kind of networks by reproducing in the quantum regime the models which describe real-world networks. In the Barabási-Albert and Erdős–Rényi model, regardless of the topology, clusters with a similar average degree $\langle k \rangle$ have a comparable overall quality. The degree $\langle k \rangle$ in complex graphs could thus be used as a benchmark for the quality of the state implemented with the optimization protocol discussed in Section 3.3.2. Moreover, analyzing “small-world networks”, that evolve from a regular network to a random network as their characteristic parameter p_{WS} increases, we found that regular graphs are optimized better than random graphs. The overall quality of a network is an important property to reduce noises that arise from finite-squeezing implementation when the resource is used, for example, in a quantum computation protocol.

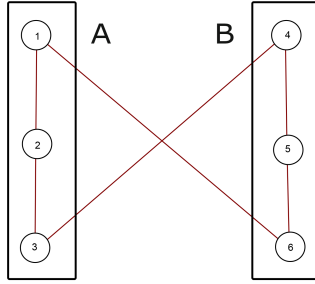
In addition, the optimization protocol permits us to concentrate the squeezing on two given nodes, with the aim of creating an EPR channel out of them by measuring and by employing feedforward procedures or by acting on the resource with a linear optical transformation. We saw that such a global transformation can always be found and we can indeed retrieve an EPR channel out of the two given nodes. If we allow only local transformations we can no longer rely on the optimization protocol of Section 3.3.2, due to the fact that we have more constraint on the form of the linear optical symplectic transformation acting on the resource. We used a Derandomized Evolutionary Strategy (DES) algorithm, whose main advantage is a high convergence speed, with respect to other optimization algorithms. Such an algorithm doesn’t guarantee however the best optimization, as in general its aim is finding local extrema and not global ones. As an additional tool, homodyne measurements can be performed to reshape the cluster with the aim of obtaining an EPR link, with the price of adding feedforward operations and some extra noise.

In the present dissertation the algorithm has been tested with a small number of nodes. We are currently implementing the algorithm on a larger number of nodes and in particular in the case of networks with complex shape. Future works will be extended to the full class of symplectic local operations and some non-gaussian operations.

Appendix A

In this appendix we report the transformations we have to perform on a given graph state to get an EPR channel out of two given nodes.

6-mode graph 1 We implemented a 6-mode cluster and we distributed its modes as shown in the following figure:



The transformations for entangling nodes 1 and 6 are already reported in Section 4.2.4.

To entangle nodes 1 and 4, with $n_{gen} = 5000$, we obtained

$$X_A = \begin{pmatrix} -0.564055 & \mathcal{O}(10^{-16}) & 0.564055 \\ 0.250315 & \mathcal{O}(10^{-16}) & 0.250315 \\ \mathcal{O}(10^{-16}) & -0.277133 & \mathcal{O}(10^{-16}) \end{pmatrix}, \quad Y_A = \begin{pmatrix} -0.426429 & \mathcal{O}(10^{-16}) & 0.426429 \\ -0.661319 & \mathcal{O}(10^{-17}) & -0.661319 \\ \mathcal{O}(10^{-16}) & -0.960831 & \mathcal{O}(10^{-16}) \end{pmatrix}$$

$$X_B = \begin{pmatrix} -0.564055 & \mathcal{O}(10^{-17}) & 0.564055 \\ -0.449914 & \mathcal{O}(10^{-17}) & -0.449914 \\ \mathcal{O}(10^{-18}) & -0.993175 & \mathcal{O}(10^{-17}) \end{pmatrix}, \quad Y_B = \begin{pmatrix} 0.426429 & \mathcal{O}(10^{-17}) & -0.426429 \\ -0.545507 & \mathcal{O}(10^{-18}) & -0.545507 \\ \mathcal{O}(10^{-18}) & -0.116635 & \mathcal{O}(10^{-17}) \end{pmatrix}$$

Using these transformations, the correlations between 1 and 4 and the other nodes are at most of the order of 10^{-15} .

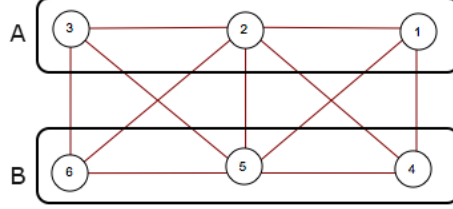
To entangle nodes 1 and 5, with $n_{gen} = 5000$, we obtained

$$X_A = \begin{pmatrix} -0.648701 & \mathcal{O}(10^{-16}) & 0.648701 \\ -0.625483 & \mathcal{O}(10^{-18}) & -0.625483 \\ \mathcal{O}(10^{-17}) & -0.901634 & \mathcal{O}(10^{-17}) \end{pmatrix}, \quad Y_A = \begin{pmatrix} -0.281402 & \mathcal{O}(10^{-16}) & 0.281402 \\ -0.329805 & \mathcal{O}(10^{-18}) & -0.329805 \\ \mathcal{O}(10^{-16}) & -0.432501 & \mathcal{O}(10^{-16}) \end{pmatrix}$$

$$X_B = \begin{pmatrix} 0.661714 & \mathcal{O}(10^{-17}) & 0.661714 \\ -0.648701 & \mathcal{O}(10^{-17}) & 0.648701 \\ \mathcal{O}(10^{-18}) & -0.999699 & \mathcal{O}(10^{-17}) \end{pmatrix}, \quad Y_B = \begin{pmatrix} 0.249267 & \mathcal{O}(10^{-17}) & 0.249267 \\ 0.281402 & \mathcal{O}(10^{-17}) & -0.281402 \\ \mathcal{O}(10^{-18}) & 0.0245157 & \mathcal{O}(10^{-17}) \end{pmatrix}$$

Using these transformations, the correlations between 1 and 5 and the other nodes are at most of the order of 10^{-15} .

6-mode graph 2 We implemented a 6-mode cluster and we distributed its modes as shown in the following figure:



The transformations for entangling nodes 1 and 6 are already reported in Section 4.2.4.

To entangle nodes 1 and 4, with $n_{gen} = 5000$, we obtained

$$X_A = \begin{pmatrix} 0.424404 & \mathcal{O}(10^{-17}) & -0.424404 \\ 0.49186 & \mathcal{O}(10^{-17}) & 0.49186 \\ \mathcal{O}(10^{-18}) & -0.0627088 & \mathcal{O}(10^{-18}) \end{pmatrix}, \quad Y_A = \begin{pmatrix} -0.56558 & \mathcal{O}(10^{-17}) & 0.56558 \\ 0.508009 & \mathcal{O}(10^{-17}) & 0.508009 \\ \mathcal{O}(10^{-18}) & -0.998032 & \mathcal{O}(10^{-17}) \end{pmatrix}$$

$$X_B = \begin{pmatrix} 0.424404 & \mathcal{O}(10^{-16}) & -0.424404 \\ -0.706958 & \mathcal{O}(10^{-17}) & -0.706958 \\ \mathcal{O}(10^{-17}) & 0.89902 & \mathcal{O}(10^{-16}) \end{pmatrix}, \quad Y_B = \begin{pmatrix} 0.56558 & \mathcal{O}(10^{-16}) & -0.56558 \\ 0.0145012 & \mathcal{O}(10^{-16}) & 0.0145012 \\ \mathcal{O}(10^{-17}) & 0.437907 & \mathcal{O}(10^{-16}) \end{pmatrix}$$

Using these transformations, the correlations between 1 and 4 and the other nodes are at most of the order of 10^{-15} .

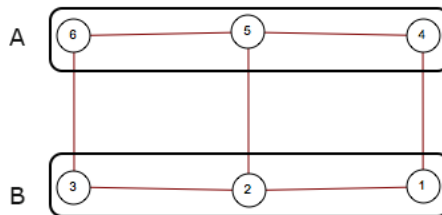
To entangle nodes 1 and 5, with $n_{gen} = 5000$, we obtained

$$X_A = \begin{pmatrix} -0.308384 & \mathcal{O}(10^{-17}) & 0.308384 \\ \mathcal{O}(10^{-16}) & 0.573929 & \mathcal{O}(10^{-16}) \\ 0.451354 & \mathcal{O}(10^{-16}) & 0.451354 \end{pmatrix}, \quad Y_A = \begin{pmatrix} -0.636317 & \mathcal{O}(10^{-18}) & 0.636317 \\ \mathcal{O}(10^{-16}) & -0.818905 & \mathcal{O}(10^{-16}) \\ 0.544315 & \mathcal{O}(10^{-16}) & 0.544315 \end{pmatrix}$$

$$X_B = \begin{pmatrix} -0.233727 & -0.362844 & -0.233727 \\ -0.308384 & \mathcal{O}(10^{-16}) & 0.308384 \\ 0.616806 & -0.269078 & 0.616806 \end{pmatrix}, \quad Y_B = \begin{pmatrix} 0.0357351 & 0.869789 & 0.0357351 \\ 0.636317 & \mathcal{O}(10^{-16}) & -0.636317 \\ 0.25228 & 0.198513 & 0.25228 \end{pmatrix}$$

Using these transformations, the correlations between 1 and 5 and the other nodes are at most of the order of 10^{-15} .

6-mode graph “grid” We implemented a 6-mode cluster and we distributed its modes as shown in the following figure:



To entangle nodes 1 and 4, with $n_{gen} = 5000$, we obtained

$$X_A = \begin{pmatrix} -0.564055 & \mathcal{O}(10^{-16}) & 0.564055 \\ 0.250315 & \mathcal{O}(10^{-16}) & 0.250315 \\ \mathcal{O}(10^{-16}) & -0.277133 & \mathcal{O}(10^{-16}) \end{pmatrix}, \quad Y_A = \begin{pmatrix} -0.426429 & \mathcal{O}(10^{-16}) & 0.426429 \\ -0.661319 & \mathcal{O}(10^{-17}) & -0.661319 \\ \mathcal{O}(10^{-16}) & -0.960831 & \mathcal{O}(10^{-16}) \end{pmatrix}$$

$$X_B = \begin{pmatrix} -0.564055 & \mathcal{O}(10^{-17}) & 0.564055 \\ -0.449914 & \mathcal{O}(10^{-17}) & -0.449914 \\ \mathcal{O}(10^{-18}) & -0.993175 & \mathcal{O}(10^{-17}) \end{pmatrix}, \quad Y_B = \begin{pmatrix} 0.426429 & \mathcal{O}(10^{-17}) & -0.426429 \\ -0.545507 & \mathcal{O}(10^{-18}) & -0.545507 \\ \mathcal{O}(10^{-18}) & -0.116635 & \mathcal{O}(10^{-17}) \end{pmatrix}$$

Using these transformations, the correlations between 1 and 4 and the other nodes are at most of the order of 10^{-15} .

To entangle nodes 1 and 5, with $n_{gen} = 5000$, we obtained

$$X_A = \begin{pmatrix} -0.648701 & \mathcal{O}(10^{-16}) & 0.648701 \\ -0.625483 & \mathcal{O}(10^{-18}) & -0.625483 \\ \mathcal{O}(10^{-17}) & -0.901634 & \mathcal{O}(10^{-17}) \end{pmatrix}, \quad Y_A = \begin{pmatrix} -0.281402 & \mathcal{O}(10^{-16}) & 0.281402 \\ -0.329805 & \mathcal{O}(10^{-18}) & -0.329805 \\ \mathcal{O}(10^{-16}) & -0.432501 & \mathcal{O}(10^{-16}) \end{pmatrix}$$

$$X_B = \begin{pmatrix} 0.661714 & \mathcal{O}(10^{-17}) & 0.661714 \\ -0.648701 & \mathcal{O}(10^{-17}) & 0.648701 \\ \mathcal{O}(10^{-18}) & -0.999699 & \mathcal{O}(10^{-17}) \end{pmatrix}, \quad Y_B = \begin{pmatrix} 0.249267 & \mathcal{O}(10^{-17}) & 0.249267 \\ 0.281402 & \mathcal{O}(10^{-17}) & -0.281402 \\ \mathcal{O}(10^{-18}) & 0.0245157 & \mathcal{O}(10^{-17}) \end{pmatrix}$$

Using these transformations, the correlations between 1 and 5 and the other nodes are at most of the order of 10^{-15} .

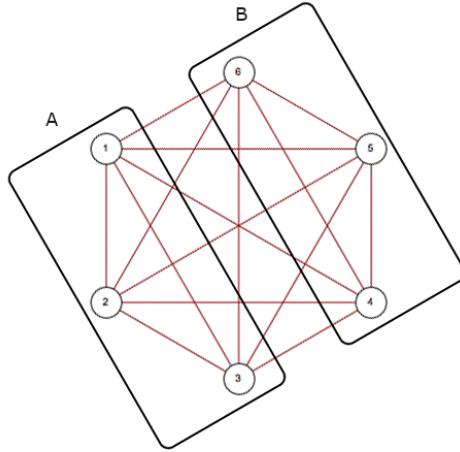
To entangle nodes 1 and 6, with $n_{gen} = 5000$, we obtained

$$X_A = \begin{pmatrix} -0.688847 & \mathcal{O}(10^{-14}) & 0.688847 \\ -0.304536 & 0.172212 & -0.304536 \\ -0.0752665 & -0.763395 & -0.0752665 \end{pmatrix}, \quad Y_A = \begin{pmatrix} 0.159655 & \mathcal{O}(10^{-16}) & -0.159655 \\ 0.617874 & -0.146023 & 0.617874 \\ 0.1408 & 0.605184 & 0.1408 \end{pmatrix}$$

$$X_B = \begin{pmatrix} -0.371646 & -0.163936 & -0.371646 \\ -0.267229 & 0.650482 & -0.267229 \\ -0.688847 & \mathcal{O}(10^{-15}) & 0.688847 \end{pmatrix}, \quad Y_B = \begin{pmatrix} 0.334483 & 0.687841 & 0.334483 \\ -0.422597 & 0.27726 & -0.422597 \\ -0.159655 & \mathcal{O}(10^{-14}) & 0.159655 \end{pmatrix}$$

Using these transformations, the correlations between 1 and 6 and the other nodes are at most of the order of 10^{-15} .

6-mode graph “fully connected” We implemented a 6-mode cluster and we distributed its modes as shown in the following figure:



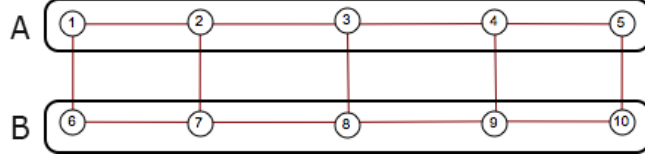
To entangle nodes 1 and 2, with $n_{gen} = 5000$, we obtained

$$X_A = \begin{pmatrix} 0.56149 & -0.397134 & -0.164356 \\ -0.56149 & 0.397134 & 0.164356 \\ 0.408248 & 0.408248 & 0.408248 \end{pmatrix}, \quad Y_A = \begin{pmatrix} -0.134394 & -0.419068 & 0.553462 \\ -0.134394 & -0.419068 & 0.553462 \\ -0.408248 & -0.408248 & -0.408248 \end{pmatrix}$$

$$X_B = \begin{pmatrix} 0.447715 & 0.293987 & 0.104392 \\ 0.436176 & 0.614297 & -0.472751 \\ 0.124502 & 0.361237 & 0.860632 \end{pmatrix}, \quad Y_B = \begin{pmatrix} -0.706639 & 0.450256 & -0.0124474 \\ 0.201155 & -0.408378 & 0.0407497 \\ 0.232375 & -0.190305 & 0.152002 \end{pmatrix}$$

Using these transformations, the correlations between 1 and 2 and the other nodes are at most of the order of 10^{-15} .

10-mode graph “grid” We implemented a 10-mode cluster and we distributed its modes as shown in the following figure:



To entangle nodes 1 and 10, with $n_{gen} = 3000$, we obtained

$$X_A = \begin{pmatrix} \mathcal{O}(10^{-9}) & \mathcal{O}(10^{-10}) & \mathcal{O}(10^{-9}) & \mathcal{O}(10^{-12}) & \mathcal{O}(10^{-10}) \\ 0.433752 & 0.208888 & 0.184265 & \mathcal{O}(10^{-10}) & -0.249487 \\ -0.119857 & -0.00616257 & -0.529232 & \mathcal{O}(10^{-9}) & -0.409374 \\ -0.0169188 & 0.964388 & -0.0334197 & \mathcal{O}(10^{-10}) & -0.0165008 \\ \mathcal{O}(10^{-11}) & \mathcal{O}(10^{-10}) & \mathcal{O}(10^{-9}) & -0.99531 & \mathcal{O}(10^{-13}) \end{pmatrix}$$

$$Y_A = \begin{pmatrix} 0.57735 & \mathcal{O}(10^{-9}) & -0.57735 & \mathcal{O}(10^{-9}) & 0.57735 \\ 0.654299 & -0.0802321 & 0.218916 & \mathcal{O}(10^{-9}) & -0.435383 \\ -0.0663495 & -0.0285936 & -0.5482 & \mathcal{O}(10^{-9}) & -0.48185 \\ -0.177099 & 0.137942 & -0.0553395 & \mathcal{O}(10^{-9}) & 0.121759 \\ \mathcal{O}(10^{-10}) & \mathcal{O}(10^{-9}) & \mathcal{O}(10^{-10}) & -0.0967379 & \mathcal{O}(10^{-11}) \end{pmatrix}$$

$$X_B = \begin{pmatrix} 0.696996 & 0.118446 & 0.0513584 & -0.247325 & -0.645638 \\ 0.0037403 & -0.083768 & 0.275009 & -0.806103 & 0.271269 \\ 0.0733984 & 0.383927 & 0.21772 & -0.120292 & 0.144322 \\ -0.309119 & 0.116546 & -0.514378 & -0.239374 & -0.205258 \\ \mathcal{O}(10^{-9}) & \mathcal{O}(10^{-10}) & \mathcal{O}(10^{-10}) & \mathcal{O}(10^{-9}) & \mathcal{O}(10^{-10}) \end{pmatrix}$$

$$Y_B = \begin{pmatrix} -0.0150675 & -0.0249436 & 0.00769078 & -0.134483 & 0.0227583 \\ 0.0507257 & -0.194465 & -0.209338 & 0.205192 & -0.260064 \\ 0.00754282 & 0.844743 & 0.088232 & 0.191228 & 0.0806892 \\ -0.277579 & 0.256789 & -0.474074 & -0.347131 & -0.196495 \\ -0.57735 & \mathcal{O}(10^{-10}) & 0.57735 & \mathcal{O}(10^{-18}) & -0.57735 \end{pmatrix}$$

Using these transformations, the correlations between 1 and 10 and the other nodes are at most of the order of 10^{-9} .

To entangle nodes 1 and 6, with $n_{gen} = 5000$, we obtained

$$\begin{aligned}
 X_A &= \begin{pmatrix} -0.0741002 & \mathcal{O}(10^{-8}) & 0.0741002 & \mathcal{O}(10^{-8}) & -0.0741002 \\ 0.414091 & \mathcal{O}(10^{-8}) & -0.148369 & \mathcal{O}(10^{-7}) & -0.562461 \\ 0.447327 & 0.125818 & 0.273404 & -0.600588 & -0.173923 \\ 0.0405618 & -0.823495 & -0.0157227 & -0.0204954 & -0.0562845 \\ -0.0760763 & \mathcal{O}(10^{-8}) & -0.346725 & -0.479288 & -0.270649 \end{pmatrix} \\
 Y_A &= \begin{pmatrix} 0.572575 & \mathcal{O}(10^{-8}) & -0.572575 & \mathcal{O}(10^{-8}) & 0.572575 \\ 0.36941 & \mathcal{O}(10^{-9}) & 0.562499 & \mathcal{O}(10^{-6}) & 0.193089 \\ 0.0501783 & 0.0487566 & -0.332644 & 0.237199 & -0.382822 \\ -0.0459603 & 0.551043 & -0.0564897 & 0.0855141 & -0.0105295 \\ -0.38284 & \mathcal{O}(10^{-7}) & -0.138526 & -0.587861 & 0.244315 \end{pmatrix} \\
 X_B &= \begin{pmatrix} -0.0741002 & \mathcal{O}(10^{-8}) & 0.0741002 & \mathcal{O}(10^{-9}) & -0.0741002 \\ -0.292924 & -0.719874 & -0.207062 & \mathcal{O}(10^{-8}) & 0.0858616 \\ 0.507739 & -0.0570439 & 0.591356 & \mathcal{O}(10^{-8}) & 0.0836171 \\ -0.254744 & 0.644631 & -0.167788 & \mathcal{O}(10^{-8}) & 0.0869557 \\ \mathcal{O}(10^{-9}) & \mathcal{O}(10^{-8}) & \mathcal{O}(10^{-9}) & -0.612348 & \mathcal{O}(10^{-8}) \end{pmatrix} \\
 Y_B &= \begin{pmatrix} -0.572575 & \mathcal{O}(10^{-8}) & 0.572575 & \mathcal{O}(10^{-8}) & -0.572575 \\ -0.16622 & -0.200272 & 0.28033 & \mathcal{O}(10^{-8}) & 0.446551 \\ -0.462094 & 0.0729278 & -0.0627612 & \mathcal{O}(10^{-9}) & 0.399332 \\ -0.130422 & 0.132483 & 0.404244 & \mathcal{O}(10^{-9}) & 0.534666 \\ \mathcal{O}(10^{-8}) & \mathcal{O}(10^{-8}) & \mathcal{O}(10^{-8}) & 0.790588 & \mathcal{O}(10^{-8}) \end{pmatrix}
 \end{aligned}$$

Using these transformations, the correlations between 1 and 6 and the other nodes are at most of the order of 10^{-8} .

Appendix B

In the characteristic function formalism an operator \hat{O} can be expanded as

$$\hat{O} = \frac{1}{(2\pi)^N} \int d^{2N} \mathbf{x} \chi_O(\mathbf{x}) \hat{D}^\dagger(\mathbf{x}) \quad (\text{B.1})$$

The right hand-side of Eq. (4.12) then can be written as

$$\begin{aligned} \text{Tr}_B [\hat{\rho}(\mathbb{1}_A \otimes |m\rangle \langle m|)] &= \text{Tr}_B \left[\frac{1}{(2\pi)^N} \int d^{2N} \mathbf{x} \chi_\rho(\mathbf{x}) \hat{D}^\dagger(\mathbf{x}) \right. \\ &\quad \left. \left(\mathbb{1}_A \otimes \frac{1}{2\pi} \int d^2 \boldsymbol{\eta}_B \chi_\omega(\boldsymbol{\eta}_B) \hat{D}^\dagger(\boldsymbol{\eta}_B) \right) \right] \end{aligned}$$

and since

$$\begin{aligned} \text{Tr}_B[\hat{D}^\dagger(\mathbf{x}_A, \mathbf{x}_B)(\mathbb{1}_A \otimes \hat{D}^\dagger(\boldsymbol{\eta}_B))] &= \text{Tr}_B[\hat{D}^\dagger(\mathbf{x}_A) \otimes \hat{D}^\dagger(\mathbf{x}_B) \hat{D}^\dagger(\boldsymbol{\eta}_B)] = \\ &= \hat{D}^\dagger(\mathbf{x}_A) \text{Tr}_B[\hat{D}^\dagger(\mathbf{x}_B) \hat{D}^\dagger(\boldsymbol{\eta}_B)] = \hat{D}^\dagger(\mathbf{x}_A) 2\pi \delta(\mathbf{x}_B + \boldsymbol{\eta}_B) \end{aligned}$$

which follows from the property $\text{Tr}[D(\mathbf{x})D(\mathbf{y})^\dagger] = (2\pi)^N \delta^{2N}(\mathbf{x} - \mathbf{y})$, Eq. (4.12) can be rewritten as

$$\begin{aligned} p(m) \hat{\rho}_A &= \frac{1}{(2\pi)^N} \int d^{2N} \mathbf{x} \chi_\rho(\mathbf{x}) \hat{D}^\dagger(\mathbf{x}_A) \int d^2 \boldsymbol{\eta}_B \chi_\omega(\boldsymbol{\eta}_B) \delta(\mathbf{x}_B + \boldsymbol{\eta}_B) \\ &= \frac{1}{(2\pi)^N} \int d^{2N} \mathbf{x} \chi_\rho(\mathbf{x}) \chi_\omega(-\mathbf{x}_B) \hat{D}^\dagger(\mathbf{x}_A) \end{aligned} \quad (\text{B.2})$$

By using Eq. (B.1), we obtain the expression of the density operator $\hat{\rho}_A$ in terms of the characteristic function, namely

$$\hat{\rho}_A = \frac{1}{(2\pi)^{(N-1)}} \int d^{2N-2} \mathbf{x}_A \chi_{\rho_A}(\mathbf{x}_A) \hat{D}^\dagger(\mathbf{x}_A)$$

and comparing this expression with Eq. (B.2) we get to Eq. (4.13).

Substituting Γ of Eq.(4.16) in Eq.(4.11), Eq. (4.13) reads

$$\begin{aligned} \chi_{\rho_A}(\mathbf{x}_A) &= \frac{1}{p(m)} \frac{1}{2\pi} \int d^2 \mathbf{x}_B e^{-\frac{1}{2} \mathbf{x}^T \Gamma \mathbf{x} - i \mathbf{x}^T \mathbf{D}} e^{-\frac{1}{2} \mathbf{x}_B^T \Gamma_\omega \mathbf{x}_B + i \mathbf{x}_B^T \mathbf{D}_\omega} = \\ &= \frac{e^{-\frac{1}{2} \mathbf{x}_A^T A \mathbf{x}_A} e^{-i \mathbf{x}_A^T \mathbf{D}_A}}{2\pi p(m)} \int d^2 \mathbf{x}_B e^{-\frac{1}{2} \mathbf{x}_B^T (B + \Gamma_\omega) \mathbf{x}_B} e^{-i \mathbf{x}_B^T [(\mathbf{D}_B - \mathbf{D}_\omega) - i C^T \mathbf{x}_A]} \end{aligned} \quad (\text{B.3})$$

where Γ_ω and D_ω are the statistical moments of the projected state, if we consider a Gaussian measurement.

Recalling that for any symmetric positive-definite matrix Q $2N \times 2N$ and \mathbf{Y} is a $2N$ -dimensional real vector the identity

$$\int d^{2N} \mathbf{x} e^{-\frac{1}{2} \mathbf{x}^T Q \mathbf{x} - i \mathbf{x}^T \mathbf{y}} = \frac{(2\pi)^N}{\sqrt{\det Q}} e^{-\frac{1}{2} \mathbf{y}^T Q^{-1} \mathbf{y}}$$

holds, Eq. (B.3) gives

$$\begin{aligned} \chi_{\rho_A}(\mathbf{x}_A) &= \frac{e^{-\frac{1}{2} \mathbf{x}_A^T A \mathbf{x}_A} e^{-i \mathbf{x}_A^T \mathbf{D}_A}}{2\pi p(m)} \frac{2\pi}{\sqrt{\det(B + \Gamma_\omega)}} e^{-\frac{1}{2} [(\mathbf{D}_B - \mathbf{D}_\omega) - i C^T \mathbf{x}_A]^T (B + \Gamma_\omega)^{-1} [(\mathbf{D}_B - \mathbf{D}_\omega) - i C^T \mathbf{x}_A]} \\ &= \frac{e^{-\frac{1}{2} (\mathbf{D}_B - \mathbf{D}_\omega)^T (B + \Gamma_\omega)^{-1} (\mathbf{D}_B - \mathbf{D}_\omega)}}{p(m) \sqrt{\det(B + \Gamma_\omega)}} e^{-\frac{1}{2} \mathbf{x}_A^T [A - C(B + \Gamma_\omega)^{-1} C^T] \mathbf{x}_A - i \mathbf{x}_A^T [\mathbf{D}_A - C(B + \Gamma_\omega)^{-1} (\mathbf{D}_B - \mathbf{D}_\omega)]} \end{aligned}$$

which corresponds to Eq.(4.17), up to normalization.

Bibliography

- [1] B. P. A. Einstein and N. Rosen, *Phys. Rev.* **47**, 777 (1935).
- [2] J. S. Bell, *Physics* **1**, 195–200 (1964).
- [3] J. P. Dowling and G. J. Milburn, *Phil. Trans. R. Soc. A* **361** (2003).
- [4] A. Aspect, “John bell and the second quantum revolution”, in *Speakable and unspeakable in quantum mechanics* (Cambridge University Press, 2004).
- [5] E. Diamanti, in *Proceedings of Quantum Information and Measurement (QIM) 2017* (2017), QF3B.1.
- [6] D. Bruss and G. Leuchs, *Quantum information: from foundations to quantum technology applications*, 2nd ed. (Wiley-VCH, 2018).
- [7] J. Roslund, R. M. de Araújo, S. Jiang, C. Fabre, and N. Treps, *Nature Photonics* **8**, 109–112 (2014).
- [8] J. Yoshikawa, S. Yokoyama, T. Kaji, C. Sornphiphatphong, Y. Shiozawa, K. Makino, and A. Furusawa, *APL Photonics* **1**, 060801 (2016).
- [9] A. Furusawa and P. van Loock, *Quantum teleportation and entanglement* (Wiley-VCH, 2011).
- [10] S. Braunstein and P. van Loock, *Rev. Mod. Phys.* **77**, 513 (2005).
- [11] E. Kashefi and A. Pappa, *Cryptography* **1**, 12 (2017).
- [12] S. Pirandola and S. L. Braunstein, *Nature* **532**, 169–171 (2016).
- [13] J. Gao, B. Barzel, and A. Barabási, *Nature* **530**, 307–312 (2016).
- [14] A. Barabási and R. Albert, *Rev. Mod. Phys.* **74**, 47 (2002).
- [15] Y. Cai, J. Roslund, F. Arzani, X. Xu, C. Fabre, and N. Treps, *Nature Communications* **8**, 15645 (2017).
- [16] J. Roslund, O. M. Shir, T. Bäck, and H. Rabitz, *Phys. Rev. A* **80** (2009).
- [17] D. Walls and G. J. Milburn, *Quantum optics*, 2nd ed. (Springer, 1994).
- [18] G. Grynberg, A. Aspect, and C. Fabre, *Introduction to quantum optics: from the semi-classical approach to quantized light* (Cambridge University Press, 2010).
- [19] O. Morin, “Non-gaussian states and measurements for quantum information”, PhD thesis (Université Pierre et Marie Curie, 2013).

- [20] H. P. Robertson, Phys. Rev. **34**, 163–164 (1929).
- [21] E. Schrödinger, Sitz. Preus. Acad. Wiss. (Phys.-Math. Klasse) **19**, 296–303 (1930).
- [22] R. Loudon, *The quantum theory of light*, 3rd ed. (Oxford University Press, 1973).
- [23] C. Gerry and P. Knight, *Introductory quantum optics* (Cambridge University Press, 2004).
- [24] R. J. Glauber, Phys. Rev. **130**, 2529 (1963).
- [25] R. M. Wilcox, Journal of Mathematical Physics **8**, 962 (1967).
- [26] N. Treps, V. Delaubert, A. Maître, J. M. Courty, and C. Fabre, Phys. Rev. A **71**, 013820 (2005).
- [27] E. Wigner, Phys. Rev. **40**, 749 (1932).
- [28] U. Leonhardt, *Measuring the quantum state of light* (Cambridge University Press, 1997).
- [29] M. A. Nielsen and I. L. Chuang, *Quantum computing and quantum information* (Cambridge University Press, 2000).
- [30] J. Preskill, *Lecture notes in quantum information*, California Institute of Technology, 2018.
- [31] Arvind, B. Dutta, H. Mukunda, and R. Simon, Pranama - J. Phys **45**, 471–497 (1995).
- [32] B. W. Lovett and P. Kok, *Introduction to optical quantum information processing* (Cambridge University Press, 2010).
- [33] S. L. Braunstein, Phys. Rev. A **71**, 055801 (2005).
- [34] J. L. O’Brien, Science **318**, 1567 (2007).
- [35] B. Hensen, H. Bernien, A. E. Dréau, A. Reiserer, N. Kalb, M. S. Blok, J. Ruitenberg, R. F. L. Vermeulen, R. N. Schouten, C. Abellán, W. Amaya, V. Pruneri, M. W. Mitchell, M. Markham, D. J. Twitchen, D. Elkouss, S. Wehner, T. H. Taminiau, and R. Hanson, Nature **526**, 682–686 (2015).
- [36] L.-M. Duan, G. Giedke, J. I. Cirac, and P. Zoller, Phys. Rev. Lett. **84**, 2722–2725 (2000).
- [37] M. D. Reid, P. D. Drummond, W. P. Bowen, E. G. Cavalcanti, P. K. Lam, H. A. Bachor, U. L. Andersen, and G. Leuchs, Rev. Mod. Phys. **81**, 1727 (2009).
- [38] J. Roslund, R. de Araújo, S. Jiang, C. Fabre, and N. Treps, Nature Photonics **8**, (2013).
- [39] P. L. Knight and V. Buzek, “Squeezed states: basic principles”, in *Quantum squeezing. springer series on atomic, optical, and plasma physics*, Vol. 27 (Springer, Berlin, Heidelberg, 2004).
- [40] A. I. Lvovsky, arXiv:1401.4118 [quant-ph], 2014.

- [41] C. H. Bennett, G. Brassard, C. Crépeau, R. Jozsa, A. Peres, and W. K. Wootters, *Phys. Rev. Lett.* **70**, 1895–1899 (1993).
- [42] D. Boschi, S. Branca, F. De Martini, L. Hardy, and S. Popescu, *Phys. Rev. Lett.* **80**, 1121–1125 (1998).
- [43] X.-S. Ma, T. Herbst, T. Scheidl, D. Wang, S. Kropatschek, W. Naylor, B. Wittmann, A. Mech, J. Kofler, E. Anisimova, V. Makarov, T. Jennewein, R. Ursin, and A. Zeilinger, *Nature* **489**, 269–273 (2012).
- [44] S. L. Braunstein and H. J. Kimble, *Phys. Rev. Lett.* **80**, 869 (1998).
- [45] A. Furusawa, J. L. Sørensen, S. L. Braunstein, C. A. Fuchs, H. J. Kimble, and E. S. Polzik, *Science* **282**, 706–709 (1998).
- [46] S. L. Braunstein, C. A. Fuchs, and H. J. Kimble, *Journal of Modern Optics* **47**, 267–278 (2000).
- [47] A. Christ, C. Lupo, and C. Silberhorn, *New Journal of Physics* **14**, 083007 (2012).
- [48] K. Husimi, *Proceedings of the Physico-Mathematical Society of Japan. 3rd Series* **22**, 264–314 (1940).
- [49] P. Shor, *SIAM Journal on Computing* **26**, 1484–1509 (1997).
- [50] R. Jozsa, arXiv:quant-ph/0508124, 2005.
- [51] M. A. Nielsen, *Physics Letters A* **308**, 96–100 (2003).
- [52] D. W. Leung, *International Journal of Quantum Information* **02**, 33–43 (2004).
- [53] R. Raussendorf and H. J. Briegel, *Phys. Rev. Lett.* **86**, 5188 (2001).
- [54] S. Lloyd and S. L. Braunstein, *Phys. Rev. Lett.* **82**, 1784–1787 (1999).
- [55] N. C. Menicucci, P. van Loock, M. Gu, C. Weedbrook, T. C. Ralph, and M. A. Nielsen, *Phys. Rev. Lett.* **97**, 110501 (2006).
- [56] M. Gu, C. Weedbrook, N. C. Menicucci, T. C. Ralph, and P. van Loock, *Phys. Rev. A* **79**, 062318 (2009).
- [57] M. A. Nielsen, *Reports on Mathematical Physics* **57**, 147–161 (2006).
- [58] H. J. Briegel and R. Raussendorf, *Phys. Rev. Lett* **86**, 910 (2001).
- [59] M. Hein, J. Eisert, and H. J. Briegel, *Phys. Rev. A* **69**, 062311 (2004).
- [60] G. Ferrini, J. Roslund, F. Arzani, Y. Cai, C. Fabre, and N. Treps, *Phys. Rev. A* **91**, 032314 (2015).
- [61] A. Dufour, “Ingénierie d’états quantiques multimodes avec des impulsions femtosecondes”, PhD thesis (Sorbonne Université, 2018).
- [62] M. Van den Nest, A. Miyake, W. Dür, and H. J. Briegel, *Phys. Rev. Lett.* **97**, 150504 (2006).
- [63] P. van Loock and D. Markham, *AIP Conference Proceedings* **1363**, 256 (2011).
- [64] K. Azuma, K. Tamaki, and H.-K. Lo, *Nature Communications* **6** (2015).

- [65] A. Barabási and R. Albert, *Science* **286**, 509–512 (1999).
- [66] D. Watts and S. Strogatz, *Nature* **393**, 440–442 (1998).
- [67] M. Cuquet and J. Calsamiglia, *Phys. Rev. Lett.* **103**, 240503 (2009).
- [68] A. Acín, J. I. Cirac, and M. Lewenstein, *Nature* **3**, 256–259 (2007).
- [69] N. C. Menicucci, S. T. Flammia, and P. van Loock, *Phys. Rev. A* **83**, 042335 (2011).
- [70] K. Zyczkowski and M. Kus, *J. Phys. A* **27**, 4235 (1994).
- [71] J. Zhang, G. Adesso, C. Xie, and K. Peng, *Phys. Rev. Lett.* **103**, 070501 (2009).
- [72] C. Weedbrook, S. Pirandola, R. García-Patrón, N. J. Cerf, T. C. Ralph, J. H. Shapiro, and S. Lloyd, *Rev. Mod. Phys.* **84**, 621–669 (2012).
- [73] J. Eisert, “Discrete quantum states versus continuous variables”, in *Lectures on quantum information* (John Wiley & Sons, Ltd, 2008) Chap. 3, pp. 39–52.
- [74] G. Adesso, S. Ragy, and A. R. Lee, *Open Systems & Information Dynamics* **21**, 1440001 (2014).
- [75] Y. Miwa, R. Ukai, J. Yoshikawa, R. Filip, P. van Loock, and A. Furusawa, *Phys. Rev. A* **82**, 032305 (2010).
- [76] G. Giedke and J. Ignacio Cirac, *Phys. Rev. A* **66**, 032316 (2002).
- [77] J. Eisert, S. Scheel, and M. B. Plenio, *Phys. Rev. Lett.* **89**, 137903 (2002).